CHALMERS
UNIVERSITY OF TECHNOLOGY

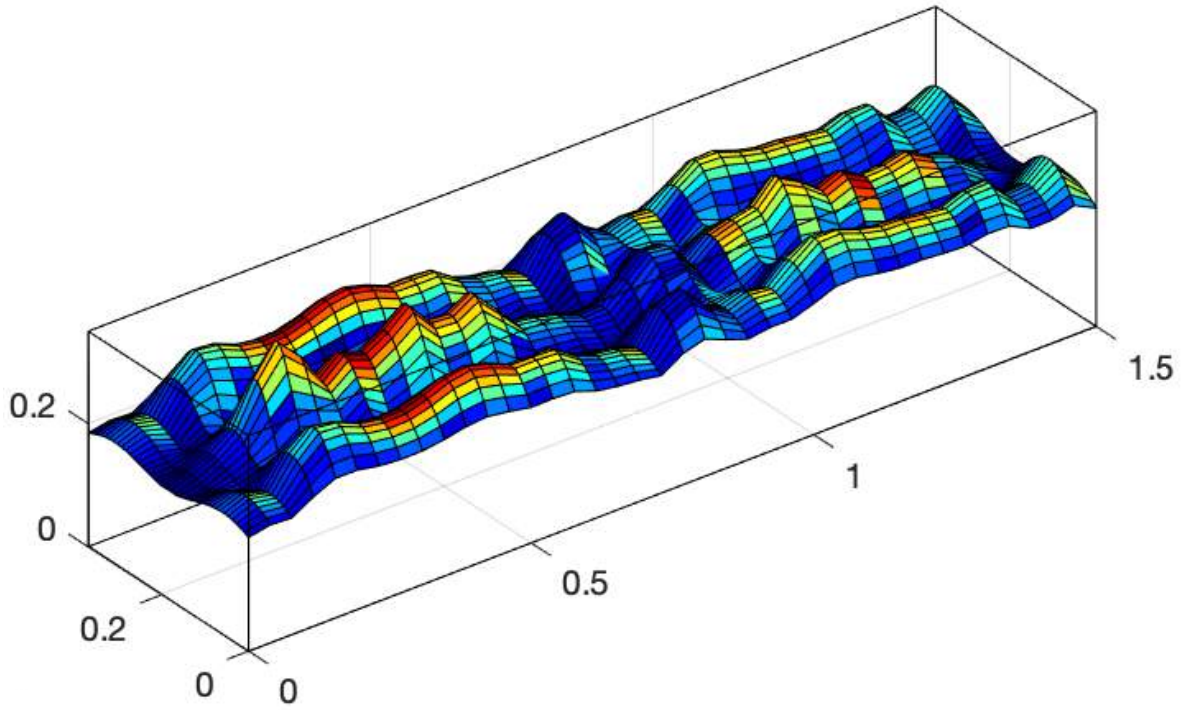

Assessment and Optimization of Sound Reproduction in Water Filled Tanks

A Pilot Study to Evaluate the Use of Shaker Excitation Techniques and an Empirical Study of Sound Field Control Methods

Master's thesis in Master Program Sound and Vibration

AXEL KINDBOM JONSSON

Division of Applied Acoustics
CHALMERS UNIVERSITY OF TECHNOLOGY
Master's thesis ACEX30
Gothenburg, Sweden 2020

Master's thesis ACEX30

Assessment and Optimization of Sound Reproduction in Water Filled Tanks

A Pilot Study to Evaluate the Use of Shaker Excitation Techniques and an Empirical Study of Sound Field Control Methods

AXEL KINDBOM JONSSON

CHALMERS
UNIVERSITY OF TECHNOLOGY

Department of Architecture and Civil Engineering
Division of Applied Acoustics
Vibroacoustics Group
Chalmers University of Technology
Gothenburg, Sweden 2020

Assessment and Optimization of Sound Reproduction in Water Filled Tanks
A Pilot Study to Evaluate the Use of Shaker Excitation Techniques and an Empirical Study of Sound Field Control Methods

AXEL KINDBOM JONSSON

Supervisor: Professor Jens Forssén, Department of Architecture and Civil Engineering
Research Institute Client: PhD Torbjörn Johansson, IVL Swedish Environmental Research Institute
Examiner: Professor Jens Forssén, Department of Architecture and Civil Engineering

Department of Architecture and Civil Engineering
Division of Applied Acoustics
Vibroacoustics Group
Chalmers University of Technology
SE-412 96 Gothenburg
Telephone +46 31 772 1000

Cover: A simulated sound pressure field in a water filled tank.

Department of Architecture and Civil Engineering
Gothenburg, Sweden 2020

Assessment and optimization of sound reproduction in water-filled tanks
A Pilot Study to Evaluate the Use of Shaker Excitation Techniques and an Empirical Study of Sound Field Control Methods
AXEL KINDBOM JONSSON
Department of Architecture and civil Engineering
Chalmers University of Technology

Abstract

Many marine biological tests have been carried out in water-filled tanks where the area of research has been the effects of noise on aquatic life. Recorded or artificial noise has then been produced using loudspeakers, hydrophones, and various other noise sources. The desired sound spectra and sound levels are however hard to produce in the tank, and the sound field that gets produced can deviate largely from the desired sound field in certain or for all frequency regions. Techniques for a more accurate reproduction of sound fields in water-filled tanks thus have the potential to facilitate valid research about the influence of certain sound fields on marine animals.

This report assesses the use of shaker excitation as a means for producing a desired sound field in water-filled tanks. In addition to this, it assesses the use of basic signal processing algorithms to equalize the sound field in the tank. A glass tank filled with 240 litres of water is used for the experiments, and the performance of the shaker is compared to the performance of an underwater loudspeaker. The performance of the signal processing algorithms is evaluated based on a comparison between the sound field with equalization applied to it, and the sound field when no equalization is applied to it. An existing analytical model is deployed to approximate the sound field distribution in the tank, and to communicate it graphically.

The findings in this thesis suggest that the use of shakers as a means of excitation provides sound fields in the tank that are comparable with the sound field produced by an underwater loudspeaker. In terms of level in low frequency regions, the shaker is able to produce higher levels than the underwater loudspeaker. In combination with digital signal processing equalizing techniques, the performance of the transducer, being either the shaker or the loudspeaker, improves.

Keywords: acoustics, equalization, shaker, excitation, underwater, marine, tank, pressure, velocity, signals.

Acknowledgements

I would like to express my sincerest gratitude to Jens Forssén at Chalmers division of Applied Acoustics and Torbjörn Johansson at IVL Swedish Environmental Research Institute who guided me through this project. I also wish to acknowledge the technical and logistical help provided by Börje Wijk at Chalmers Division of Applied Acoustics, as well as PhD Jan Hallander at SSPA, who lent me necessary measurement equipment. Ultimately, all staff and students at the department were supportive and contributed to small and big. This is with emphasis on Michael Sikora, Hannes Helmholz, Pablo Panter and Shivam Bahuguna. A special thanks goes to Antonin Novak, a research fellow at Université du Mans, Le Mans, France, who generously gave detailed help and guidance regarding the modelling part of this project.

Axel Kindbom Jonsson, Gothenburg, August 8, 2020

Contents

List of Figures

List of Tables

1
Introduction

1.1 Background

Underwater noise levels due to human activities are getting higher. In certain frequency regions, the amount of background noise in seas like the North Pacific and the North Sea increased with up to 20 dB between the years 1960 and 2000 [5] (Ch. 9), [6]. Noise from ships, construction sites, deep-sea mining activities, and from newer technologies such as seismic airgun surveys are some of the sources of sound in the ocean. These sources are all contributors to the health threats[1] and behavioural effects on marine life that is becoming an increasing area of concern [5] [7] [8].

Many marine biological tests on the effects of noise on aquatic life have been carried out in aquariums and tanks. Recorded or artificial noise has then been produced using loudspeakers, hydrophones, and various other noise sources. The desired sound spectra and sound levels are however hard to produce in the tank, and the actual sound field that gets produced can deviate largely from the desired sound field in certain or for all frequency regions. Adding to the complexity of the matter, most marine animals have a hearing sensitivity for particle motion, why not only pressure should be considered during a test. The deviations in the produced sound field (pressure and velocity) from the desired sound field might lead to test results that are in fact not valid for the scenario that the test intends to investigate [9] [10] [11]. Thus, a technique for more accurate reproduction of desired sound fields in aquariums and tanks have the potential to facilitate research about the influence of certain sound fields on marine animals.

There are many factors affecting the sound field in a water filled tank. These factors are made up by a combination of the type and character of the transducer used for the production of sound, water temperature, composition and depth (pressure), external background noises as well as geometry and boundary conditions of the tank. In this project, mainly the influence of the enclosure and of the transducer will be considered. Specifically, regarding the influence of the transducer, the use of shaker excitation techniques will be examined. Except of for the cases when a researcher simply has access to a shaker but not an underwater loudspeaker, the evaluation of shaker excitation techniques should attract the interest of the researcher because of these main reasons:

- This thesis is based on the assumption that the single parameter manipulated

[1] Loud noises could cause masking effects, hearing damage, behavioral effects, etc. [5] [7] [8].

during a potential future marine biological sound experiments will be the noise. Therefore, any possible disturbance from alien objects such as a loudspeaker in the tank that might affect the behaviour of the animal should be avoided.
- Shakers might be more durable than underwater loudspeakers. This idea was nourished by the fact that the underwater loudspeaker used in this project broke down twice during the coarse of the project. The problem of non-durable underwater loudspeakers was originally pointed out by this projects research institute client T. Johansson in a personal communication.
- The ability of an underwater loudspeaker to produce low frequency sounds is limited. As an example, the underwater loudspeaker used in this project, has a useful frequency range only above 200 Hz[2]. Additionally, due to the properties of a tank as an environment for the water to be kept in, the sound field in low frequency regions is attenuated very quickly with distance from the sound source. The ability of a shaker to produce lower frequency sounds than this at a sufficient level will be examined.

If the use of shakers as means for producing a desired signal in a tank proves favourable, the findings in this thesis might help the end target group, the marine biologists, perform their research in a more accessible, reliable, valid and economically justifiable manner.

1.2 Aim

Assess, develop and optimize methodology for sound reproduction in water-filled tanks, in terms of
1. Spectrum
2. Level

reducing undesirable effects caused by laboratory settings.

1.3 Objective and Scope

This thesis is a pilot study to evaluate the use of shaker excitation techniques and an empirical study for the optimization of sound field control methods. It is a pilot study in the sense that the scale of the research conducted in it is small and is only carried out on one of many types of shakers and in one particular environment. Additionally, and importantly, the performance of the shaker is examined only through studying its ability to produce sound fields of desired spectrum and level, (which however are the primary aims making this pilot study interesting in the first place). Many other aspects of its performance could (and maybe should) however also be studied[3]. The results presented should be a part of the readers' resources in the process of determining the feasibility, cost, duration and possible improvements of future larger-scale research about the potential of shaker excitation techniques [12].

The thesis is an empirical study for the optimization of sound field control methods

[2]See Appendix A.6 for specifications.

[3]For example durability, the cost compared to other transducers, ease of use, etc.

in the sense that the techniques that will be used for sound equalization of the sound field in the tank are already established in other fields of science. No documented research was however found about the use of the techniques in situations similar to the one presented in this thesis, why the collection of empirical data in this area of research would fill a knowledge gap in academic literature [13].

The combination of equalizing techniques (the empirical study) with shaker excitation techniques (the pilot study) makes sense since the system that the shaker will be used upon will modify the sound field produced in it so much that without the equalization, the performance of the shaker would be hard to determine in some aspects.

In this thesis, the spectrum and level are two separated aims where spectrum refers to the characteristic distribution of what is measured, but without specific demands on the level. "Level" is referring to the amplitude of what is measured without any specific demands on the distribution of what is measured. One part of the results should show that the implementation of a chosen methodology leads to a difference between a desired sound spectrum and a measured sound spectrum that is as small as possible. Another part of the results should show that the implementation of a chosen methodology leads to a produced level that is higher than a reference level. The reference sound level should be measured from a conventional source intended for the purpose of producing sound in water. The emphasis on the results regarding sound level should additionally be on low-frequency regions where the reference sound source is not able to produce levels that are sufficiently high[4]. Improvements are detected by comparing the produced sound field in the tank with the desired sound field on a before-and-after implemented methodology basis.

As for the relation between pressure and particle velocity, the instruments needed for physical underwater particle velocity measurements were not available. Therefore, theoretical results based on the expected pressure field are derived and analyzed in contrast to the results found in the literature.

1.4 Societal, Ethical and Ecological Aspects

This thesis is based on the premise that it will attract the interest of marine biologists or other researchers with the aim to find ways to better understand the effects of noise on marine animals. No animals were subjected to any tests in this project, but as declared, the findings in this thesis aim to be used in contexts where animals are involved in physical tests. It is expected that if the findings in this thesis are used in physical animal tests, these tests will be conducted taking any legal, ethical and ecological aspects and regulations into account. The sole long term ethical and ecological purpose of this thesis is to promote prosperity for marine animals and

[4]The ability to produce low frequency noise in water-filled tanks is generally hard, which will be shown in later chapters.

their respective ecosystems.

As for the ethical, societal aspects, the broad science of underwater acoustics might promote activities that are neither sustainable nor peaceful. Examples of these activities could be oil and gas prospecting, or military. These kinds of activities have historically been a large motivation for research and development in the field of underwater acoustics [14]. Any use of the findings in this thesis for unethical societal purposes are opposed by the author of this thesis.

2
Theory

2.1 Material Properties

The means of investigating the material properties of the aquarium are limited. A glass inner wall with the dimensions 0.35x0.15x0.05 m was taken away from the aquarium and weighted to 0.7 kg This gives an approximate density $\rho \approx 2.66{\cdot}10^3$ kg/m^3. The speed of sound for longitudinal waves is given by

$$c = \sqrt{\frac{1}{\rho}\frac{E(1-\mu)}{(1+\mu)(1-2\mu)}} \tag{2.1}$$

giving a speed of sound of roughly $c \approx 5.634 \cdot 10^3$ m/s [15]. The Young's modulus and Poisson's ratio are, from tables in literature [15], assumed to be $E = 70$ GPa and $\mu = 0.27$ respectively. The calculated speed of sound approximately lies in the same range as suggested in literature (for example [16], ch. 6), why normal glass material properties are assumed. As will be elucidated in Section 2.2, any shear and bending movement or stress in the glass walls are neglected for the case of modelling, and only longitudinal waves are considered. Shear movement will not be excited by the pressure waves and shear stress is not an issue in terms of sound transmission in this case [1]. Only the stress in normal direction towards the wall is considered and the flexural waves of the glass walls is accounted for in later equations.

Approximate properties of the media, as from tables in literature, and used in [1] (for example [17] ch. 9 or [16] ch. 6) will be used in this project and are found in Table 2.1 below.

Table 2.1: Approximate properties of the media

Material	**Density,** ρ kg/m^3	**Speed of Sound,** c m/s
Glass	2500	5600
Tap water	1000	1500
Air	1.225	340

The dimensions of the tank under study is found in Table 2.2 below.

Table 2.2: Dimensions of the aquarium

Dimensions	L_x m	L_y m	L_z m
Tank	1.5	0.37	0.45
Water depth			0.35
Wall and floor thickness			0.008

A further description of the tank under study is found in Section 3.5.5.4.

2.2 Modeling

An analytical model, as developed by [1], is used to describe the properties of a sound field in a water-filled tank. In this model, a volume of water inside a rectangular shaped glass tank with water-to-air boundary on top and water-to-glass-to-air boundaries on all other sides is considered. It includes the effects of the damping and phase shifts that take place in the sound field due to the boundaries in the aquarium as well as leakage into the surrounding air through elastic glass walls. The model is based on modal analysis, i.e., it uses the properties of the system to find the periods of vibrations at which the system naturally resonates (general description of modal analysis found in, for example [16], chapter 28). When an arbitrary number of modes is calculated for, a superposition of the modes provides the response of the system.

Using the equations presented in the following sections 2.2.1 to 2.2.8, with the same material parameters and geometries, as presented in [1], provides the same results as is found in [1], as expected (Figure 2.1 below). This is mentioned for two main reasons:

1. By reconstructing the findings in [1] in this thesis, reliability is given to the fact that that the methodology presented in [1], including numerous repeatedly executed detailed mathematical expressions, is interpreted and implemented correctly in this project.
2. The results presented in [1] is verified with physical measurements for various cases with different simple rectangular tanks, providing reliability to the results for ideal cases.

In the present context, an ideal case is a tank with walls and a floor of the same thickness, that are not reinforced in any way, and additionally, that are not supported in any way except at the interfaces between the walls and between the walls and the floor. The glass walls are thus modelled as simply supported plates. The tank at Chalmers that is used for the physical measurements in the present study does not represent an ideal case. This is because it is reinforced transversely with additional glass plates in various places, restraining the movement of the glass walls. Additionally, the tank at Chalmers is placed on soft foam pads on top of a concrete floor, which could create a physical boundary condition that differs from the modelled boundary condition. A closer description of the real tank under study, as well as photos, is found in Section 3.5.4. Even though the results provided from the

model will lack some validity for the case of the Chalmers aquarium, the overall characteristics in the modeled and in the measured sound fields are comparable[1], making the model a convenient tool for approximating and explaining the behaviour of the sound field within the tank.

For the convenience of the reader regarding reliability, below is a frequency response function (FRF), originally from [1], that is recalculated in this project and that turns out to be identical.

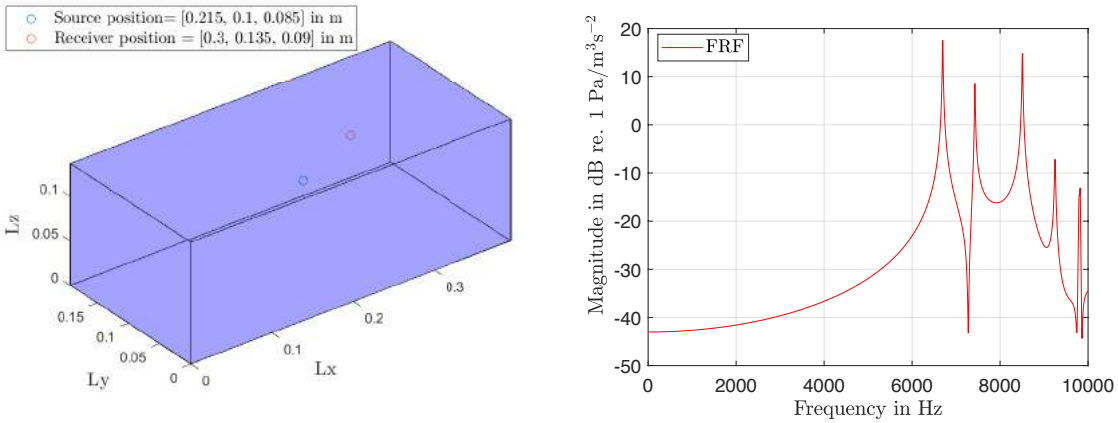

(a) Tank dimensions and source and receiver coordinates.

(b) Frequency Response Function.

Figure 2.1: Tank with parameters from [1].

If nothing else is clearly stated, the following Sections 2.2.1 to 2.2.8 is based on the theory of [1], that in turn is a further development of classical equations of acoustics. Additional literature sources are used as tools to communicate the basis for the equations.

2.2.1 Coordinates, Subscripts and Superscripts

In Figure 2.2 below, the coordinates used in the model are illustrated.

[1]This will be shown in Section 4.2.

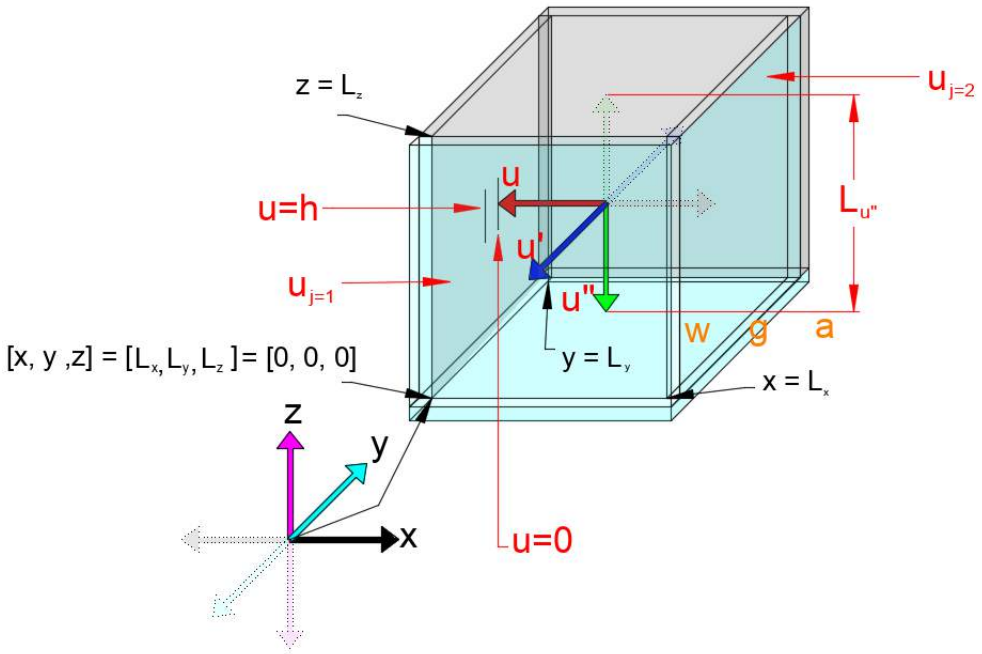

Figure 2.2: Coordinate system used in the model.

The superscripts (w), (g) and (a) seen in the above figure will be used in the equations to denote the media water, glass and air respectively. The symbols u, u' and u'' represents mutually orthogonal local axes that is pointing in normal direction towards either a wall, a floor or the water surface depending on what is calculated. For example, a modal wavenumber component $k_{m_u}^{(g)}$ will be calculated in Eq. 2.9, in which the superscript (g) will be referring to the medium glass, m is the mode $[m_x, m_y, m_z]$ and u means that the modal wavenumber component for the two walls perpendicular to the u-axis will be calculated. In Eq. 2.9 there is also a $L_{u'}$ and a $L_{u''}$ where $L_{u'}$ is the length of the side(s) of the tank that is perpendicular to the u'-axis and $L_{u''}$ is the length of the side(s) that is perpendicular to the u''-axis. If the u has an additional subscript 1 or 2, it means that one single side of the tank is calculated for, which is necessary for the case when the properties of one side of the tank is not the same as the properties for its parallel neighbour[2]. $u = 0$ denotes locations at the interface water-to-glass[3].

2.2.2 Characteristic Impedance

The characteristic impedance of the media for a longitudinal wave is the ratio of pressure to velocity, and can be expressed by

$$Z^{(w)} = \rho^{(w)}c^{(w)},\ Z^{(g)} = \rho^{(g)}c^{(g)},\ Z^{(a)} = \rho^{(a)}c^{(a)} \tag{2.2}$$

in Ns/m^3 [15]. These impedances will at a later stage (Eq. 2.12) represent the boundaries tendency to retain its state of rest when no force is acting upon it

[2]The surface of the water in the tank and the bottom of the tank.
[3]Or water-to-air at the surface of the water where there is no "glass roof".

(inertia) as well as its elastic properties. Additionally, but not directly used in deriving this analytical model, the reflection coefficient

$$r = \frac{Z^{(w)} - Z^{(a)}}{Z^{(w)} + Z^{(a)}} \tag{2.3}$$

shows that any airborne sound hardly will influence the sound field in the tank water, which will be discussed in further sections [18].

2.2.3 Early Approximation

The wave number k (in m^{-1}), being the spatial analog to the angular frequency $\omega = 2\pi f$, is expressed by

$$k^{(w)} = \frac{\omega}{c^{(w)}} \tag{2.4}$$

in water [15]. With L_x, L_y and L_z being the tank extent in x, y and z direction respectively, the modal wavenumber components can, as a first approximation be expressed as

$$k_{m_x}^{(w)} = \frac{m_x \pi}{L_x},\ k_{m_y}^{(w)} = \frac{m_y \pi}{L_y},\ k_{m_z}^{(w)} = \frac{m_z \pi}{L_z}, \qquad m_x, m_y, m_z = 1, 2, 3... \tag{2.5}$$

giving the modulus of the wavenumber (eigenvalue) in water as

$$k_m^{(w)} = \sqrt{(k_{m_x}^{(w)})^2 + (k_{m_y}^{(w)})^2 + (k_{m_z}^{(w)})^2} \tag{2.6}$$

As can be seen in Eq. 2.5, the indices m_x, m_y and m_z starts from 1 and not 0. Correspondingly, the minimum resonant frequency is expressed as the mode [1,1,1]. The index 0 is excluded, because a mode with such an index, for example mode $[1, 0, 1]$ will have an amplitude that is very low, and that will contribute very little to the resonances in the tank [1] [19].

From Eq. 2.5 an equation for the orthonormal (mutually orthogonal unit vectors [20]) eigenfunctions is expressed as

$$\psi_m^{(w)}(x, y, z) = A_m \sin(k_{m_x}^{(w)} x) \sin(k_{m_y}^{(w)} y) \sin(k_{m_z}^{(w)} z) \tag{2.7}$$

with $A_m = \sqrt{2^3/(L_x L_y L_z)}$ being a normalization factor. Note that when one or more of the $x, y, z = 0$ or $x = L_x$, $y = L_y$ or $z = L_z$ in Eq. 2.7, the total acoustic pressure at the wall becomes zero. Glass walls are easily bent by the sound pressure in water, causing close to acoustically "invisible" boundaries, and a close to zero sound pressure at the walls[4]. This boundary condition is called pressure release, or a "Dirichlet boundary condition" and is used as a first approximation to develop a more realistic boundary condition, i.e. one that includes damping, leakage, and a non-90° degree phase shift upon wall reflections. In a number of papers, [21], [22], [19] etc, this assumption of "acoustically soft" boundaries is seen as sufficient, and can

[4]The pressure release condition is also valid for the boundary water-to-air and, *"for most tanks"* ([5] Ch. 115) in addition valid for a water-to-tank-floor boundaries.

be used to calculate simplified FRFs between a source and a receiver through using Eq. 2.5 to 2.7 with Eq. 2.17 that is derived in a later section of this chapter (Section 2.2.5). The use of such a simplified FRF is evaluated briefly in Section 4.2.

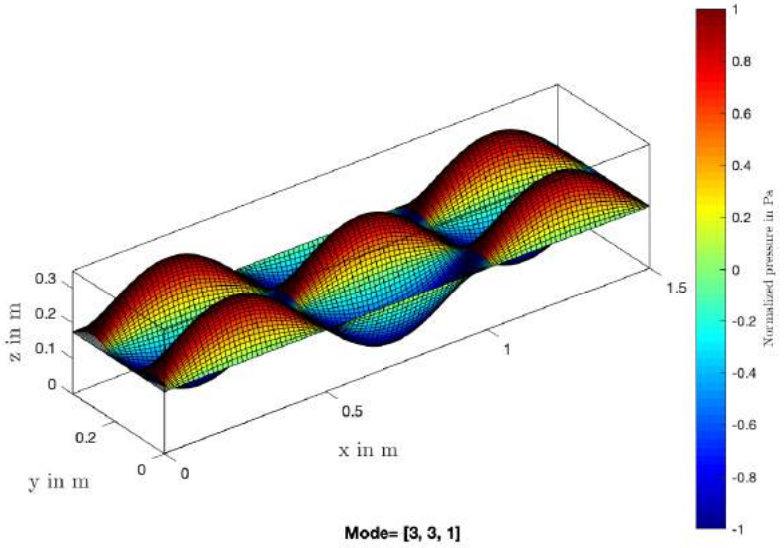

Figure 2.3: Orthonormal eigenfunction in the tank. Mode [3,3,1].

In Figure 2.3 above, the basic orthonormal eigenfunction for mode [3,3,1] is seen. It is calculated in MATLAB® through Eq. 2.6 for 75x75x75 points within the aquarium with the material properties given in Section 2.1. Note that the pressure at the boundaries u=0 is zero. Assuming this (simplified) boundary condition, it can be shown that the (non-zero) particle velocity is normal to each wall under consideration, and that the particle velocity that is parallel to the wall under consideration vanishes (similar tendencies will be shown later in Section 2.2.6, although for a more developed approach). Important to clarify for Figure 2.3 is that the wave is in fact longitudinal (compressional wave) and does not move transversely. The wave extending in z-direction in Figure 2.3 is only a graphical tool to represent the relative and normalized magnitude of the compression and decompression of the medium in the xy-plane, at height $L_z/2$ from the bottom of the tank.

2.2.4 Further Approximation

In Eq. 2.4 to 2.8, the simplified approach with a Dirichlet boundary condition has been used. The approximate properties of the media glass and air will further on be included. This will give boundary conditions ranging from Dirichlet (pressure release) to Neumann (zero velocity at the interface) boundary conditions. These mixed boundary conditions will include the dissipation of energy through the walls (absorption), small damping in the wall, and damping due to reflections at the walls.

The modal wavenumber in the wall and in the air can be expressed as a function of

the modal wave number in water (Eq. 2.5) through

$$k_m^{(g)} = \frac{c^{(w)}}{c^{(g)}} k_m^{(w)}(1 - i\delta), \quad k_m^{(a)} = \frac{c^{(w)}}{c^{(a)}} k_m^{(w)} \tag{2.8}$$

where $i\delta$ ($i = \sqrt{-1}$) represents a small, but not negligible, attenuation (damping) of the waves in the wall[5]. Since certain properties of the glass are unknown, this value is to be fitted within the ranges that are suggested in literature (in for example [23]).

The modal wavenumber component in the wall can, from Eq. 2.8 be obtained as in Eq 2.9 below.

$$k_{m_u}^{(g)} = -i\sqrt{-(k_m^{(g)})^2 + \left(\frac{m_{u'}\pi}{L_{u'}}\right)^2 + \left(\frac{m_{u''}\pi}{L_{u''}}\right)^2} \tag{2.9}$$

Similarly, the modal wavenumber component in air can be expressed as

$$k_{m_u}^{(a)} = -i\sqrt{-(k_m^{(a)})^2 + \left(\frac{m_{u'}\pi}{L_{u'}}\right)^2 + \left(\frac{m_{u''}\pi}{L_{u''}}\right)^2} \tag{2.10}$$

Equations 2.9 and 2.10 are calculated three times respectively[6]. A modal specific impedance at the walls can be expressed through

$$\zeta_u = \frac{\xi_{m_u}^{(a,w)} + \mathrm{i}\xi_{m_u}^{(g,w)} \tan\left(k_{m_u}^{(g)} h\right)}{1 + \xi_{m_u}^{(a,g)} \tan\left(k_{m_u}^{(g)} h\right)} \tag{2.11}$$

with

$$\xi_{m_u}^{(\alpha,\beta)} = \frac{Z^{(\alpha)}}{Z^{(\beta)}} \frac{k_{m_u}^{(\beta)}}{k_m^{(\beta)}} \frac{k_m^{(\alpha)}}{k_{m_u}^{(\alpha)}} \tag{2.12}$$

The $Z^{(\alpha)}$ and $Z^{(\beta)}$ in Eq 2.10 is calculated in Eq. 2.2. Subscript (α, β) is either (a, w), (g, w) or (a, g). Correspondingly, Eq. 2.12 must be calculated nine times: (α, β) for each of the three u-coordinates. Eq. 2.11 is calculated three times, while the interface glass to air at the top of the aquarium can be reduced to just

$$\zeta_{u_2} = \xi_u^{(\alpha=a,\beta=w)} \tag{2.13}$$

(giving a total of 4 different dimensionless ζ). In Eq 2.12, the "absorption" of energy through leakage though the walls is included, as well as its elastic and inertial properties (see Eq. 2.2). The modal wave number components in water (as calculated in Eq. 2.4) can now be reformulated as

$$k_{m_u}^{(w)} \cong \frac{m_u\pi + i(\zeta_{u_1} + \zeta_{u_2})}{L_u} \tag{2.14}$$

[5]The attenuation in water is however negligible.

[6]These three times are corresponding to the walls orthogonal to axes u, u' and u'', see Figure 2.2.

Then, the compensated complex expression (compare with Eq. 2.6) for the modal solution can be written as

$$\psi_m(x, y, z) = A_m \sin(k_{m_x} x - i\zeta_{x_1}) \sin(k_{m_y} y - i\zeta_{y_1}) \sin(k_{m_z} z - i\zeta_{z_1}) \tag{2.15}$$

From the above equation and onward, the superscripts (w), (g) and (a) will be omitted, since they no longer are needed to distinguish between the different media. Through computing Eq.2.15 for 75x75x75 equally spaced points with coordinates within the aquarium, and material properties as given in Section 2.1, Figure 2.4 below is produced.

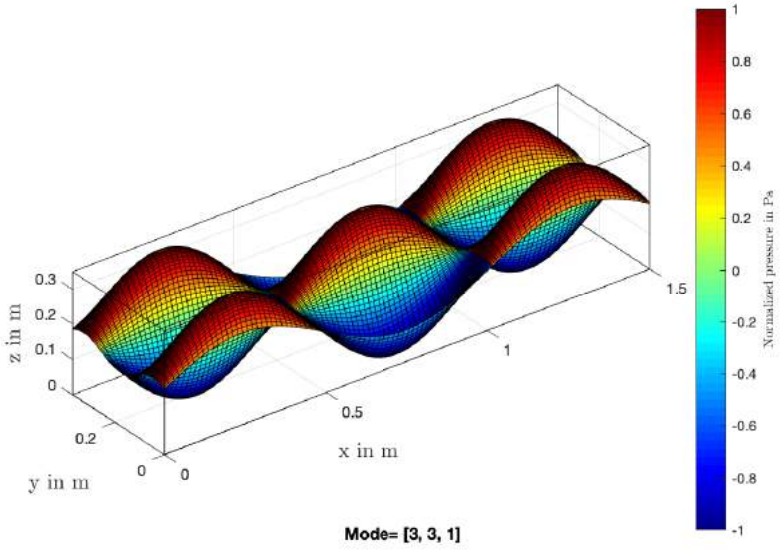

Figure 2.4: Real part of Eq. 2.15. Mode [3,3,1].

Figure 2.4 shows that the boundary condition in fact is not a Dirichlet boundary condition, but rather a mix of Neumann and Dirichlet boundary conditions. The pressure is however very close to zero at the corners of the aquarium, showing that the aquarium walls behave similar as to simply supported plates. Furthermore, if computing the solution for the acoustic pressure mode in time domain

$$p_m(x, y, z; t) = \psi_m(x, y, z) \mathrm{e}^{j\omega_m t} \tag{2.16}$$

the transient behaviour of the modal wave is seen and shown in Figure 2.5 below.

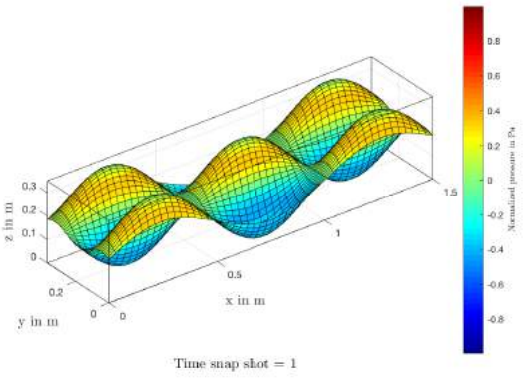

(a) Fisrt snap shot in time.

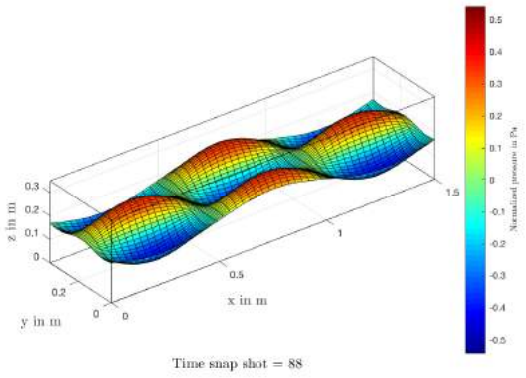

(b) Second snap shot in time.

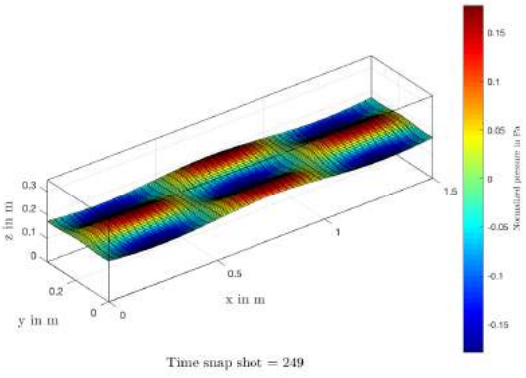

(c) Third snap shot in time.

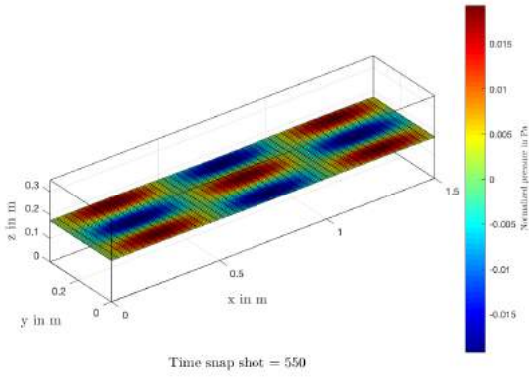

(d) Fourth snap shot in time.

Figure 2.5: Real part of Eq. 2.16. See video of the transient behaviour of the mode online on https://youtu.be/zaa6ZlAx1Sw.

It should be noted that Figure 2.5 represents one single mode [3, 3, 1], and that no sound source is taken into consideration. The figure only provides limited information about the behaviour of the sound field, and interpreting actual sound decay times in seconds from it is possible or the purpose here.

2.2.5 Modelled Frequency Response Function

Finally, the modal response (FRF) between a source with coordinates $[x_0, y_0, z_0]$ m and a receiver with coordinates $[x, y, z]$ m is given by

$$P(x, y, z; \omega) = \rho \frac{q}{V} \sum_{m=0}^{\infty} \frac{\psi_m(x_0, y_0, z_0)\psi_m(x, y, z)}{\Lambda_m(k_m^2 - k^2)} \tag{2.17}$$

in Pa, where q in $\mathrm{m^3 s^{-2}}$ is volume acceleration of an assumed point source at $[x_0, y_0, z_0]$ m and Λ_m is given by

$$V\Lambda_m = \iiint_V \psi_m(x, y, z)\psi_m^*(x, y, z)dV \tag{2.18}$$

The pressure FRF in dB is given as

$$\text{FRF} = 20\log_{10}\left(\left|P(x,y,z;\omega)\right|\right) \tag{2.19}$$

with the references dB re. 1 Pa/m^{3}s^{-2}. In simple words, this FRF indicates what pressure (in Pa) is going to be measured at the receiver position in the aquarium (at a hydrophone) if a small omnidirectional source[7] is producing a signal at the source position. This (noise) signal is assumed to have equal intensity at different frequencies[8]. Furthermore, ρ, q, V and Λ in Eq. 2.17 are all constants and could be neglected if the signal strength specifically is not of particular interest.

Eq. 2.4 to Eq. 2.17 is calculated for each mode between [1, 1, 1] and a number of modes that provides a steady FRF, i.e. one that changes only insignificantly when adding more modes. The number of modes providing a steady FRF was found experimentally to be around 16^3 ($m_{x,y,z} = 1, 2, 3, ..., 16$). In Figure 2.6 below, four different FRFs are calculated using different numbers of modes. Subfigure 3.13d shows a FRF calculated with 16^3 modes, which is what is going to be used further.

[7] This could in practice be approximated by a sound emitting hydrophone [1].
[8] I.e. a white noise, see for example [24].

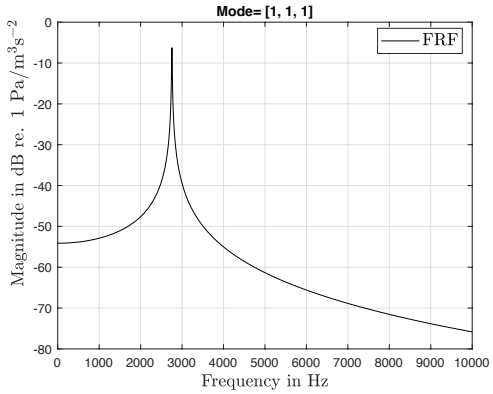

(a) Mode [1, 1, 1].

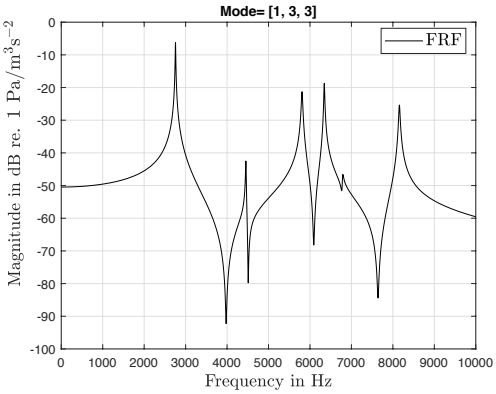

(b) Mode [1, 1, 1] to mode [1, 3, 3].

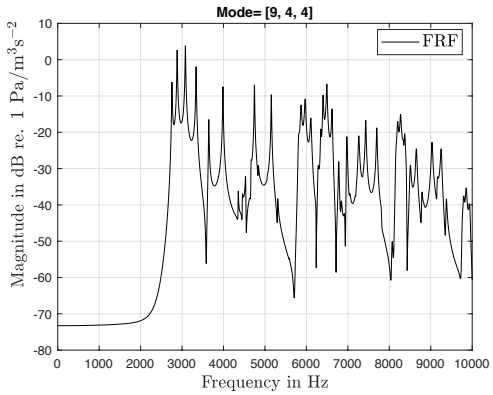

(c) Mode [1, 1, 1] to mode [9, 4, 4].

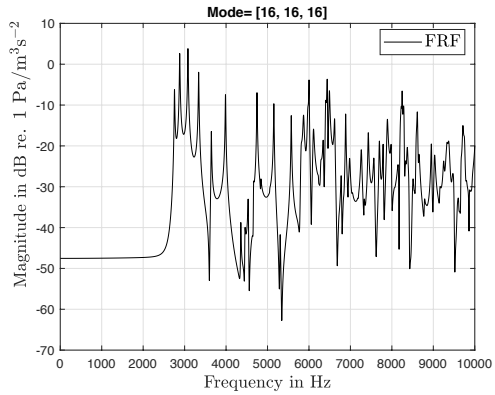

(d) Mode [1, 1, 1] to mode [16, 16, 16].

Figure 2.6: Addition of modes from one single mode (top left) [1, 1, 1] to all modes from [1, 1, 1] to [16, 16, 16] (bottom right) added. The impact of the number of modes calculated for can be seen online on: https://youtu.be/Pqi68TKIHnM.

2.2.6 Modelled Particle Velocity

Fish, and probably also most invertebrates, have hearing systems that are based on a sensitivity for a relative contribution of pressure *and* particle motion. The relation between these two quantities is only linear under certain circumstances and even if a researcher manages to produce a desired pressure field in a tank, the corresponding velocity field might still lack the desired properties [11]. In this section, the theoretical particle velocity field in the tank will be derived from the theoretical pressure results.

The relationship between sound pressure and particle velocity in the tank can described by the Euler's equation

$$\nabla P = -\rho \frac{\partial \vec{v}}{\partial t} \tag{2.20}$$

where P is pressure, ∇ is a 3D gradient operator[9] and ρ is the density of the water in this case (see, for example [18] and [1]). In the frequency domain, by calculating the gradient of a grid of equally spaced $P(x, y, z; \omega)$ (Eq. 2.17) with the MATLAB® function `gradient` [2] and normalizing with $\rho\omega$, so that $\vec{v}(x, y, z; \omega) = \nabla P/(\rho\omega)$, three components in x, y and z are obtained that are proportional to the particle velocity.

2.2.7 Graphical Presentation

In Figures 2.7 to 2.10, top left, the pressure field in the xy-plane at height $L_z/2$ in the aquarium is represented by the absolute value of the FRF calculated through Eq. 2.17. The FRF is calculated between a source with x, y, z coordinates = [0.2, 0.185, 0.175] m and a 3D-grid of 40x40x40 receiver positions with coordinates fitting within the boundaries of the aquarium. The frequency range calculated for is 1 Hz to 10 kHz with 5 Hz frequency steps (which provides reasonable computational speed), and the number of modes calculated for is 16x16x16. The field is normalized to have a dynamic range between 0 and 1 Pa, and so that regions of the field at height $L_z/2$ represents zero pressure and regions of the field at height $L_z = z$ represent maximum pressure (1 Pa).

At the top right, the corresponding particle velocity field is shown. It is obtained from the normalized gradient of the absolute value of the FRF between the source and receiver positions. The arrows represent velocity vectors with magnitude and direction proportional to the velocity within the aquarium in the xy-plane. Included in the velocity field plot is the contours of the absolute value of the velocity field. Both the velocity arrow and velocity contours are normalized to have a dynamic range between 0 and 1 m/s.

It should be pointed out that the pressure field and the velocity field in the two top plots respectively are normalized at each individual frequency calculated for. This means that the magnitude at different point in the field always will be relative to a maximum of 1 somewhere in the field at that particular frequency. This normalization was a compromise that was made because when normalizing to a single quantity-wise common value for the whole frequency range, hardly any spatial dynamics was seen in the plot for portions of the frequency range[10]. An alternative representation, with a common frequency independent medium-wise normalization value, will be demonstrated briefly at the end of this chapter.

The down left figure is the FRF in dB-scale between a source at position [0.2, 0.185, 0.175] m and a receiver at position [1.2, 0.185, 0.175] m. The location of the source and the receiver is marked with a blue and a red circle in the two top figures.

[9] For carthesian coordinates, $\nabla = \frac{\partial}{\partial x}i + \frac{\partial}{\partial y}j + \frac{\partial}{\partial z}k$ where i, j and k are standard unit vectors in the directions of the x, y and z coordinates respectively.

[10] i.e. the field could be all just deep blue or deep red at certain frequency ranges, while in fact some regions of the fields at that frequency range had normalized pressure or velocity values many times bigger or smaller than other regions of the field.

The downright figure is the corresponding velocity FRF in dB-scale. The velocity at position [1.2, 0.185, 0.175] is calculated from the root of the square of the velocity components in x, y and z-direction.

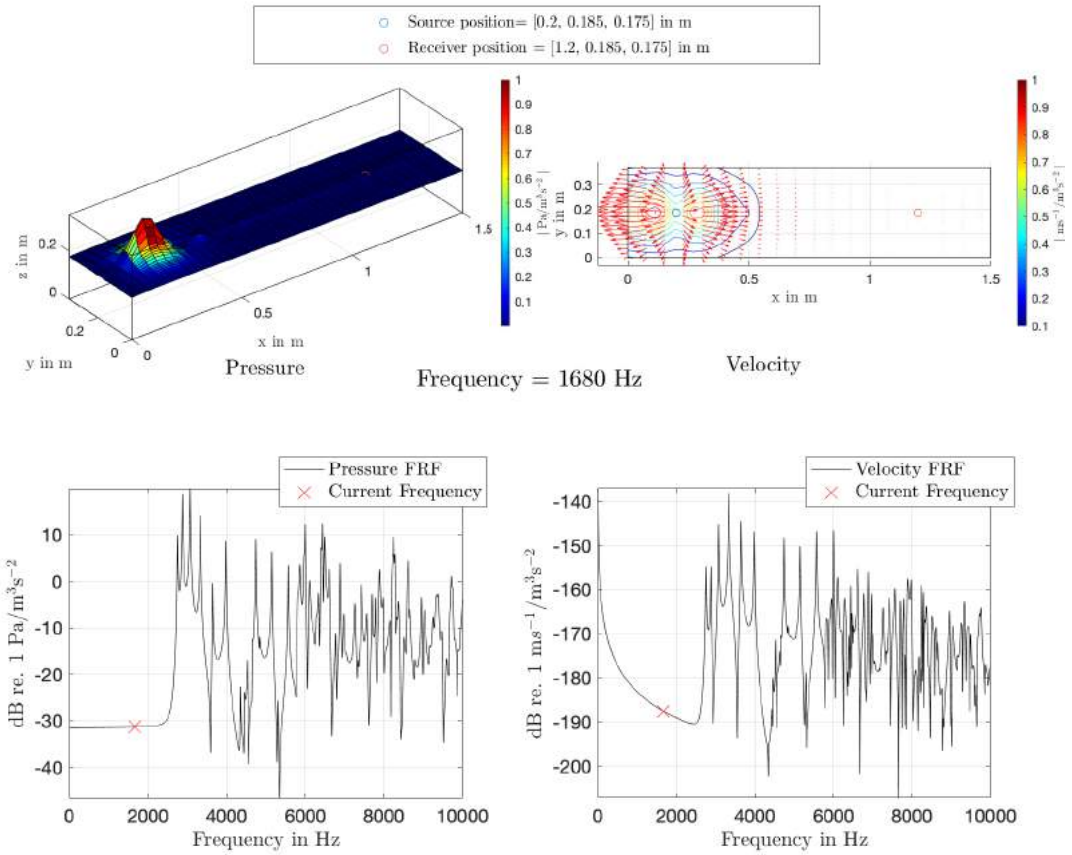

Figure 2.7: Response in aquarium at 1680 Hz, below the first eigenmode. From top left to down right: Pressure field, particle velocity, pressure at receiver and velocity at receiver. Dynamic plot can be seen online on https://youtu.be/d0seW5q0EC8.

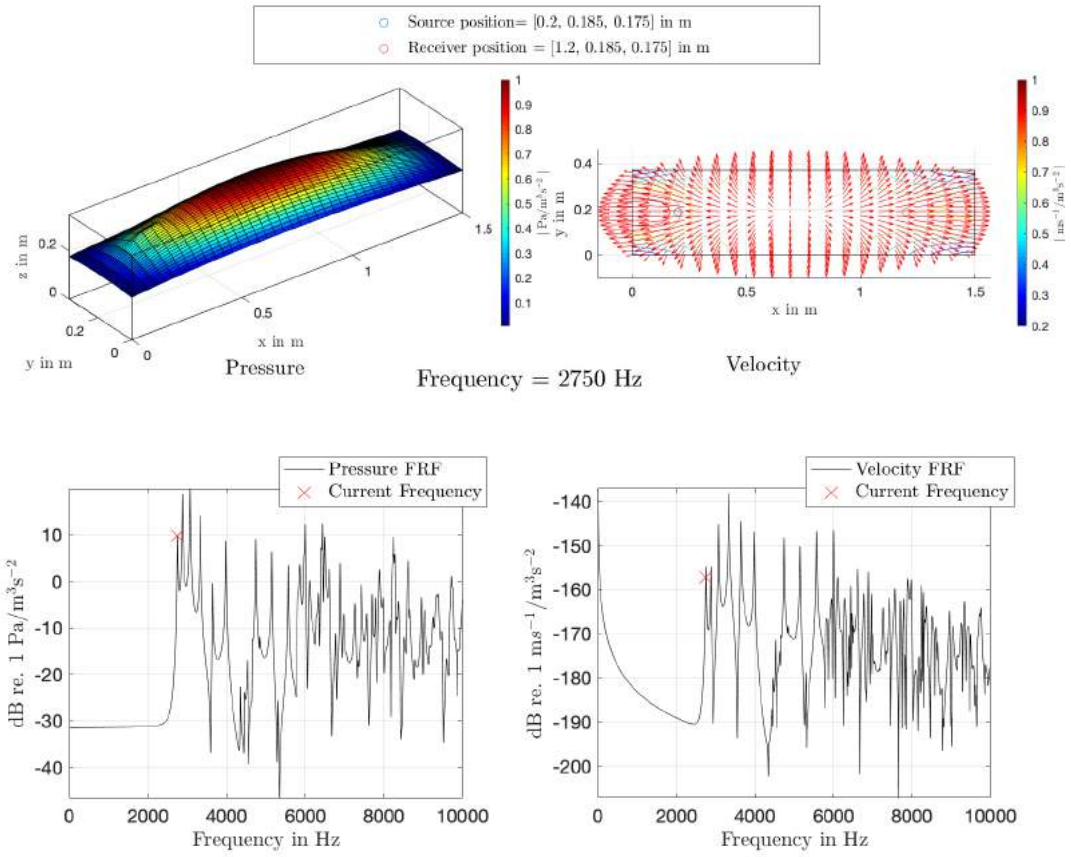

Figure 2.8: Response in aquarium at 2750 Hz. Close to the first eigenmode [1, 1, 1] From top left to down right: Pressure field, particle velocity, pressure at receiver and velocity at receiver. Dynamic plot can be seen online on https://youtu.be/d0seW5q0EC8.

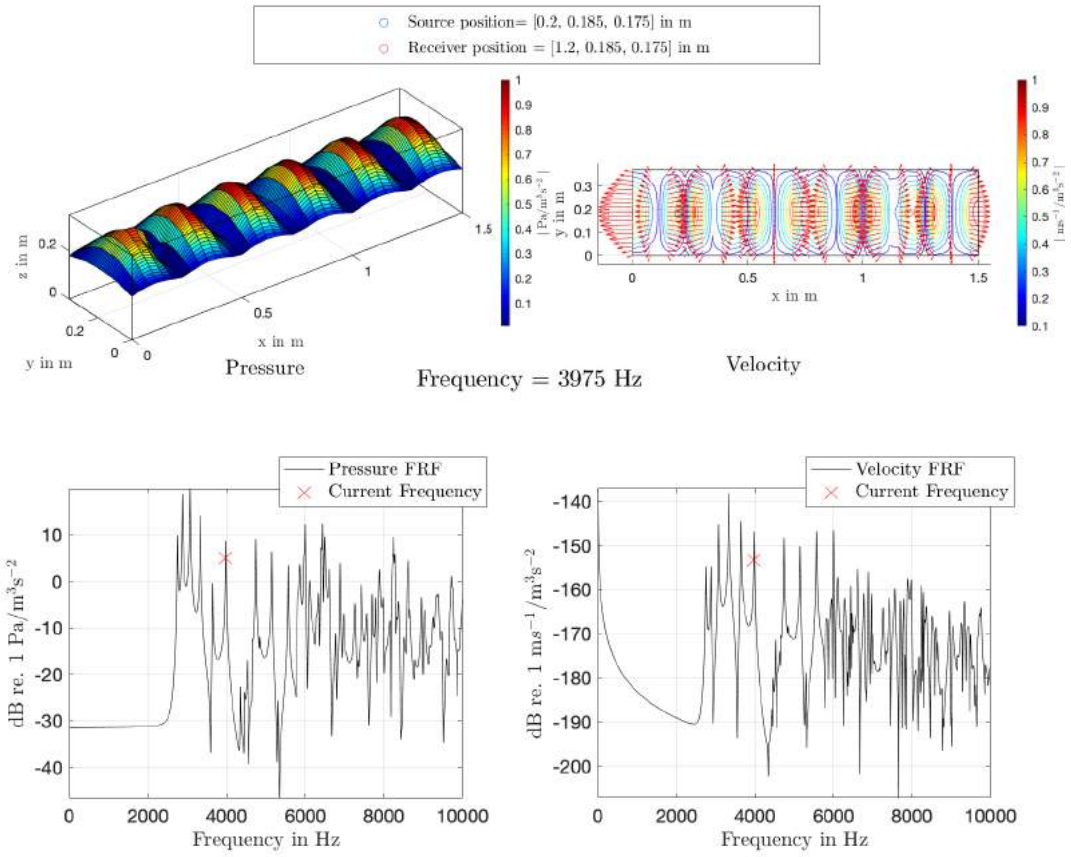

Figure 2.9: Response in aquarium at 3975 Hz. From top left to down right: Pressure field, particle velocity field, pressure at receiver and velocity at receiver. Dynamic plot can be seen online on https://youtu.be/d0seW5q0EC8.

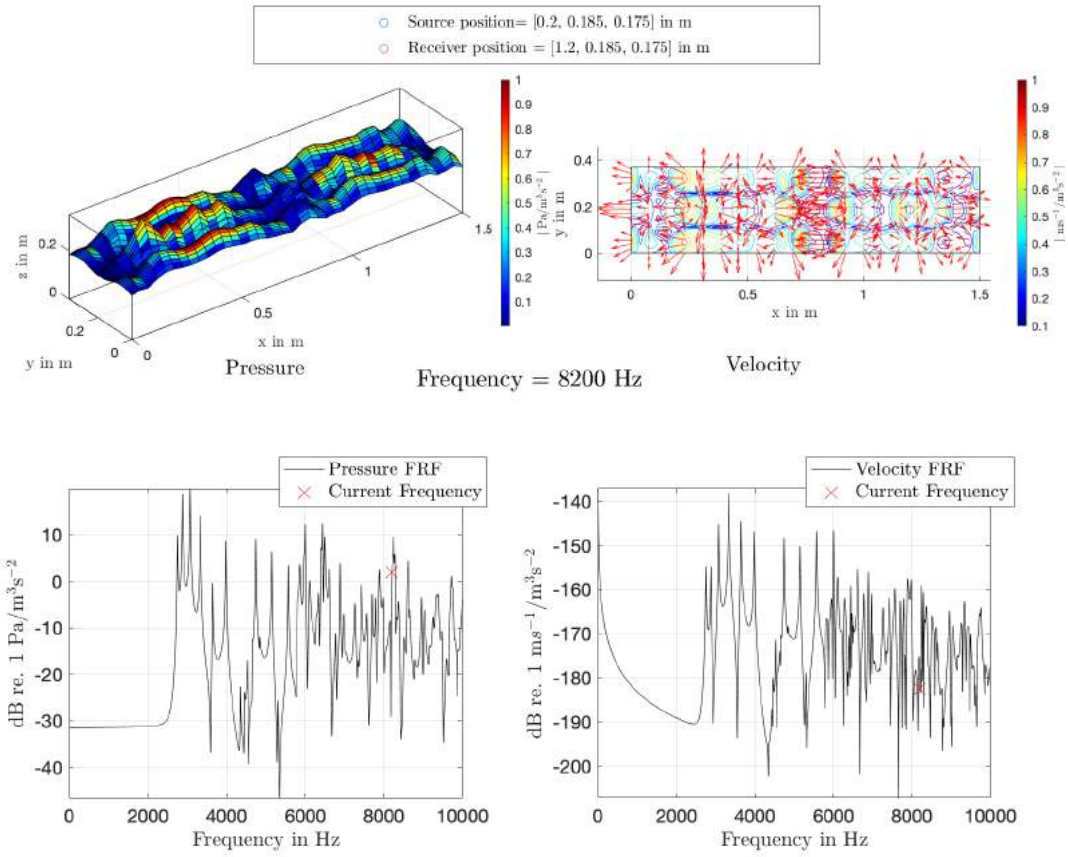

Figure 2.10: Response in aquarium at 8200 Hz. From top left to down right: Pressure field, particle velocity field, pressure at receiver and velocity at receiver. Dynamic plot can be seen online on https://youtu.be/d0seW5q0EC8.

In Figures 2.7 to 2.10 some features of the system can be distinguished:

- The boundary condition is not a Dirichlet boundary condition, but rather a mix of a Dirichlet boundary condition and a Neumann boundary condition. This can be seen from the non-zero pressure and movement of particles at the boundaries of the aquarium in Figures 2.7 to 2.10.
- In a free acoustic far-field, the particle velocity for a given sound pressure in a plane wave can be calculated in one direction as

$$\text{PVF} = \frac{\tilde{p}}{\rho c} \tag{2.21}$$

where PVF stands for far-field particle velocity in ms^{-1}, $\tilde{p}$ is the root mean square[11] pressure in Pa (ρc making up the characteristic impedance of water)

[11]The root mean square value of several values is calculated through

$$y_{\text{RMS}}(n) = \sqrt{\frac{1}{N}\sum_{n=1}^{N}|y_n|^2} \quad n = 1, ..., N \tag{2.22}$$

[25]. The field in the aquarium is, however, far from free because of the numerous wall reflections that cause negative and positive interference between emitted and reflected waves. A big part of the frequency range of interest also lies within the acoustic near-field of the sound source. In the near-field, the travelling wave cannot be considered plane, and Eq. 2.21 is not valid. Depending on the context, the approximate transition from near- to far-field varies, but one definition comparable with the situation in this study is found in [26] and states that in the far field, $kr >> 1$, where r is the distance from a source to a receiver. The ratio of particle velocity to pressure in the aquarium that corresponds to the two lower plots in Figure 2.7 to 2.10 is calculated to correspond to what is viewed in Figure 2.11 below:

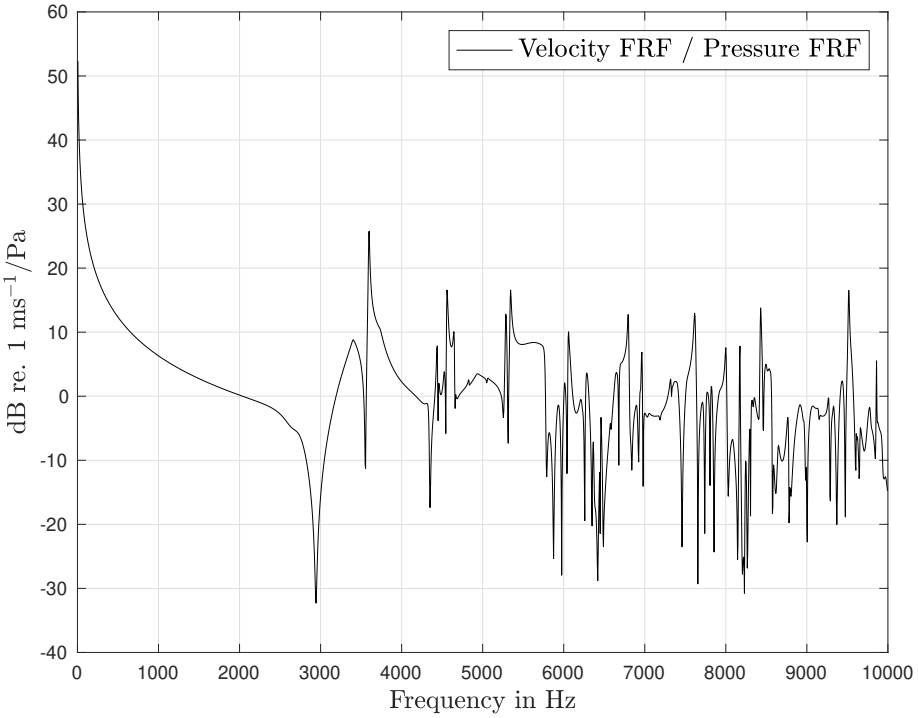

Figure 2.11: Ratio of the magnitude of the particle velocity to the sound pressure in the tank.

Similar observations (ratios of particle velocity to pressure) can be found in [21] and [11]. If the field in the tank was free and in the far-field, the ratio of particle velocity to pressure would just correspond to 1 according to Eq. 2.21 (a horizontal line at 0 dB re. 1 ms^{-1}/Pa in Figure 2.11) [11]. The effect of the near-field, excluding the reflections from the tank walls and the surface of the water would, for a point source, correspond to

$$PNF = \frac{\tilde{p}}{\rho c}\left(1 + \frac{i}{kr}\right) \tag{2.23}$$

Here, the near field contribution to the particle velocity is shown through the expression within the brackets, and thus it is understood that with increasing

distance r from the source or increasing frequency, the contribution to the particle velocity from the near field is decreasing, and the ratio of particle velocity to pressure is approaching 1 ms^{-1}/Pa [11]. This behaviour, the decreasing ratio of velocity to pressure with increasing frequency (distance of 1 m between source and receiver kept constant), can be seen in Figure 2.11 below approximately 2500 Hz. Because of the normalization at each frequency step in the velocity field at the top right plot in Figures 2.7 to 2.10, the information about the decreasing near field contribution as a function of increasing frequency is unfortunately lost. An alternative representation, where the field is normalized to a common value that is independent of frequency is found on https://youtu.be/5sVUeiSQUvk, with a screenshot of the video at 745 Hz in Figure 2.12 below.

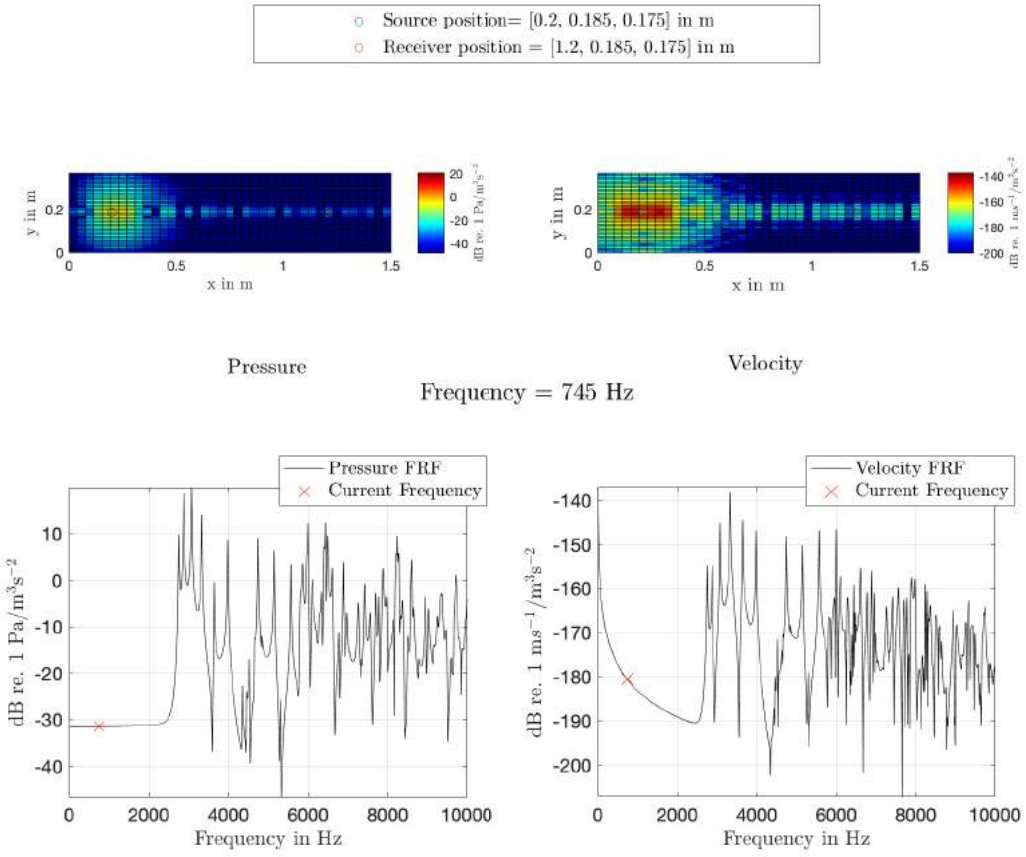

Figure 2.12: Response in aquarium at 745 Hz. From top left to down right: Pressure field, particle velocity field, pressure at receiver and velocity at receiver. Dynamic plot can be seen online on https://youtu.be/5sVUeiSQUvk.

The velocity field is here represented by the root of the square of the velocity components in x, y and z-direction. Additionally, in difference to in Figure 2.7 to 2.10, both the the pressure field and the velocity field is here in dB-scale.

- The tank has high-pass characteristics where sound above the first resonance frequency travels as normal modes, and sound below the first resonance fre-

quency (mode [1, 1, 1]) is attenuated very quickly. The reason for this is the Dirichlet boundary condition, where low-frequency pressure waves reaching the boundaries of the aquarium are reflected back with almost completely inverted phase, but with a still high amplitude [1]. A shortcut to approximate the lowest resonance frequency (the cutoff frequency) of a rectangular tank with acoustically soft boundaries (Dirichlet boundary conditions) is suggested by [21] and [22] among others, as:

$$f_0 = \frac{c}{2}\sqrt{\frac{1}{L_x^2} + \frac{1}{L_y^2} + \frac{1}{L_z^2}} \tag{2.24}$$

giving a lowest resonance frequency of 2992 Hz if inserting values from Table 2.1 and 2.2. This estimation gives a lowest resonance frequency that is around 242 Hz higher than the lowest resonance in Figure 2.8. Another estimate from [21] that is taking a rigid floor into account (acoustically hard boundary) is calculated as

$$f_0 = \frac{c}{2}\sqrt{\frac{1}{L_x^2} + \frac{1}{L_y^2} + \frac{1}{4L_z^2}} \tag{2.25}$$

giving a lowest resonance frequency of 2423 Hz. This places the resonance frequency calculated with Eq. 2.17 in between the estimates from Eq. 2.24 and Eq. 2.25.

- Comparing the FRF of the tank in Figure 2.1b from [1] with the FRF of the tank in this study, some differences in characteristics are noted
  - The first resonance frequency is lowered when the dimensions of the tank are increased.
  - The complexity of the FRF in the frequency range of interest increases as the lowest resonance frequency is decreased but is also affected by material parameters, boundary conditions and positions of the source and the receiver. A clear example of this is found in comparing the calculated FRF in Figure 2.1, with material properties and geometries from [1], with the FRF calculated for in this project, and displayed in 3.13d. The FRF for the tank under study in this project and for the chosen frequency range is much more complicated than the FRF for the tank in [1].

2.2.8 Validity of the Model

The tank under study in this thesis has irregular boundary conditions, more advanced than those of the tanks found in [1]. The field in the aquarium is dependent on the mechanical and acoustical properties of the tank boundaries, and each additional parameter that is taken into account results in advanced mathematical descriptions and greater computational efforts. (A closer description of the tank under study in this thesis is found in Section 3.5.5.4.) Additionally, the above model from [1] is considering a point source exciting the system. A hydrophone was tried out as a source to approximate the properties of a point source, but it proved to produce too low power to excite the present tank above the background noise levels. An underwater loudspeaker, lacking the characteristic properties of a point source, was

therefore used when comparisons to real laboratory measurements were made. The above model should thus only be used to understand the behaviour of the sound field in the tank from a qualitative standpoint, even though many qualitative similarities with the measured results remain, as will be shown in Section 4.2.

2.3 Choice of Measurement Parameters

The hearing range of fishes and invertebrates can be as high as at least 100 kHz ([27] p. 88) and as low as 0.1 Hz [28]. In a personal communication with this projects research institute client T. Johansson Aug 2020, it was pointed out that the animals that most likely would be subjected for tests in an aquarium of the dimensions used in this project, would have an effective hearing range primarily below 10 kHz. A sampling frequency, f_s, is therefore defined as $25.6 \cdot 10^3$ Hz for all measurements in this project. This sampling frequency is chosen to get alias-free results in the frequency range 0.3 Hz to 10 kHz in a way that will be explained later in Section 2.4.5. Duration of measurements is set to $T = 15$ s, at which it is seen that the averaging process has stabilized (see Section 2.4.4 below). The reference value for underwater sound pressure measurements is set to $p_{ref} = 1\mu$ Pa as is standard for underwater sound pressure measurements [16].

The choice of signal to send to the tank depends on the type of measurement carried out, i.e. measurements of single frequency tones, a wider frequency range, recorded sounds, etc. The signals that is used in this project are presented below:

- None
  - No input signal is chosen. Choice made for calibration or measurement of background noise.
- White Noise
  - Random signal having equal intensity at all frequencies. The signal has a constant power spectral density([16], ch.14). Created using the function found in Appendix B.1.
- Logarithmic sweep sine
  - Logarithmically increasing frequency and constant amplitude during a defined time period. Created using function found in Appendix B.2.
- Sine wave
  - Single frequency tone with constant amplitude, created using function in Appendix B.3.
- Audio file, for example, a field recording of sound in water.

2.4 Data Processing

From below Section 2.4.1 to Section 2.4.9, the MATLAB® code in Appendix B.4 was used to calculate the autospectra (Section 2.4.5), transfer functions (Section 2.4.6) and the coherence as well as SNR (Sections 2.4.8 and 2.4.9). This code provides equivalent results to the in-house software used and presented in Section 3.6.

2.4.1 Windowing

The blocks (vectors of measured data in digital format) are windowed to avoid spectral leakage (the phenomenon that the signal contents appear at different frequencies than it originally was ([16] Ch. 28)). This is done through a sample-wise multiplication of the block with a Hanning window, which is a widely used window function for general-purpose measurements [16] Ch. 15. the Hanning window being defined as

$$h(n) = \frac{1 - \cos(\frac{2\pi n}{N+1})}{2} \quad n = 1, ..., N, \tag{2.26}$$

in MATLAB® ([2], see `hanning`), where n is the sample number [3]. The windowed signal is normalized in order to conserve the power from before the windowing:

$$\sum_n |x(n)|^2 = \sum_n |x_{hw}(n)|^2 \tag{2.27}$$

x being the signal before the windowing and x_{hw} being the signal after windowing. The normalized Hanning window is calculated through

$$h_s(n) = \frac{h(n)}{\sqrt{\frac{\sum_n h(n)^2}{N}}} \tag{2.28}$$

A window length of 2^{13} is used for this project if nothing else is stated.

2.4.2 Fourier Transform

The blocks are transfered to the frequency domain through the Discrete Fourier Transform ([3] Ch. 8):

$$X(k) = \sum_{n=1}^{N} x_{hw}(n) e^{-j2\pi \frac{(k-1)(n-1)}{N}} \quad n = 1, ..., N \tag{2.29}$$

(as defined in MATLAB® ([2], see `fft`) k being the Fourier component number. The Fourier components are then scaled according to

$$X_s(k) = \frac{X(k)}{N_f} \tag{2.30}$$

N_f being the total number of frequency components in the block.

2.4.3 Double Sided and Single Sided Auto- and Cross-Spectra

Double sided auto-spectra of the signal sent to the system and the signal that is measured in the system ([3] Ch. 10) is calculated through

$$S_{xx}(k) = X_s(k) \cdot \overline{X_s(k)} \tag{2.31}$$

and

$$S_{yy}(k) = Y_s(k) \cdot \overline{Y_s(k)} \tag{2.32}$$

respectively. ($Y_s(k)$ is calculated in the same way as $X_s(k)$, but using the measured time domain signal $y(n)$ instead of $x(n)$). The overline over the last term in Eq. 2.31 and 2.32 denotes the complex conjugate.
Double sided cross spectrum of the signal sent to the system and the signal that is measured in the system is calculated in frequency domain through

$$S_{yx}(k) = Y_s(k) \cdot \overline{X_s(k)} \tag{2.33}$$

and

$$S_{xy}(k) = X_s(k) \cdot \overline{Y_s(k)} \tag{2.34}$$

respectively .

2.4.4 Averaging

The cross- and auto spectra are averaged block-wise to reduce the effects of random background noise through

$$AS_{xx}(n_b) = AS_{xx}(n_b - 1) - \frac{(AS_{xx}(n_b - 1) - S_{xx}(n_b))}{n_b} \qquad n_b = 2, ..., N_b \tag{2.35}$$

with $AS_{xx}(n_b = 1) = S_{xx}(n_b = 1)$

2.4.5 Singe Sided Auto - and Cross Spectra

The spectra are converted from double sided to single sided spectra through:

$$AG_{xx}(k = 1) = AS_{xx}(k = 1) \tag{2.36}$$

$$AG_{xx}(k) = 2 \cdot AS_{xx}(k) \qquad 1 < k < \frac{f_s}{2.56} \tag{2.37}$$

A division with 2.56 in the denominator in Eq. 2.37 is chosen to avoid aliasing in the sampled signal (sampling theorem [16] Ch. 14) as well as to avoid a region between 10 kHz and approximately 12.8 kHz where a lowpass transition region (magnitude goes from 1 to 0) occurs caused by lowpass filters in the measurement chain (both the B&K Type 2635 Charge Amplifier and the NI Type 9234, see Section 3.5.1). The single-sided auto spectrum contains the squared RMS-amplitudes and is used to present the measured data according to Eq. 2.38 below. The sound pressure level (SPL) measured at the hydrophone positions is presented as the magnitude of the auto spectra in dB-scale as

$$\mathrm{SPL}_{\mathrm{hydrophone}} = 10 \cdot \log_{10}\left(\frac{AG_{yy}(k)}{p_{ref}^2}\right) \tag{2.38}$$

The single sided auto spectrum (which, when is referred to in the text, should be thought of simply as the "sound pressure level, no fuzz") will in the future simply be termed auto spectrum.

2.4.6 Frequency Response Function

The frequency response function, FRF ((for example [16] Ch. 18)), is the relation between the input signal and the output signal and is calculated through

$$H_{yx,1}(k) = \frac{AG_{yx}(k)}{G_{xx}(k)} \tag{2.39}$$

and

$$H_{xy,2}(k) = \frac{AG_{yy}(k)}{AG_{xy}(k)} \tag{2.40}$$

If nothing else is stated, $H_{yx,1}$ will be used as FRF. This is because the noise in the system is assumed to be uncorrelated with the input signal, (Input signal is measured between item No. 18 and item No. 7 in Figure 3.3 in Section 3.5.4) and random noise in the output is removed through the averaging process of the cross spectrum (Eq. 2.35).

The frequency response function ($H_{yx,1}$) will be expressed in dB as

$$\mathrm{FRF}_{(\mathrm{dB})} = 20 \cdot \log_{10}\left(\left|H_{yx,1}(k)\right|\right) \tag{2.41}$$

with reference value given as 1 Pa/V.

2.4.7 Impulse Response

The impulse response (IR) of the system is calculated through the inverse Fourier transform ([3] Ch. 8)

$$\mathrm{IR} = \frac{1}{N}\sum_{k=1}^{N} H_{yx,1}(k)e^{j2\pi\frac{(k-1)(n-1)}{N}} \quad n = 1, ..., N \tag{2.42}$$

with $H_{yx,1}$ coming from Eq. 2.39.

2.4.8 Coherence

The coherence is used to express the quality of the measurements. It does so by displaying the rate of linearity between the input signal and the output signal on a scale from 0 to 1, where 1 indicates a completely linear relationship [29]. The coherence is defined as

$$\gamma^2_{xy}(k) = \frac{|AG_{xy}(k)|^2}{AG_{xx}(k)AG_{yy}(k)} \tag{2.43}$$

Low coherence can be caused by noise in the signal chain, which includes transducers, amplifiers and acquisition systems. Low signal-to-noise ratio[12] also causes low coherence, as well as noises, for example tapping against the glass tank in this case, which will be interesting later in this report.

[12] See Section 2.4.9 below.

2.4.9 Signal to Noise Ratio

The signal to noise ratio, SNR, is used to express the ratio of signal power to noise power. There are variations on how to calculate the signal-to-noise ratio, and the different variations can be used to present different content of related information. In Section 2.4.9.1 below, a SNR based on the coherence as calculated in Eq. 2.43 is presented. This SNR treats everything that is not coherently existing in the input and output of the system as noise. This SNR ($\text{SNR}_{\text{coherence}}$) will in this report primarily be used in relation to the transfer functions of the system. In Section 2.4.9.2, a SNR is calculated that is simply the difference between the measured background noise and the measured signal noise. This SNR ($\text{SNR}_{\text{subtract}}$) will primarily be used in relation to sound pressure level measurements.

2.4.9.1 Coherence-based SNR

Calculating the SNR in terms of the coherence [30] can be done as follows:

$$\text{SNR}_{\text{coherence}} = \frac{\gamma_{xy}^2(k)}{1 - \gamma_{xy}^2(k)} \tag{2.44}$$

The SNR is given in dB as

$$\text{SNR}_{\text{coherence,dB}}(k) = 10 \cdot \log_{10}(\text{SNR}) \tag{2.45}$$

2.4.9.2 Subtraction-based SNR

The subtraction-based SNR, is simply calculated through subtracting a measured background noise with no signal fed to the system $AG_{yy,\text{background}}(k)$, from the noise measured in the system with a signal fed to it $AG_{yy,\text{signal}}(k)$. In dB the $\text{SNR}_{\text{subtract}}$ is given as

$$\text{SNR}_{\text{subtract,dB}}(k) = 10 \cdot \log_{10}\left(\frac{AG_{yy,\text{signal}}(k)}{AG_{yy,\text{background}}(k)}\right) \tag{2.46}$$

2.4.10 Convolution

A convolution is a form of cross-merging of two signals. One signal is often in the form of an impulse response carrying the modifying properties of a system, and the other is an arbitrary signal [3]. The discrete-time convolution of two signals can, as defined in MATLAB® [2], be expressed as

$$w(k) = \sum_j \text{IR}(j)x(k - j + 1) \tag{2.47}$$

where j and k in this case is the index of the discrete time sample of an impulse response IR and a x.

2.5 Sound Field Equalization

As has been shown in Section 2.2, the response of the system will greatly affect the signal that is sent to it. With this said, any sound reproduced in the tank will be

far from the original sound. An original sound might, for example, be one that is recorded in the ocean (see later Section 3.5.2).

There exists a number of approaches to undo the undesired modifications caused to a signal from the system it is sent to (equalization). Common for these methods is that they, from a reasonable effort put into the task, only apply for discrete points or limited areas within the system [31]. Common for these methods is also that they are developed for sound fields in air. Two of these approaches that provided equalization algorithms giving desirable results are presented in the two following sections. Both of them take a starting point in the measured FRF of the system, see Section 2.4.6. The performance of the equalization algorithms are partly depending on high coherence in the measurements, see Section 2.4.8. If the measured FRF is wrong, which is indicated by low coherence, so will the equalization algorithm be.

2.5.1 Least Mean Square

The Least Mean Square (LMS) algorithm is a simple and robust adaptive filter [32] that is used in many contexts. In this project, the use of the LMS algorithm to equalize the signal sent to the system will be evaluated. Since there exists a vast knowledge on the subject of how to refine the performance of an LMS algorithm (in, for example, [32]), the use of it in this study will merely be to show its potential use in this particular application, and no further optimizations will be presented.
The basic LMS algorithm can be written as

$$w(n+1) = w(n) + \mu u(n)e(n) \tag{2.48}$$

where w is a weight vector that is adjusted to minimize the error e between the desired signal (the input signal x(n)) and a signal that is going to be equalized u(n)). μ is a step size that determines the stability and speed of the algorithm.

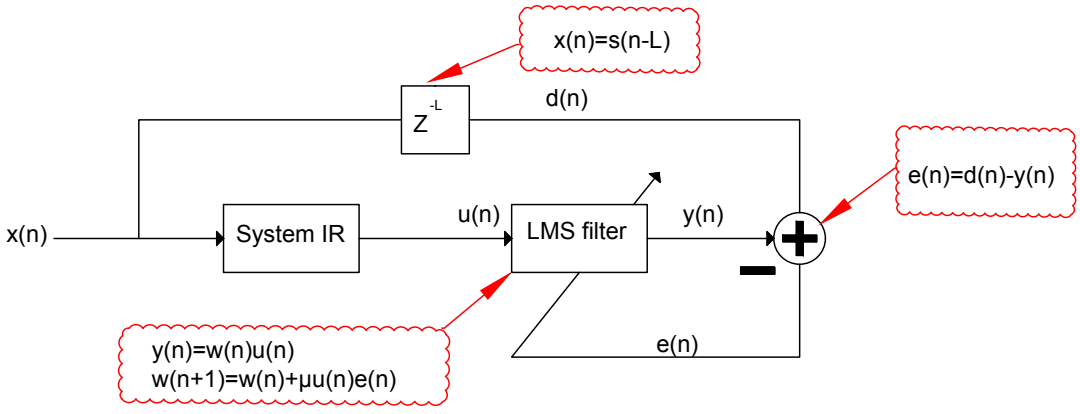

Figure 2.13: Block diagram showing the inverse signal modeling using an adaptive filter.

In Figure 2.13 above, a discrete time signal x is convolved with the system impulse response in the block "System IR", producing the new signal u. The same signal x

is delayed (i.e. zeros are added "in front of" the signal in MATLAB®, see Appendix B.6) with L samples in block $\mathrm{Z}^{-\mathrm{L}}$ and saved for a "later" calculation of the error e. u is filtered with w from Eq. 2.48 in block "LMS filter" through

$$y(n) = w^T(n)u(n) \tag{2.49}$$

where T denotes a transpose operation.
Finally, the error is calculated through

$$e(n) = d(n) - y(n) \tag{2.50}$$

whereafter the algorithm (block "LMS filter") is updated. After a certain number of iterations (loops in MATLAB®, see Appendix B.6), the error e minimizes to a range that is determined by the chosen step size μ and length of w, as well as delay L in the signal $d(n)$. The delayed version of $x(n)$, namely $d(n)$ is delayed to compensate for the overall propagation delay caused by the LMS filter, and from the system IR. The calculated weight vector w will in this project be used to filter the signal that is sent to the tank. The LMS algorithm code used in this thesis is found in Appendix B.6.

Below, the properties of the LMS filter is displayed using different settings. The case that the LMS filter is tested on is a $T = 1$ s, $f_s = 25.6$ kHz white noise created with the code provided in Appendix B.1, that is convolved with an arbitrary impulse response $h = [0.1,\ -0.4,\ 0.1,\ -20,\ 8,\ 1,\ -40,\ -2,\ 0,\ 1,\ 1,\ 1,\ -1]$ in MATLAB® using Eq. 2.47. Computing the FRF between the input signal and the result from the convolution with Eq. 2.4.6 results in the plot below:

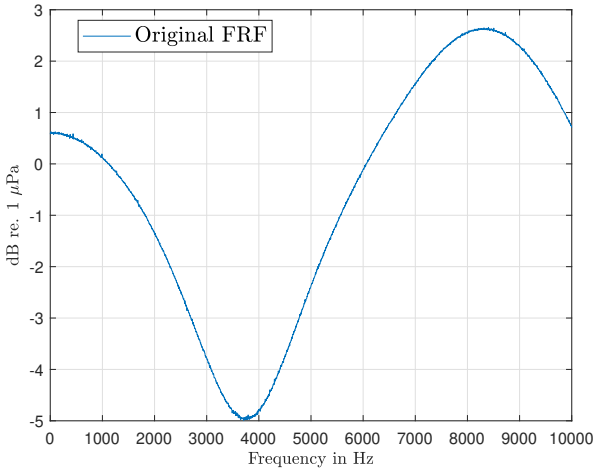

Figure 2.14: FRF between a $T = 1$ s, $f_s = 25.6$ kHz white noise and the product of a convolution between a white noise and an arbitrary impulse response $h = [0.1,\ -0.4,\ 0.1,\ -20,\ 8,\ 1,\ -40,\ -2,\ 0,\ 1,\ 1,\ 1,\ -1]$.

The frequency response plotted in Figure 2.14 above will in this theory section be seen as an unrealistically simple frequency response between a signal that is sent through a, for example, underwater loudspeaker and the signal that is recorded at a

hydrophone within the tank. The simplicity of the FRF will make it easier to trace the properties of the LMS filter.

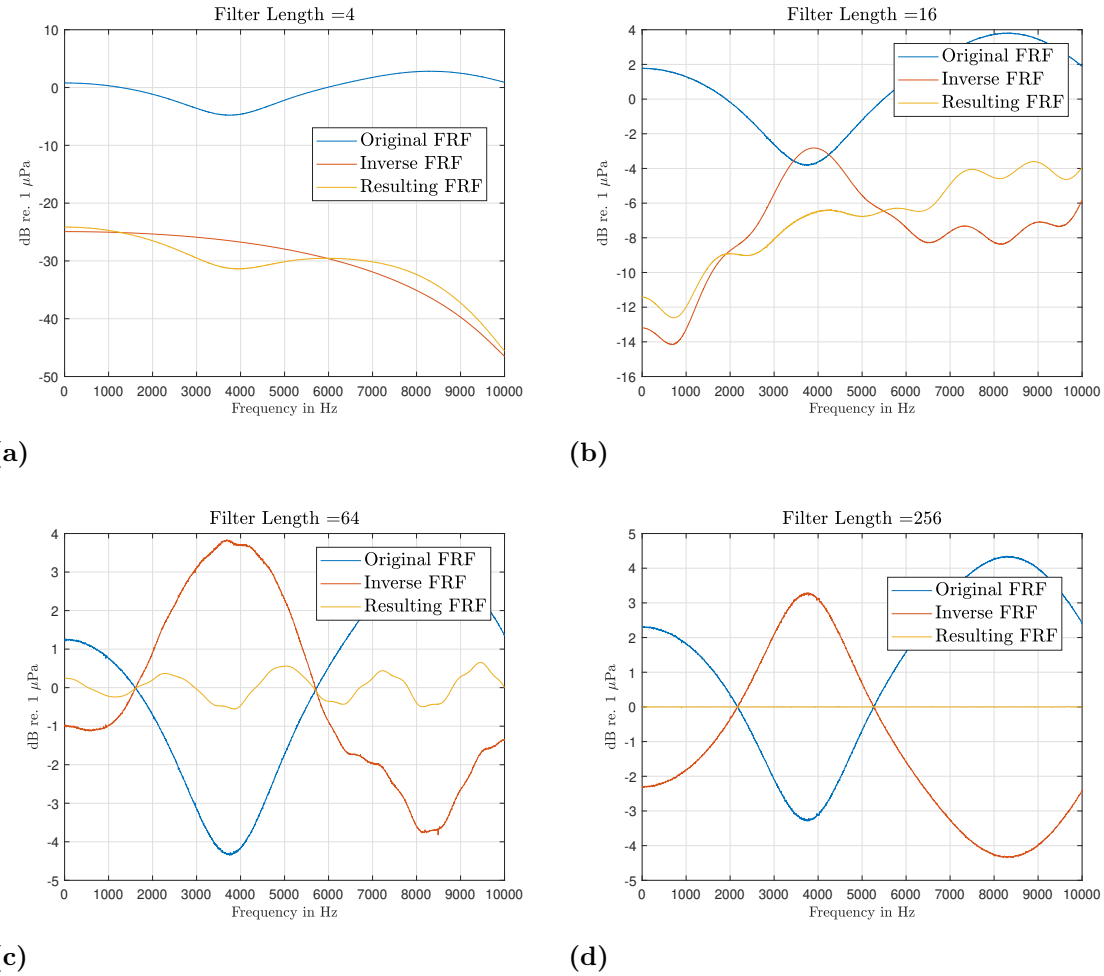

Figure 2.15: Blue curve: FRF between a $T = 1$ s, $f_s = 25.6$ kHz white noise and the product of a convolution between the white noise and an arbitrary IR $h = [0.1, -0.4, 0.1, -20, 8, 1, -40, -2, 0, 1, 1, 1, -1]$. Red curve: Inverse of the original FRF using an LMS algorithm. Yellow curve: The resulting FRF after convolution. Step size μ is 0.02.

In Figure 2.15 above, Subfigures 2.15a to 2.15d show the increasing performance of the LMS algorithm with increasing filter length and constant step size $\mu = 0.02$. When the filter length is 256 taps, as in Subfigure 2.15d, the inverse FRF looks very close to a mirror image of the original FRF, and the error value e has stabilized. The blue curve FRF is calculated between x and u, as explained in Section 2.4 with the settings manifested in the same section. The red curve is the inverse FRF. It is calculated through first convolving the delayed original signal d with w through Eq. 2.47, and then calculating the FRF between the result and d. The resulting FRF (yellow curve) is simply a multiplication between the original FRF and the inverse FRF. The error value e from Eq. 2.50 as a function of filter length is displayed in Figure 2.16 below:

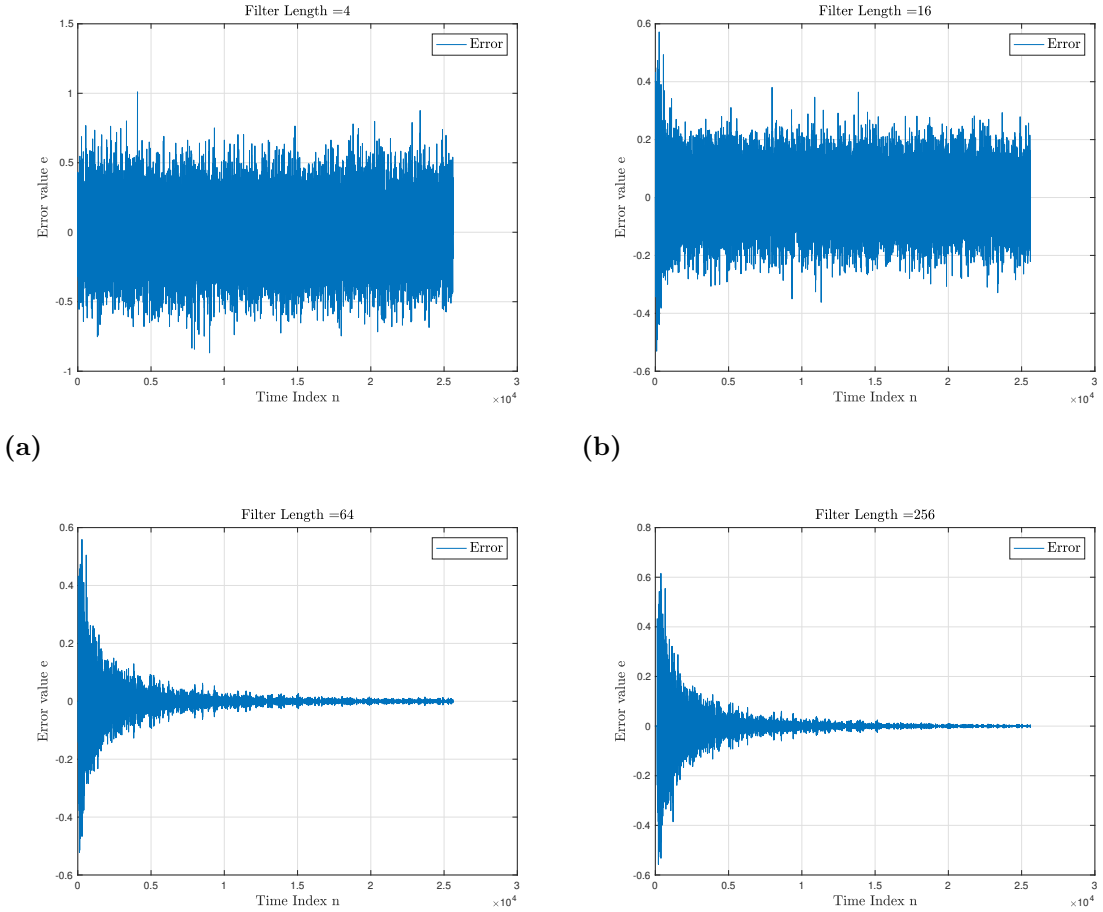

Figure 2.16: Effect on the error e of the LMS algorithm when increasing its length.

Figure 2.16 above can be seen as a first indication that a very complicated impulse response, like the one indicated by the complicated FRF in for example Figure 2.9, will require a long LMS filter. This statement is valid for the basic LMS approach as used in this thesis. The IR of the blue curve in Figure 2.16 is constituted of 13 coefficients. The strong resonances and antiresonances with narrow peaks and dips make the spotting of the w coefficients in the LMS algorithm statistically harder. In fact, even a very short impulse response that causes high amplitude narrow peaks or dips might be too much for the LMS algorithm to handle, as is shown in Figure 2.17 below.

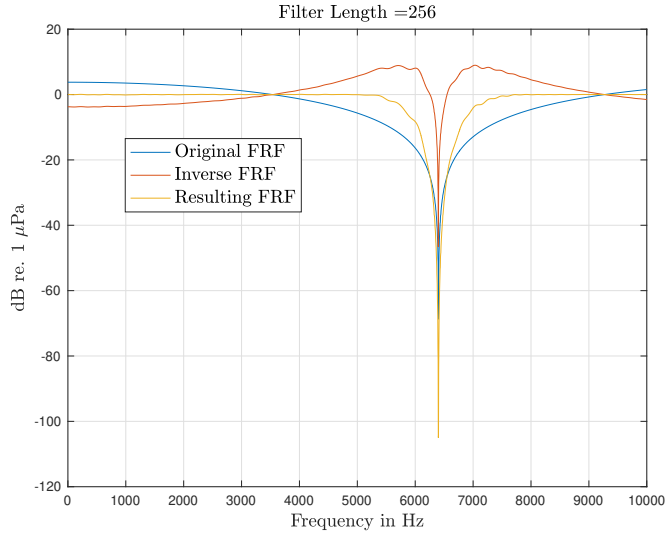

Figure 2.17: Blue curve: FRF between a $T = 1\text{s}, fs = 25.6\text{kHz}$ white noise and the product of a convolution between the white noise and an arbitrary IR h= [1 0 1]. Red curve: Inverse of the original FRF using an LMS algorithm. Yellow curve: The resulting FRF after convolution. Step size μ is 0.02 and filter length M=256 taps.

In Figure 2.17 above, the LMS calculation parameters are identical to those that produced the inverse FRF in Figure 2.15d, but the IR is now set to h = [1 0 1]. Results with varying choice of step size, keeping the filter length of 256 taps can be seen below:

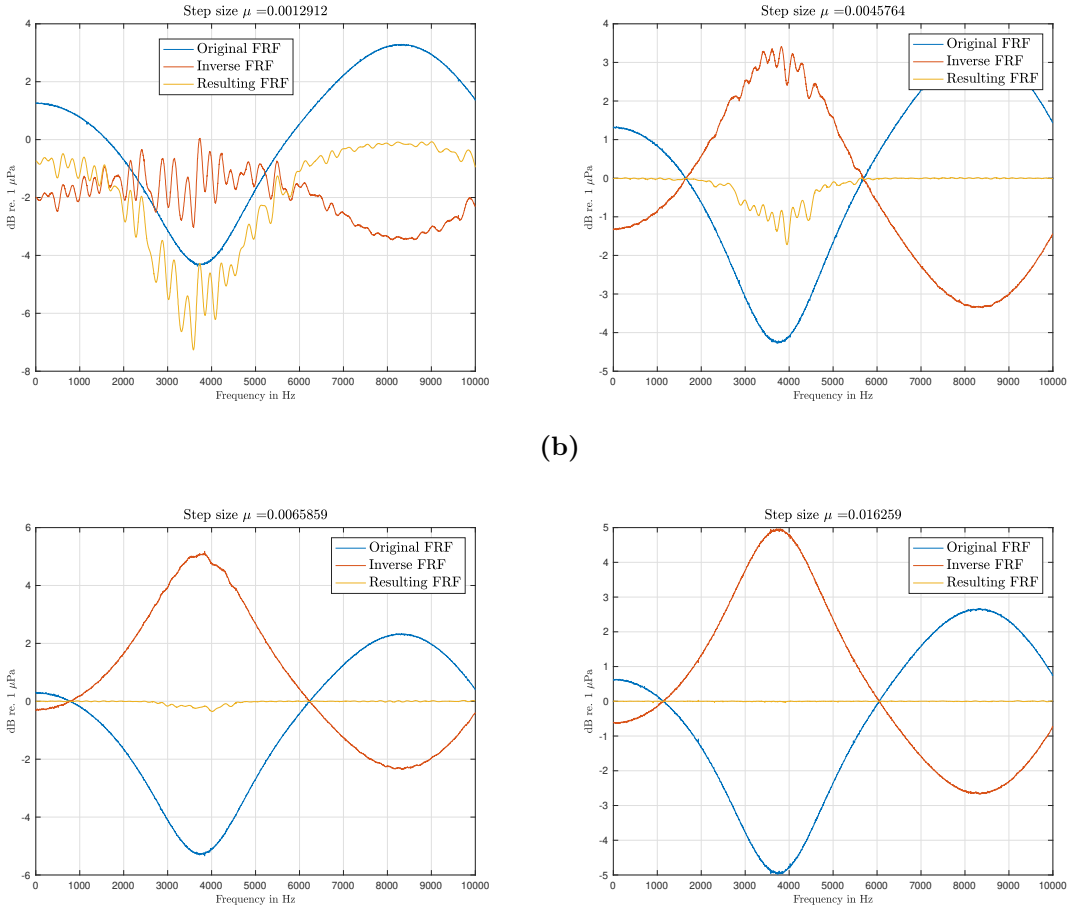

Figure 2.18: Effect of varying the step size. Filter length is 256.

Theoretical and actual results based on the measured IR of the physical tank can be seen in Section 4.3.
In the real test results that will be presented in Section 4.3 was obtained with the step size μ =0.0492 and the filter length $M = 1024$ taps, which was found experimentally to give satisfactory results.

2.5.2 Inverse Filtering with Regularization

Another way of equalizing the signal sent to the tank that is relying on the tanks measured impulse response is simply based on

$$H_{inv}(\omega) = \frac{1}{C(\omega)} \tag{2.51}$$

where $C(\omega)$ is the transfer function measured in the tank, and $H_{inv}(\omega)$ is its inverse [33].

However, this basic approach in finding the inverse filter would cause undesired side

effects, involving the requirement of a very large gain on high and low frequencies, why a "built-in" regularization is proposed:

$$H(\omega) = \frac{\overline{C(\omega)}}{|C(\omega)|^2 + \beta Rg(\omega)} \tag{2.52}$$

In Eq. 2.52 above, $\beta Rg(\omega)$ is a regularization factor [34] [35]. This regularization factor can in practice be calculated through defining a frequency range of interest between f_{low} and f_{high} where in between there is a passband region, and of which outside there is a stopband region. Before and after the passband region, a $f_{\text{low}}/3$ and a $f_{\text{high}}/3$ transition region will be allowed. A bandpass filter[13] R_{log}, is created as in Appendix B.7, with the appearance as in Figure 2.19 below.

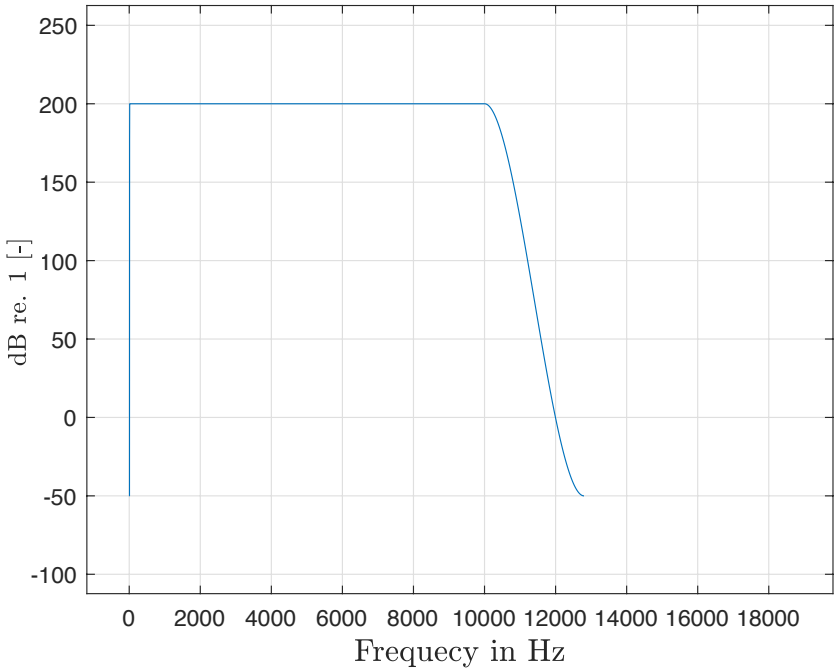

Figure 2.19: Bandpass filter appearance.

R_{log} is transferred from logarithmic to linear scale ($R = 10^{-R_{log}/20}$), flipped (note the minus sign before R in previous equation), made double sided[14] symmetrically around the Nyquist frequency and transferred to the time domain through an inverse Fourier transform (Eq. 2.42). This provides an IR, r, that is then shifted symmetrically towards the sample located at half the length of the IR, see Figure 2.20 below.

[13] A bandpass filter is a filter that is attenuating sound outside of a certain frequency range (and that is optionally, as in this project, amplifying the sound within the frequency range) [3].

[14] Double sided spectrum is required for the frequency domain, compare with Section 2.4.

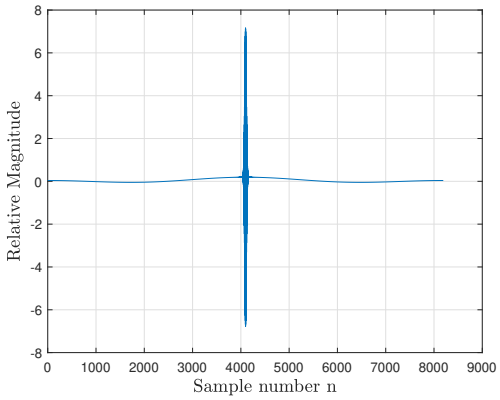

Figure 2.20: Bandpass filter in time domain, shifted symmetrically towards the sample located at half the length of the IR

The shift in time is performed to make the non-causal (requirement of future inputs [3]) part causal (output depends upon present and past inputs [3]). The r is then windowed with a Hanning window (See Section 2.4.1). The z-transform[15] of r, at this point, provides a pole-zero plot as in Figure 2.21 below.

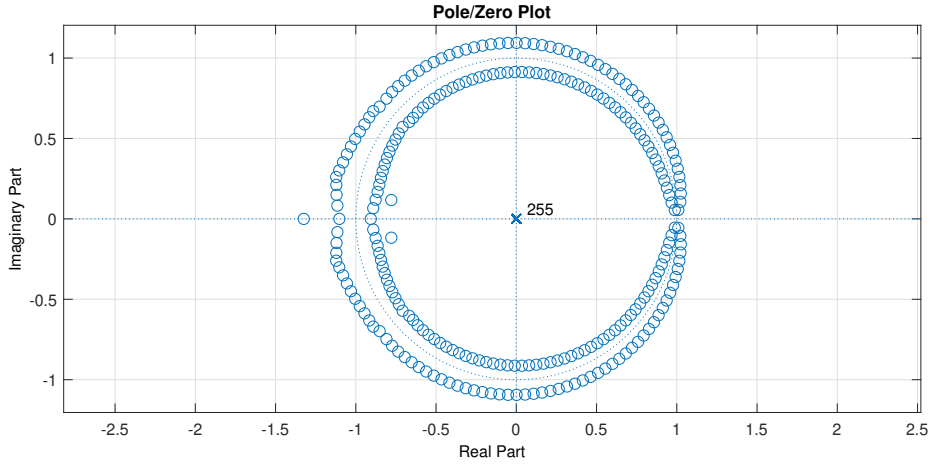

Figure 2.21: Pole-Zero plot from r. Plotted using the MATLAB® function `fvtool` (See [2] and [3]).

As the zeros not all are located within the unit circle in Figure 2.21, an unstable IIR is indicated (the poles are all located at 0 in this case). With unstable, it is for example meant that the output of the filter can get infinitely large. This unwanted filter characteristic is dealt with, in short, through "squeezing" the zeros within the unit circle with the MATLAB® function `rceps` (See [2], based on theory in [3]), resulting in the Pole-Zero plot as below:

[15]The z-transform is found probing the impulse response with sinusoids and exponentials to find the systems poles and zeros, where the roots of the poles and the zeros are the numerator and denominator polynomials of the r rational transfer function [36].

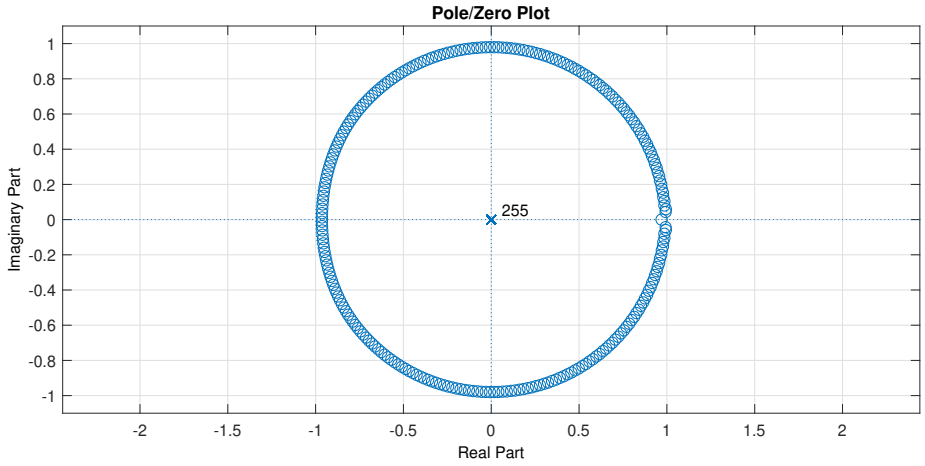

Figure 2.22: Pole/Zero plot from r after modification. Plotted using the MATLAB® function `fvtool` (See [2] and [3])

Finally, the IR r is transferred back to the frequency domain thorugh a Fourier transform as in Eq. 2.29 obtaining what in Eq. 2.52 would be referred to the regularization factor $\beta Rg(\omega)$. The result using this approach, with an impulse response h=[0.1 -0.4 0.1 -20 8 1 -40 -2 0 1 1 1 -1 1] convolved with a white noise, is displayed in Figure 2.23 below:

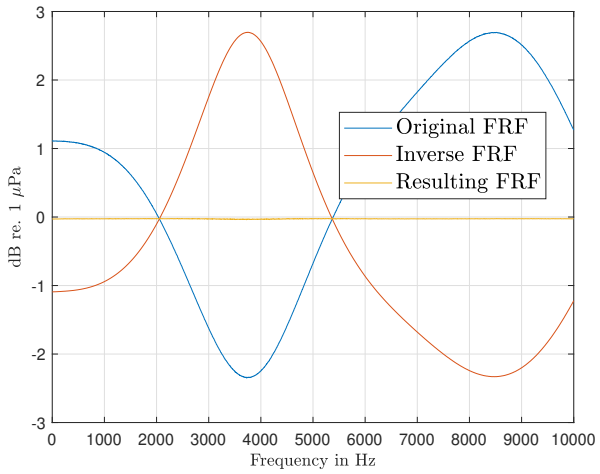

Figure 2.23: Blue curve: FRF between a $T = 1$ s, $f_s = 25.6$ kHz white noise and the product of a convolution between the white noise and an arbitrary IR $h = [0.1 \ -0.4 \ 0.1 \ -20 \ 8 \ 1 \ -40 \ -2 \ 0 \ 1 \ 1 \ 1 \ -1 \ 1]$. Red curve: Inverse of the original FRF using Eq. 2.52. Yellow curve: The resulting FRF after convolution.

The regularization in the passband region and in the stopband region will for the physical tests be 70 dB and -70 dB respectively and the length of the filter will be $n = 8192$ taps.

Theoretical and actual results based on the measured IR of the physical tank can

be seen in Section 4.3.2. The abbreviation IFR will furthermore be used instead of Inverse Filtering with Regularization.

2.6 Sound Pressure Levels in Water and in Air

Making a direct comparison between sound pressure levels in water and in air is not practical. Even though the same reference pressure of 1 μPa would be used for both air[16] and water when presenting measured sound pressure levels, the impedance of air and water differ. Because of this, the power flow in air and in water will differ, also in any cases where the measured pressure would be the same. Another impractical actuality is the difference between the atmospheric pressure in air compared to the hydrostatic pressure in water, etc. Additionally, the human hearing system loses many of the properties it has in air when it is used in water. This can also be linked to the higher impedance of water. Since the impedance of water lies within the same range as the impedance for human tissue, much of the sound perceived in water travels through the human tissue. The eardrum, which is evolved to pick up sound waves in air travelling through the ear canal, loses much of its function [38]).

2.7 Underwater Loudspeakers

The underwater loudspeaker used in this project is an electroacoustic moving-coil transducer that is designed to convert electrical energy into acoustic energy for under-water applications. Its difference from a loudspeaker for air applications is, among other things, that its membrane is stiffer, and therefore has an impedance that is better matching the impedance of water. Another feature of it is that when it is put into water, a compensation chamber is flooded which creates an internal air pressure that is equal to the water pressure that surrounds the speaker. The principles of its function was involuntarily examined as it broke down and had to be fixed. Its function is similar to that of the USRDJ9 transducer, which can be read more about in [4]. Figure 2.24 below contains an assembly drawing of the USRDJ9 transducer in Subfigure 2.24a, and the disassembled underwater loudspeaker used in this project in Subfigure 2.24b.

[16]Presenting sound pressure levels in air with a reference pressure of 1 μPa is not conventional. The sound pressure level in air is usually given with the reference pressure 20 μPa [37].

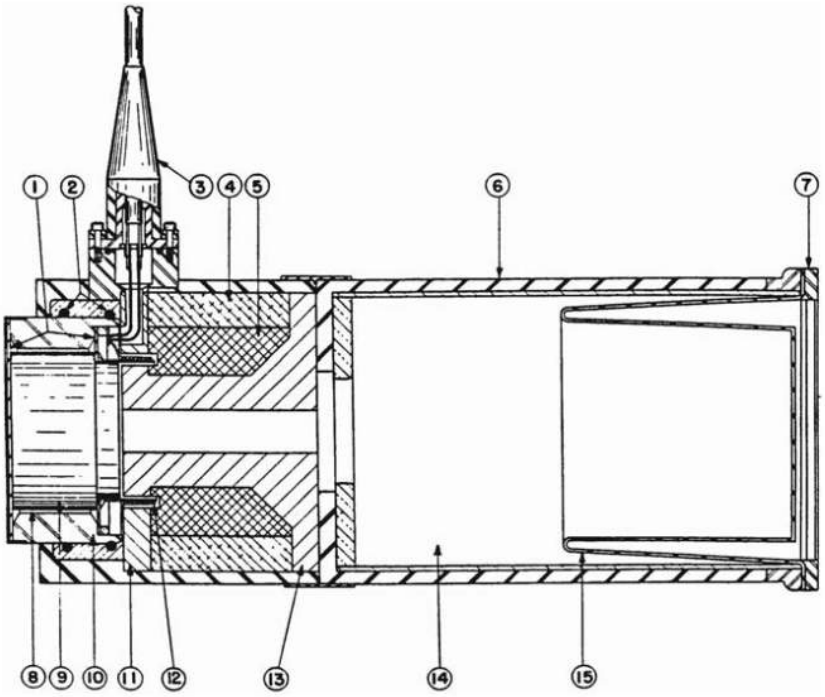

FIGURE 2.12. Assembly drawing of the USRD J9 transducer; 1, rubber seals; 2, rubber O-rings; 3, cable gland; 4, magnet; 5, lead; 6, rubber jacket; 7, grille; 8, slit filled with silicone oil response 9, magnesium diaphragm; 10, diaphragm housing; 11, front pole pieces; 12, coil; 13, back pole piece; 14, compensating air chamber; 15, rubber compensating bag. Overall length, 11 in.; diameter, 4-1/2 in. (adapted from Bobber, 1970).

(a)

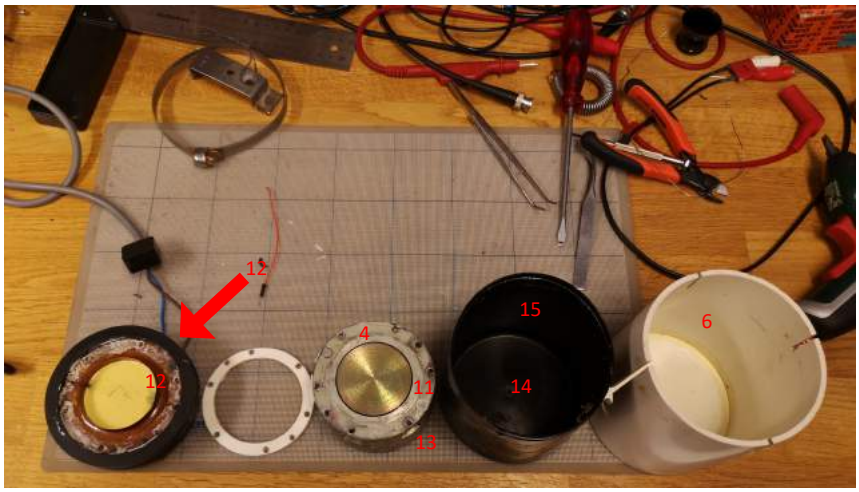

(b)

Figure 2.24: Subfigure 2.24a is an assembly drawing of a USRDJ9 transducer from [4]. Subfigure 2.24b is the disassembled underwater loudspeaker used in this project. The red numbers in Subfigure 2.24b indicates the corresponding numbered items in Subfigure 2.24a.

The similar features of the two transducer in Figure 2.24 above are pointed out by the numbers in the subfigures that are matched element wise. Some of the elements

that exists in the transducer depicted in the lower plot are not visible and their corresponding numbers are therefore not included in the figure.

Some general design aims for a loudspeaker membrane is that is should be stiff enough to avoid uncontrolled motions, have a low mass to allow as low as possible starting force demands and to store as little energy as possible. Additionally it should be well damped to prevent ringing effects [24]. In Section 2.8 below, the principles of a shaker, which is a form of transducer, will be introduced. A shaker does not have a loudspeaker membrane. Mounting the shaker stinger against the glass tank will make the glass tank itself a "substitute" for a membrane. Unfortunately, the design goals of an ideal loudspeaker membrane will through this application not be met, and lower coherence in the measurements than for the loudspeaker case is expected.

The underwater loudspeaker used in this project is further introduced in Section 3.5.5.2.

2.8 Shakers

The principles of the shaker used in this project, a permanent magnet electrodynamic shaker, resembles the principles of a common loudspeaker. Inside the shaker, as for a common loudspeaker, is a coil of wire that is suspended in a fixed radial magnetic field. When a current is passed through this coil, an axial force is induced in proportion to the current, and so on [39]. In difference to a common loudspeaker, the shaker is however designed for vibration testing, fatigue and resonance tests, and modal and structural analyse. As stated in the previous section, it does not have a loudspeaker membrane, but will induce vibrations directly into whatever structure the shaker stinger is mounted to. It is expected that the structure that the stinger is mounted to will not have the desired properties of a loudspeaker membrane, and that this will show up as lower coherence in the measurements.

The shaker used in this project is further introduced in Section 3.5.5.

2.9 Theory - the rest

This section will cover contrasting fields of theory that is not fitting in in other parts of Chapter 2 in any obvious way, but is necessary for the proceeding of the thesis.

2.9.1 Ground loops

A ground loop is resulting from a scenario when two points of a circuit have a different potential between them, but are meant to have the same ground reference potential between them ([40], p. 494). It is often a source of unwanted noise in measurements.

2.9.2 Butterworth Filter

A Butterworth filter is designed to have an as flat as possible frequency response in the passband. It is used to filter out signals below, and above two frequencies[17]. In between the two frequencies is the passband region (see [41] and the "butter" command in MATLAB® [2]).

2.9.3 The Difference Equation

A signal can be filtered using the difference equation

$$\begin{aligned} a(1)y(n) = b(1)x(n) + b(2)x(n-1) + ... + b(n_b+1)x(n-n_b) \\ -a(2)y(n-1) - ... - a(n_a+1)y(n-n_a) \end{aligned} \tag{2.53}$$

where y is the filtered signal, x is the unfiltered signal, b is the denominator coefficient, a is the numerator coefficient ($n_b = n_a$ and is the number of the 1,...,5 coefficients) [3]. The numerator and denominator coefficients could, for example, originate from the design of a Butterworth filter, described in Section 2.9.2 above.

2.9.4 Calibration

In the context of this project, a calibration procedure is carried out to obtain the correct relation between charge sensitivity in pC/Pa for the hydrophones, and voltage sensitivity in V/Pa for the microphones. A loaded sensitivity value is an overall sensitivity of the microphone and preamplifier combined. The microphones are calibrated with microphone calibrators, and the hydrophones are calibrated with a pistophone. A pistophone follows the principle of a piston that is mechanically driven to push at a fixed cyclic rate, moving a fixed volume of air to which the hydrophone under test is coupled. See the B&K Webpage for more information.

2.9.5 1/3rd Octave Bands

Some of the autospectra that will be presented in this report are summed in 1/3rd octave bands. The centre frequencies of these 1/3rd octave bands are $f_{\text{centre}} = [12.5, 16, 20, 25, 31.5, 40, 50, 63, 80, 100, 125, 160, 200, 250, 315, 400, 500, 630, 800, 1000, 1250, 1600, 2000, 2500, 3150, 4000, 5000, 6300, 8000, 10000]$ Hz as defined in [42]. The upper and the lower frequency limit of each 1/3rd octave band are calculated through

$$f_{\text{lower}} = f_{\text{centre}}/f_d \tag{2.54}$$

and

$$f_{\text{upper}} = f_{\text{centre}} \cdot f_d \tag{2.55}$$

where $f_d = 2^{1/6}$.

[17] A Butterworth filter can in fact also be used to filter out sound above, or below a certain frequency as well.

2.9.6 A-weighting

Sound spectra are often frequency weighted with something that is called A-weighting. The A-weighting is applied to some sound signals after they are measured and transferred to the frequency domain, so that the spectra they produce better will resemble how the human perceives the measured sound [37]. An A-weighted sound pressure level can be calculated through

$$\mathrm{LA} = \mathrm{SPL} + \mathrm{A}(f) \tag{2.56}$$

where $\mathrm{A}(f)$ is calculated through

$$\mathrm{A}(f) = 20\log_{10}(\mathrm{R_A}(f)) - 20\log_{10}(\mathrm{R_A}(1000)) \tag{2.57}$$

and $\mathrm{R_A}(f)$ is calculated through

$$\mathrm{R_A}(f) = \frac{12194^2 f^4}{(f^2 + 20.6^2)\sqrt{(f^2 + 107.7^2)(f^2 + 737.9^2)(f^2 + 12194^2)}} \tag{2.58}$$

The above equations give equivalent results to those obtained if using table values given in [43]. The SPL in Eq. 2.56 is calculated as in Eq. 2.38 but with the reference pressure chosen depending on if the measurement is for water or for air situations.

2.9.7 Equivalent A-weighted Sound Pressure Level

To get a single value representation of the perceived level of a sound that is measured over a period of time, an equivalent A-weighted sound pressure level can be calculated as

$$\mathrm{LAeq} = 10\log_{10}\left(\frac{1}{N}\sum_{k=1}^{N} 10^{LA_k/10}\right) \tag{2.59}$$

A-weighting, 1/3rd octave bands and equivalent sound pressure levels are of little significance in this thesis, since they most often are associated with sound pressure measurements undertaken in air, but it will briefly be used, why it is explaied here in the theory section.

3
Methods

3.1 Literature study

To accomplish the aims stated in Section 1.2, a comprehensive literature study was conducted, both before the start of the project and continuously during the project. Except of the literature that exists on the subject of underwater acoustics, previous experiments in the area of research have been carried through and are well documented. The literature study supported the development of a method, measurement procedure and setup, as well as provided the necessary theory about the physics associated with water as the medium for sound propagation. Much of the literature study was a repetition or expansion of knowledge gained at classes at the Chalmers Master's Program Sound and Vibration.

3.2 Modelling

From the literature study, an analytical modelling approach was identified, which is presented in previous Section 2.2. This analytical model provided information about what sound field characteristics could be expected in the tank. Furthermore, the theoretical transfer function of the system (the water filled tank, excited with a point source) that was obtained from the model, provided the basis for the development of digital filters used to equalize the sound field within the tank (see Section 2.5). The design of a digital filter was conducted utilizing the information found in literature.

3.3 Data Processing

The project required code to process and present collected physical data. The coding required for this thesis, including the code required for numerical modeling, was produced using the software MATLAB®. The theory behind the code is presented in Chapter 2. The code used to process and present the collected data sprung from knowledge gained at classes at the Chalmers Master's Program Sound and Vibration with additional support from literature. Exceptions regarding the last statement is for the real-time data acquisition part of the data processing, where an in-department developed MATLAB® program was used. For this part, trial and error methodology was deployed. This was since the program lacks documentation and the developers were unavailable.

3.4 Resources

Location for the physical measurements was at the Chalmers University of Technology. A tank (aquarium) was provided by IVL Swedish Environmental Research Institute. Some essential measurement equipment was provided by SSPA Sweden, and the rest was provided by Chalmers University of Technology. Christian Berner AB provided Sylomer® for vibration isolation purposes.

3.5 Measurement Setup

In this section, the equipment associated with the physical measurements will be presented. Section 3.5.1, 3.5.2 and 3.5.3 lists the instruments. In Section 3.5.4, a graph and several photos of the setup is presented, and the setup is explained.

3.5.1 Measurement Instruments

The instrument associated with the measurement of the sound in the aquarium are found in Table 3.1

Table 3.1: Measurement equipment.

Item no.	Instrument	Model	Use
1.	Hydrophone 1	B&K Type 8103	Underwater sound pressure measurement
2.	Hydrophone 2	B&K Type 8103	Underwater sound pressure measurement
3.	Microphone x 2	B&K Type 4133 B&K Type 4166	Air sound pressure measurement
4.	Charge Conditioning Amplifier 1	B&K Type 2635	Filter and amplify signal from Hydrophone 1
5.	Charge Conditioning Amplifier 2	B&K Type 2635	Filter and amplify signal from Hydrophone 2
6.	Pre-amplifier	B&K Type 2669	Amplify signal from microphone
7.	Signal Conditioner	B&K Type 1708	Condition signal from microphone by applying gains and filters
8.	Signal Acquisition Module	NI Type 9234	ADC
9.	Hydrophone Calibrator	B&K Type 4229	Calibration of hydrophones
10.	Microphone Calibrator	B&K Type 4231	Calibration of microphone

Hydrophone 1, Hydrophone 2, the Microphones, the Hydrophone Calibrator and the Microphone Calibrator in Table 3.1 comes with the calibration charts that is found in Appenix A.

3.5.2 Signal Generation

The instruments associated with the signal generation is found in Table 3.2 below:

Table 3.2: Signal generation equipment.

Item no.	Instrument	Model	Use
11.	Shaker 1	B&K LDS Type V406	Sound source
12.	Shaker 2	B&K LDS Type V406	Sound source
13.	Power Amplifier 1	LDS Type PA100E	Driving shaker 1
14.	Power Amplifier 2	LDS Type PA100E	Driving shaker 2
15.	Underwater Loudspeaker	G&W Type UW60	Sound source
16.	Stereo Amplifier	NAD 3020	Driving underwater loudspeaker
17.	Matlab	R2017b	Signal generation and data acquisition
18.	External Sound Card	Focusrite Scarlett 2i2	Outputs audio signal
19.	Amplifier	B&K Type 2735	Driving the Loudspeaker
20.	OmniSource Loudspeaker	B&K Type 4295	Sound source

The signals sent to the tank has been further introduced in Section 2.3. In addition to these signals, three field recordings are used to verify the performance of the transducer in use, as well as the equalizing process. The measurement location is Gåsö in Sweden, position 58,23458 degrees N, 11,4146 degrees O as shown in Figure 3.1 below.

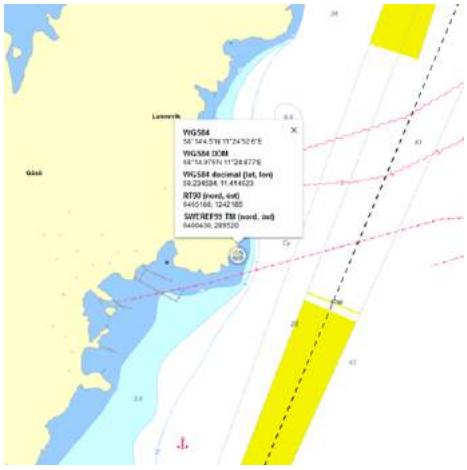

Figure 3.1: Measurement location for the field recordings.

The date for the recording is 11 augusti 2016. The water temperature was 16°C, wave height of 40-60 cm, south west wind of 5-6 m/s with gusts of wind reaching 10 m/s. No precipitation and blue skies.

The sound of two motor boats with the work names "Motorbåt" and "Miami Vice", see Figure 3.2 below, was recorded.

(a) "Motorbåt".

(b) "Miami Vice".

Figure 3.2: Photos of the two motor boats whose sound was recorded.

The recordings were made at a distance of 155 m between the hydrophone and the "Motorbåt" (Subfigure 3.2a), and at a distance of 216 m between the hydrophone and the "Miami Vice" (Subfigure 3.2b). The hydrophone was located 4 m below sea level. Settings for the recording (wav-format) was a sampling frequency of 96 kHz and a highpass filter of 3 Hz. The recordings were re-sampled to 25.6 kHz for the case of this project, using the MATLAB® function `resample` (See MATLAB® documentation [2] and [3]). One additional background noise recording was made when no boats were in sight. The sounds are presented further before, and after implemented equalization in Section 4.4.

3.5.3 Miscellaneous

Other equipment used is listed in Table 3.3 below:

Table 3.3: Miscellaneous equipment.

Item no.	Device	Use
21.	Tank	Carry the water
22.	Metal Frame 1	Holding the hydrophones
23.	Metal Frame 2	Holding the underwater loudspeaker
24.	Plastic tubes x 6	Mounted on Metal Frame 1 on fixed positions
25.	Strap x 2	Keeping the shakers at place
26.	Sylomer®	Vibration isolation
27.	Foam Pads	Protect the tank from uneven ground surfaces

3.5.4 Setup graphs and photos

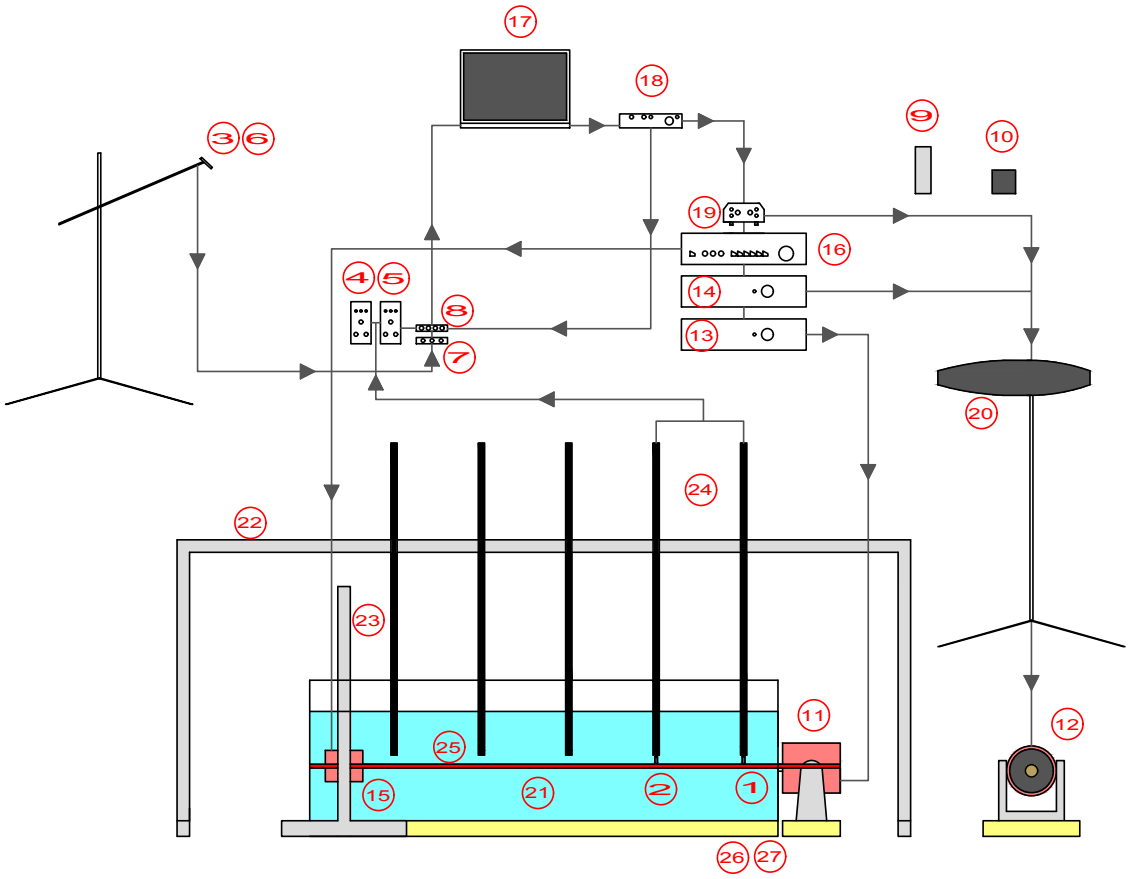

Figure 3.3: Setup graph. Encircled numbers represents the item numbers in Table 3.1, 3.2 and 3.3.

The components in Figure 3.3 are not accurately scaled. Figure 3.3 is for communicating the measurement setup only.

(a) Shaker 1. Newtonmeter shows a pre stress of approximately 42 N.

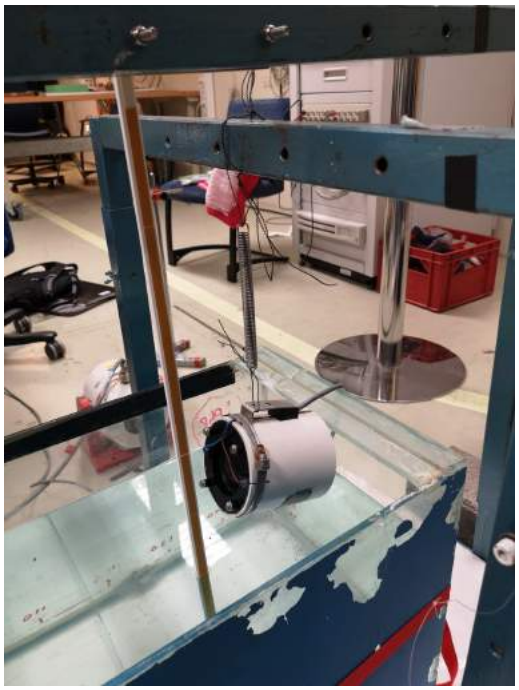

(b) Raised underwater loudspeaker mounted on metal stand.

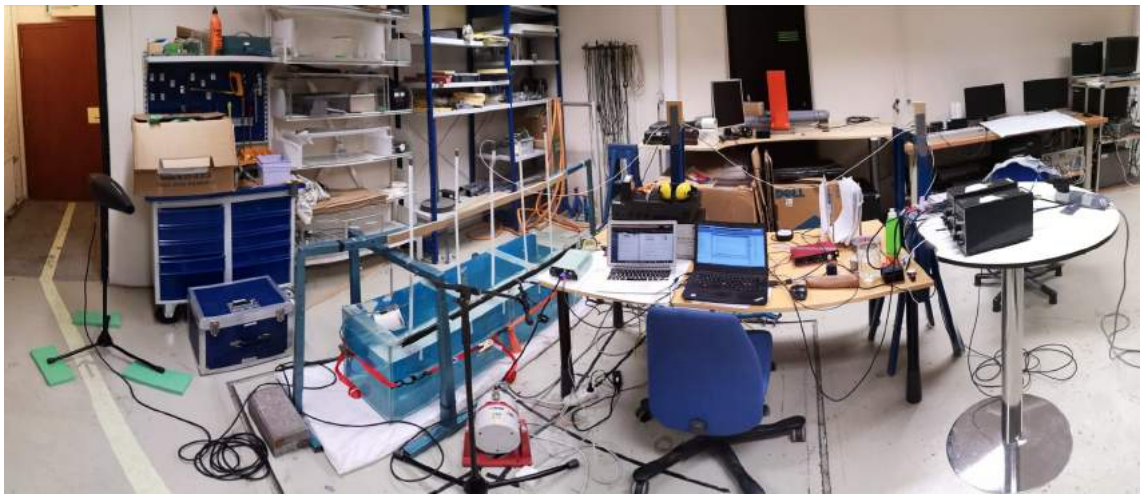

(c) Complete Physical Setup.

Figure 3.4: Setup photographies.

An alternative support for the water filled tank was tried out in order to isolate the tank from external vibrations. The support was then in the form of Sylomer® and wooden planks, as shown in Figure 3.5 below.

Figure 3.5: Alternative support for the water filled tank in the form of Sylomer® SR55 and wooden planks.

3.5.5 Mounting of equipment

3.5.5.1 Shaker

In Subfigure 3.4a above, the pre-stressed shaker B&K LDS Type V406 is shown. The shaker can produce forces up to 196 N according to the shaker data sheet[1]. For the purpose of not risking to break the glass, the gain 5/10 is the gain that is going to be used when a normalised signal is sent to the shaker. Above this gain, around gain 5.5/10, the coherence in the measurements gradually starts to show lower values, and at around 6.5/10, audible impact noises from the shaker stinger against the tank glass is heard. This is true for situations when a (pseudo)random white noise[2] normalized to 1 is sent to the LDS PA100E amplifier. The amplifier additionally has an indicator that prevents overload on the instruments[3]. This level was however never reached on purpose.

Taking the general brittleness of glass into account, it is further decided that the shaker should not be fixed to the ground. The shaker is initially pre-stressed through a combination of its own weight and friction against a 12.5 mm layer of Sylomer® SR55 below it, rubber bands and adjustable straps mounted around the aquarium. Through this arrangement, it is assumed that the shaker will be pushed back, rather

[1] Sine Peak Force. See *B&K* Webpage for more information.
[2] See Appendix B.1.
[3] 'SIGNAL CLAMP' LED illuminated, see PA100E Amplifier Manual.

than breaking the glass if forces produced against the glass becomes too large. The static force from the shaker stinger against the aquarium glass is measured to approximately 42 N with a newton meter. This is the force required to hold the shaker stinger statically 3.5 mm into the shaker body.

Additional measurements was done with the shaker stinger glued to the aquarium glass. The idea behind this is further discussed in Section 3.9.1.

3.5.5.2 Underwater Loudspeaker

In Subfigure 3.4b, the underwater loudspeaker G&W Type UW60 is seen hanging from a spring and wire on a metal frame. The position of the underwater loudspeaker can be adjusted through moving the metal frame and adjusting the length of the wire.

The specifications for the underwater loudspeaker is found in Appendix A.6. Among other things, it specifies a frequency range between 200 and 7 kHz. It is for all measurements driven to the point just below where the amplifier indicates overload, which corresponds to a gain of 6.5/10, playing a random white noise.

3.5.5.3 Hydrophones

In Subfigure 3.4c the complete measurement setup is seen. The white plastic tubes that can be seen in the tank water is for the hydrophones to be put through. The hydrophone will after have been put through the plastic tubes point out in the water. The plastic tubes are mounted on the metal frame with a distance of 30 $\pm$ 1 cm from each other (tube ends). The position of the hydrophone closest to the glass wall where the shaker is mounted is 10 $\pm$ 1 cm from the wall, and the position of the hydrophone closest to the underwater loudspeaker is 10 $\pm$ 1 cm from the loudspeaker membrane. The metal frame is movable and adjustable heightwise in 3 different positions, 7, 17 and 27 cm from the aquarium floor. This arrangement makes repeatable and easily controlled measurements at fixed positions in the aquarium possible.

3.5.5.4 General description of the laboratory environment

The aquarium has the outer dimensions [L_x, L_y, L_z]=[1.5, 0.37, 0.5] m and is filled up to L_z=0.35 m with water. The thickness of the glass walls are h=8 mm. The total aquarium weight is $m^{(g)}$=46.57 kg. The weight of the water volume $V^{(w)}$=0.181 m^3 is $m^{(w)}$=180.8 kg. The aquarium is strengthened with four glass beams that stretches transversely at the top of the aquarium in its longest dimension. Two additional glass beams are fixed vertically at the two walls in the aquariums longest dimension[4]. The edges are leaks protected with additional silicone after the aquarium was acquired.

[4]The glass beams was permanently mounted on the tank when the tank was acquired.

3.6 Processing

An in-house software modified for underwater sound recordings is used to create a connection to the NI Type 9234 signal acquisition module (item no. 8, Section 3.5.1) and start the real-time data acquisition. The inputs and outputs to the software are as in the following Table 3.4.

Table 3.4: Inputs and output of the modified in-house software.

Inputs	Description	Outputs	Description
Number of channels	Item no. 1, 2, 3 and 17 in Table 3.1 and 3.2 equals 4 channels	Data	Measured time domain signals (in V, uncalibrated)
Measurement Type	Voltage		
Name	Channel names are Input Signal, Hydrophone 1, Hydrophone 2 and Microphone		
Sampling Frequency	25.6 kHz (if nothing else is stated)		
Calibration Value	Value obtained from the calibration procedure (See Section 3.7)		
Unit	Voltage for Item no. 17. Pa for item no. 1, 2 and 3		
Reference Value	1 V for item no. 17. 1μ Pa for item no. 1, 2 and 3		

Measurement data is collected in blocks during the time T. The blocks size is chosen to be N= 8192 samples which corresponds to a time length of 0.32 seconds per block ($N \cdot 1/f_s$), exceeding the length of the impulse response of the system with a factor of more than 10. The ending of the last block is zero padded to obtain the desired block length. A plot of the measured time domain and frequency domain signals is updated after each block is acquired. The real-time processing gives early indications of possible clipping, which is an, for this application, undesired alteration of the wave forms in the signal caused by too high voltage in the measured signal compared to the dynamic range of the data acquisition instruments [44].

The data is scaled to the correct relation between V/Pa (volts per pascal) through division with a calibration value (see further explanation in Section 3.7 below).

3.7 Calibration

To be able to present reliable measurement results, Hydrophone 1, Hydrophone 2 and the Microphone (see Section 3.5.1) was calibrated at the start of each mea-

surement session. For the hydrophones, the charge sensitivity was adjusted on the Charge Condition Amplifiers 1 and 2 (see Section 3.5.1) whereafter any necessary corrections are made through a division of the measured data with a calculated calibration value (accounted for in Section 3.7.2 below). The measurement data from the microphone is directly calibrated with a division of calculated calibration value. Since the provided calibration data for the measurement devices range from year 1974 to 2013 (see Appendix A), a multi-step verification procedure was carried out to verify accuracy of the instruments.

3.7.1 Calibration of Microphones

The microphones B&K Type 4133 and B&K Type 4166 was calibrated using a microphone Calibrator B&K Type 4229. The calibration charts for the B&K Type 4133 and the B&K Type 4229 is found in Appendix A.4 and A.5 respectively. Frequency resolution during the data acquisition is chosen to match 1 Hz step intervals (See Section 2.3). The calibration procedure, here exemplified for the B&K Type 4133 with the same principle applying for the B&K Type 4166, is done through

1. Turning on the B&K Type 4231 that is assumed to produce a 1000 Hz sine tone at 1 Pa (See Appendix A.5).
2. Insert the microphone in the coupler in the B&K Type 4231
3. Start data acquisition
4. The signal measured by the microhone is band passed using a 4th order infinite impulse response (IIR) Butterworth filter. The bandpass filter has the the frequency response as in Figure 3.6 below.

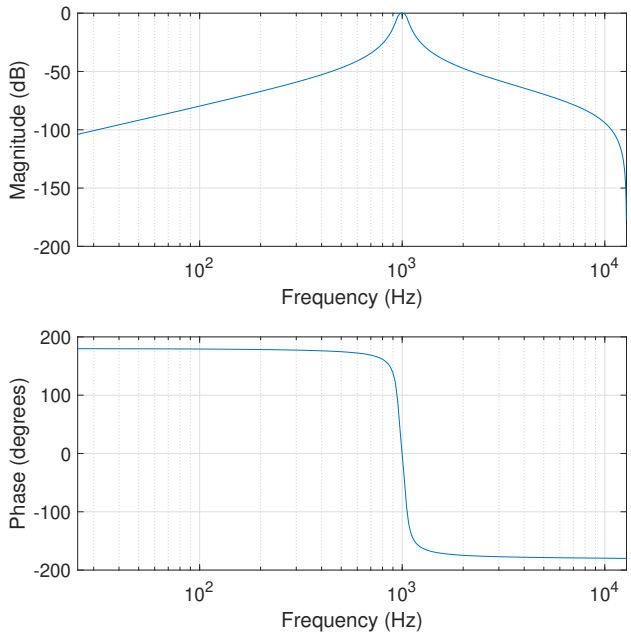

Figure 3.6: Frequency response of the 4th order Butterworth band pass filter.

The passband is designed to have cutoff-frequencies 5% below and 5% above

the center frequency, that is set to 1000 Hz. The signal is filtered using Eq. 2.53. The signal is bandpassed around the expected frequency of 1000 Hz to obtain the true voltage induced in the microphone at that frequency and to avoid any voltage induced caused by disturbing noise.

5. The root mean square value is calculated through Eq. 2.22 This provides the voltage sensitivity 11.6 mV/Pa for the B&K 4133. This value differs from the 1974 loaded sensitivity value with 1.0 mV/Pa (calibration chart in Appendix A.4) and could possibly be due to age of either the microphone, the microphone calibrator, the preamplifier or all three.
6. Start a new data acquisition session and divide the acquired data with the calculated voltage sensitivity. Results are shown in Figure 3.7 below

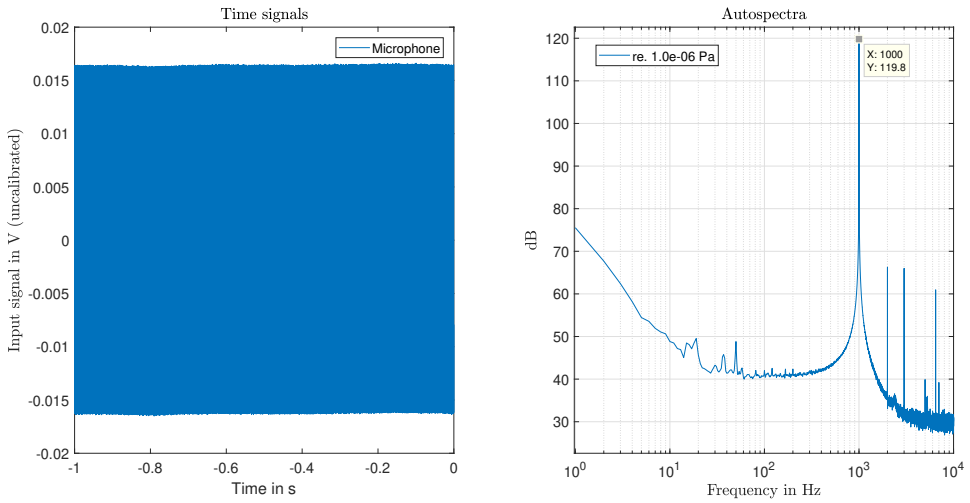

Figure 3.7: Measurement data from the microphone B&K Type 4231 inserted in the microphone calibrator.

The 119.8 $\approx$ 120 dB re. 1 μPa peak that can be seen at 1000 Hz in the right hand plot in Figure 3.7 above corresponds to a measured 1 Pa sound pressure that the microphone calibrator supposedly produces. Any deviations from exactly 120 dB re. 1 μPa is due to a finite precision in the data processing steps (Section 2.4).

3.7.2 Calibration of Hydrophones

The Hydrophones 1 and 2, both being B&K Type 8103 were calibrated using a B&K Type 4229 Calibrator. The calibration charts for both the B&K Type 8103 are found in Appendix A.1 and A.2 respectively. The calibration chart for the hydrophone calibrator is found in Appendix A.3.

The B&K Type 4229 has a coupler to 1/2 inch microphones of types such as the B&K Type 4133 microphone, see Figure 3.8 below.

Figure 3.8: B&K Type 4229 pistophone on a metal stand with the B&K Type 8103 hydrophone and the B&K Type 4133 microphone inserted.

The Microphone B&K Type 4133, calibrated as in Section 3.7.1, is therefore used to monitorthe sound pressure level inside the coupler volume during the hydrophone calibrations, as suggested by the manufacturer[5].

Going through steps 1 to 5 in Section 3.7.1 again, but now using the hydrophone calibrator together with the microphone, and using the code found in Appendix B.5[6], an RMS voltage of 2.15 V is measured. Assuming that the voltage sensitivity of the microphone is correct, this means that the pistophone produces a SPL re. 1 μPa of approximately

$$\mathrm{SPL}_{\mathrm{pistophone}} \approx 10 \cdot \log_{10} \left(\frac{\frac{(2.15\ \mathrm{V})^2}{(0.016\ \mathrm{V/Pa})^2}}{p_{ref}^2} \right) \approx 165.39\ \mathrm{dB\ re.\ } 1\mu\ \mathrm{Pa} \tag{3.1}$$

compared to the 165.8 $\pm$0.2 dB re. 1 μ Pa that is described in the data sheet.

Hydrophone 1 is the measurement instrument that was calibrated professionally most recently, namely year 2013 (see Appendix A.3). Adjusting the Charge Conditioning amplifier according to the Amplifier Manual[7] to the Hydrophone 1 Calibration Chart values results in the settings in Table 3.5 below.

[5]See the B&K Webpage for more information.

[6]The code in Appendix B.5 is a modification of the in-house code that is used for calibration of ordinary microphones. The modification of the code is to make it suitable for hydrophone calibration.

[7]See the B&K Webpage for more information.

Table 3.5: Settings for Charge Conditioning Amplifier 1 for Hydrophone 1

Setting	**Range**	**Unit**	**(Unit on the panel of the device)**
TRANSDUCER SENS. Range switch	0,1 - 1	10^{-1} pC/Pa	pC/m/s^2
TRANSDUCER SENS. conditioning knobs	0,995	pC/Pa	pC/m/s^2
ACC.-VEL.DISPL.	1 0,2	Pa Hz	m/s^2
UPPER FREQ. LIMIT	10	kHz	
mV/UNIT OUT	100	mV/Pa	mV/Unit Out

Using these settings, an RMS value of 0.00982 V/Pa (almost 0.01 V/Pa) normalized to the expected SPL of $\approx$ 165.39 dB re. 1μ Pa, is measured. This indicates that the hydrophone only needs a limited adjustment from what is stated in the calibration chart.

Going through the same procedure with Hydrophone 2, being of the same type as Hydrophone 1, shows that it, for some reason, seem to have lost much of its precision.

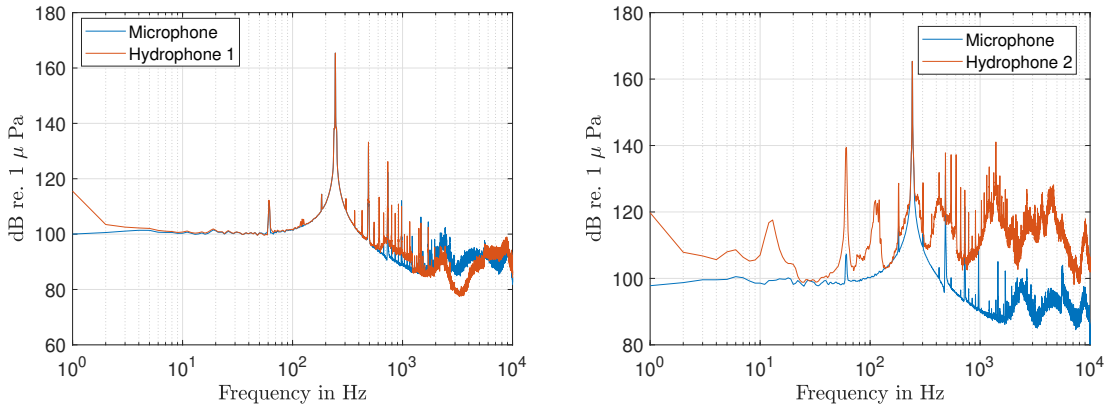

(a) Hydrophone 1 and microphone. **(b)** Hydrophone 2 and microphone.

Figure 3.9: Autospectra of SPL measured from the pistophone using Hydrophone 1 (left) and Hydrophone 2 (right) together with the Microphone

As can be seen from Figure 3.9b above, hydrophone 2 does not match the measurements with the microphone and Hydrophone 1 very well. A switch of Charge Conditioning Amplifier between the hydrophones was carried out, giving the same results. Another possible indication of the faultiness of Hydrophone 2 is that none of the charge conditioning amplifiers shows an overload when connected to it, independent of setting. Because of the doubts of the state of Hydrophone 2 that these observations induce, only Hydrophone 1 will be used for data collection.

3.8 Measurements

At the time of the project implementation (spring year 2020), no known standard procedure of measuring sound environments in aquariums was found. Therefore, a repeatable measurement procedure was developed with possible variations that will be accounted for if done.

Measurement of sound pressure was conducted at 30 fixed hydrophone positions within the aquarium. These fixed hydrophone positions correspond to the combinations of locations x = 0.1, 0.40, 0.7 1.0, 1.3 m, y = 0.12, 0.185 m and z = 0.07 0.17, 0.27 m, (all locations being in the range of ± 1 cm precision). The results presented in this report will generally only be for five of the measurement positions. This is to keep the report reasonably short and to be able to communicate the findings and observations in a clear manner. Additionally, the characteristics of the measurement results from the other 25 measurement positions did not further contribute to the proceedings of this project. The five measurement positions most commonly used are x = 0.1, 0.40, 0.7, 1.0, 1.3, y = 0.185 m and z = 0.17 m.

3.9 Alternative Setups

The Measurement Setup is, if nothing else is stated, as presented Section 3.5 in this report. Some experimental variations has in addition been tried out, which are presented below.

3.9.1 Alternative Mounting of Shaker

At high amplitudes, especially at low frequencies, the shaker stinger tends to start tap against the glass wall of the aquarium. With this said, the stinger of the shaker is at certain instances in time not in contact with the glass. This creates impacts that are undesirable because of the uncontrolled noises they produces. In Subfigure 3.10a below, the effect of impact noises can be seen in the small peaks between 30 Hz and approximately 300 Hz (aurally, the peaks are very prominent). Overall, the level below approximately 1000 Hz is raised in the whole frequency region, which is an undesirable effect caused by the tapping. A sine tone of 1000 Hz did not cause tapping noises or raised levels in other frequency regions, see Subfigure 3.10b.

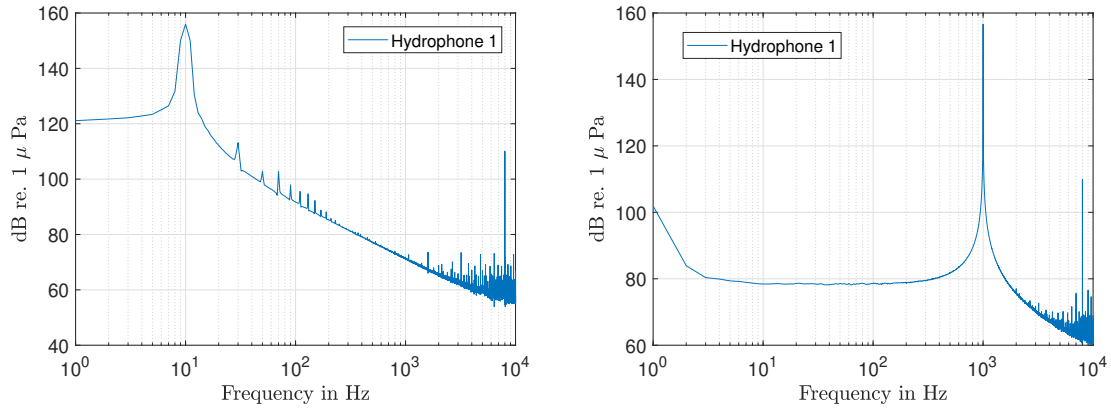

(a) A 10 Hz tone that produces tapping.

(b) A 1000 Hz tone that does not produce tapping .

Figure 3.10: Autospectrum of 10 Hz and 1000 Hz sine tones played through the shaker (at gain 3/10) on a distance of 40 cm from the hydrophone. The sine tone is created usng the code found in Appendix B.3.

To remove the undesired effects of tapping between the shaker stinger and the glass, the stinger was, for some experiments, glued against the glass with cyanoacrylate[8]. The issues with the stinger tapping against the tank glass were through the gluing procedure removed, and the coherence in FRF-measurements were improved. However, since the glue broke after two or three measurements and thereafter needed to be re-done with a drying time of several hours, the approach was abandoned.

3.9.2 Vibration Sound Isolation

An unidentified low frequency background noise was present for all measurements. This background noise varied between different measurement times, but was probably lower during night (results displayed in Figure 3.11a below) and higher during day (results displayed in Figure 3.11b below) according to measurements done at 02.00 and 14.00 respectively.

[8]The brand and name of the glue used was "Loctite Glass Bond super glue".

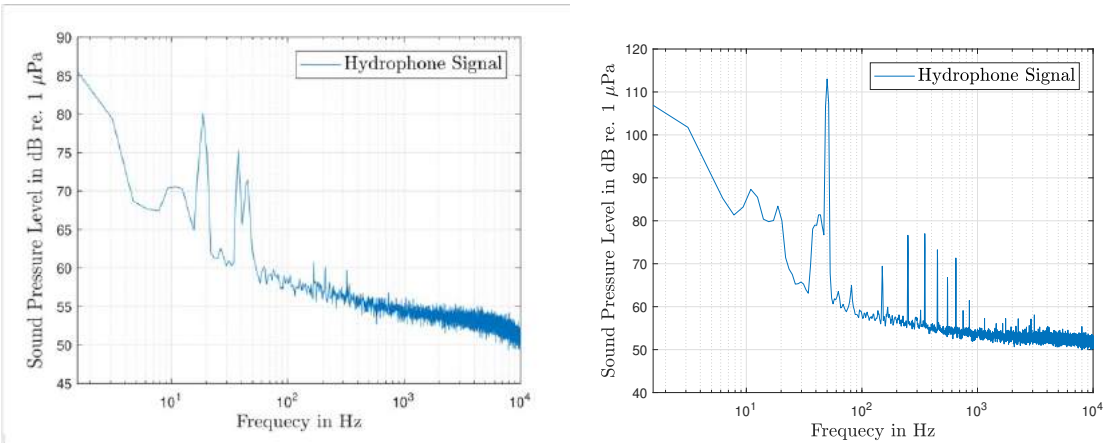

(a) Background noise level measured at 02.00.

(b) Background noise level measured at 14.00 .

Figure 3.11: Auto Spectrum. Background noise levels in the aquarium at different times during the day.

The measurements resulting in the graphs in Figure 3.11 above were carried out repeatedly around the times during the night at 02.00 and during the day at 14.00, giving results ranging from ± 5 dB re. 1 μPa of what is displayed.

The Sylomer®SR55 mentioned in Section 3.5.4 was obtained with help from the company Christian Berner AB. It was installed below the tank as displayed in Figure 3.5 in Section 3.5.4. Its properties was calculated bases on the physical model of a harmonic oscillator with a massless spring on a rigid and plane subsoil and chosen to match the weight and dimensions of the tank. The product data sheet with further details is found in Appendix A.7. Unfortunately, due to the quite large variations in low frequency background noise levels in the aquarium, any clear differences are hard to distinguish from before and after the vibration isolation. In Figure 3.12, the auto spectrum of the background noise levels in the tank is displayed, and can be compared with the background noise levels displayed in Figure 3.11b

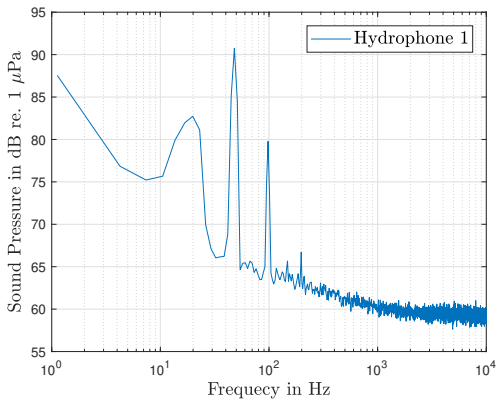

Figure 3.12: Auto Spectrum. Background noise level measured at 14.00 with Sylomer®SR55 below the aquarium for vibration isolation.

Lower background noise levels approximately below 100 Hz are identified with the Sylomer®SR55 installed compared to without the Sylomer®SR55 installed, but the possibility of external factors influencing the results was not possible to exclude. External factors are in this context factors that can not simply be controlled or identified and that originates from outside of the lab. This could for example be ventilation systems in the building that is turned on or off, and that produces low frequency vibrations that spreads through the building elements, or the interference of God.

3.9.3 Electrical Humming

The problem with electrical humming appearing as high amplitude peaks in any measurement has proven to be hard to resolve. The measurement equipment can be completely driven by batteries, which only partly resolves the issue. Any amplifier driving the shaker or underwater loudspeaker needs to be connected to a power outlet in the wall, which seems to produce ground loops[9] and thus high peaks will appear in the autospectra resulting from some measurements. A special in-department power connector is used to partly resolve this issue, but clear peaks still remain.

In Subfigure 3.13a below, the background noise in the tank is again presented, showing the electrical humming in peaks ranging up to approximately 3500 Hz. Note that Figure 3.13a shows results of measured background noise when electrical appliances are connected to power outlets in the wall without the special in-department power connector. Additionally, this plot originates from when the electrical appliances where stacked closely together, which might have worsened the ground loop effect. The background noise measurement results presented earlier, i.e. those displayed in Figure 3.11, are from when the special in-department power connector is used, and when the electrical appliances are well separated.

[9]See Section 2.9.1 for a description of ground loops.

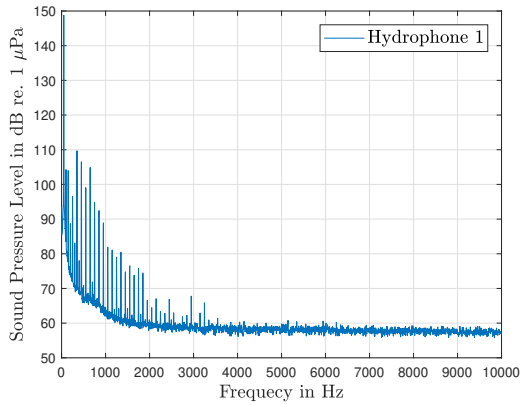

(a) Autospectrum of background SPL

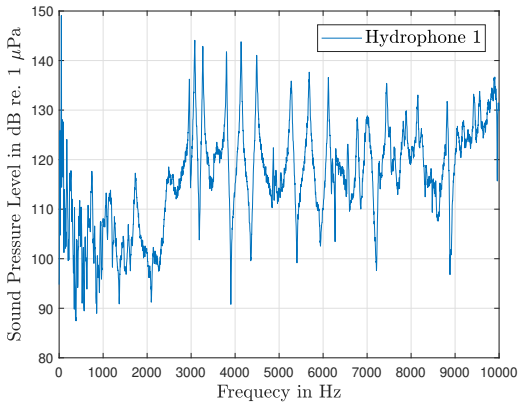

(b) Autospectrum of white Noise SPL at level (5/10)

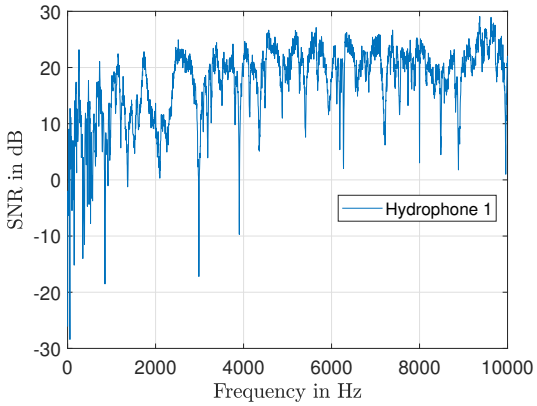

(c) Coherence based SNR

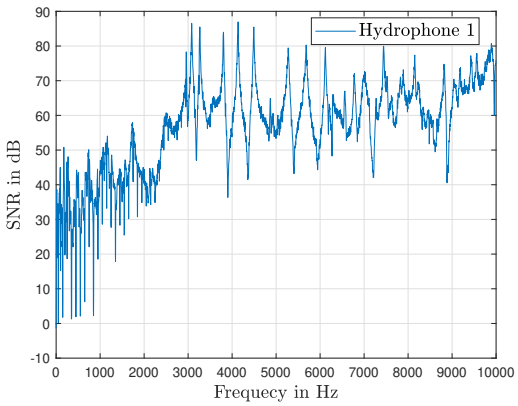

(d) Subtraction based SNR

Figure 3.13: Signal-to-noise ratio measurements

In Subfigure 3.13b, the SPL measured when a white noise is fed to the system with a gain of 5/10 on the LDS Type PA100E power amplifier is displayed. This figure is included to give intuition of the magnitude of the electrical humming noise problem before any measures were taken to reduce the ground loop problem[10]. Subfigure 3.13c is the SNR as calculated using Eq. 2.45, and Subfigure 3.13d is the SNR as calculated using Eq. 2.46. Poor signal-to-noise ratio at low frequencies due to electrical humming seems to be most visually clear if comparing the shape and positions of the high peaks up to approximately 2500 Hz in Subfigure 3.13a, with the low dips up to approximately 2500 Hz in Subfigure 3.13d.

3.9.4 Background Sound Pressure Levels in the Lab

The background sound pressure level in the air of the lab with the conventional reference pressure 20 μPa, and in addition A-weighted, is shown in Figure 3.14 below.

[10]This could be something worth keeping in mind for other researchers in future experiments.

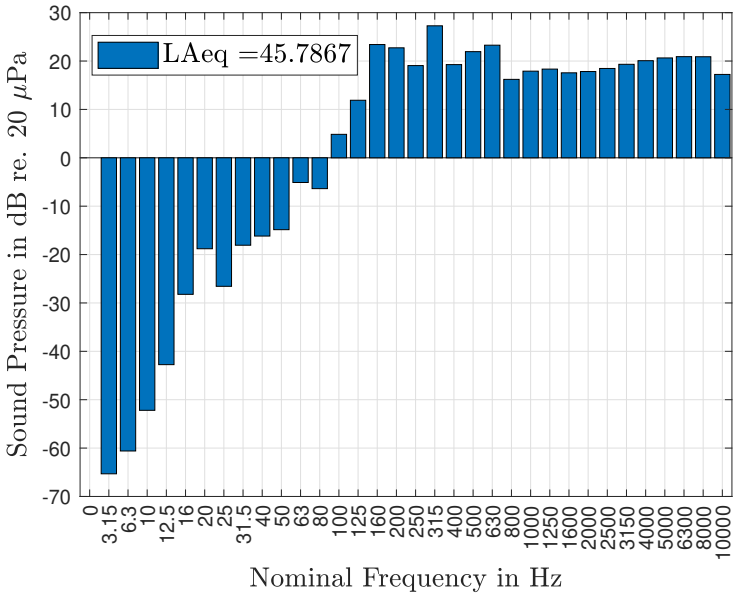

Figure 3.14: A-weighted background sound pressure in dB re. 20 μPa in the vibrolab. Summed in third-octave bands from the autospectra

Figure 3.14 is included to show the environmental settings in the air in the vibrolab. The A-weighting is done because it is conventional for sound pressure level measurements in air to be presented in this way, and because it gives a closer representation of how humans perceive sound in air than without the A-weighting (see Section 2.9.6).

Additionally, below, two graphs of the background sound pressure level measured in the lab room and in the tank, measured simultaneously[11], is seen.

[11]The impracticalities when comparing sound pressure levels in water and in air are discussed in Section 2.6.

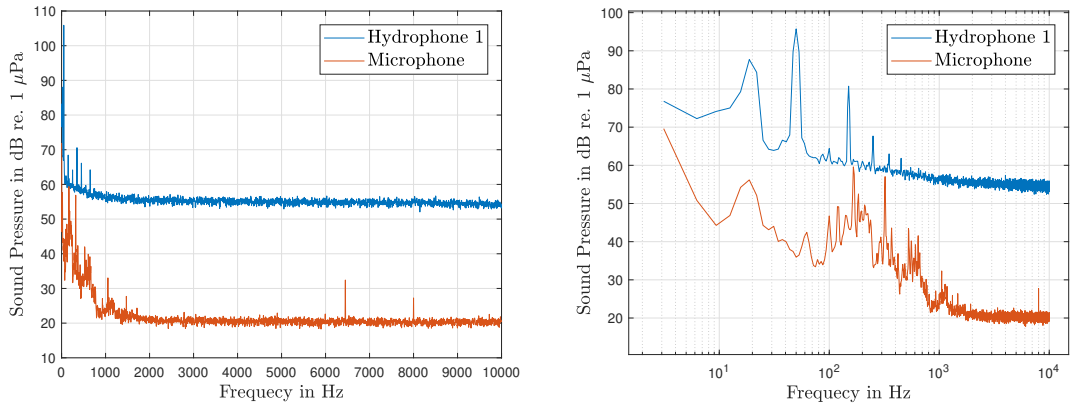

(a) Linear frequency axis **(b)** Log frequency axis

Figure 3.15: AutoSpectra of the background sound pressure levels in lab air and in the aquarium water

The reason for Figure 3.15 above being included is to show that the airborne sound in the laboratory environment outside of the water-filled tank will have little effect on the sound pressure level inside the water filled tank, see Section 2.2.2. For example, the SPL in air outside of the tank in Figure 3.15 is varying in level between approximately 35 and 60 dB re. 1 μPa between approximately 50 and 1000 Hz. These variations does not match the much smaller variations in the same frequency range for the SPL in water. That observation is important, because it tells us that the cause of high background noise levels in the tank is most likely not due to high noise levels in the air outside the aquarium[12]. It also gives the reader of this paper means to conclude that using a sound source placed at a separating distance from the tank, such as a common loudspeaker, is an unpractical way of inducing a sound field in it. The last statement is clarified in the following example, where a white noise is played through the OmniSource Loudspeaker Type 4295. The sound pressure level in dBA re. 20 μPa is measured at position $L_x/2$, $L_y/2$, $L_z + 0.1$ m (with reference to Table 2.2) which resulted in the following spectrum in Figure 3.16 below.

[12]Even though high noise levels in the air outside of the tank potentially could be caused by the same structure borne vibrations that cause high levels inside the tank. This might be the case, especially for frequency ranges below approximately 50 Hz, where the blue and the orange graphs in Figure 3.15 seem to follow the same pattern in terms of dips and peaks.

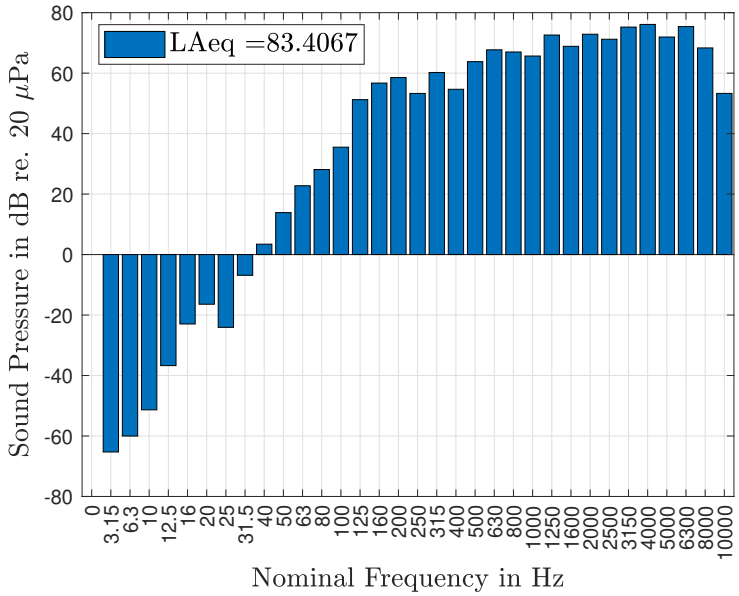

Figure 3.16: Sound pressure in dBA re. 20μPa from the OmniSource Loudspeaker in the vibrolab. Summed in third octave bands.

The SNR in water and in air respectively that results from the measurement is displayed in Figure 3.17 below.

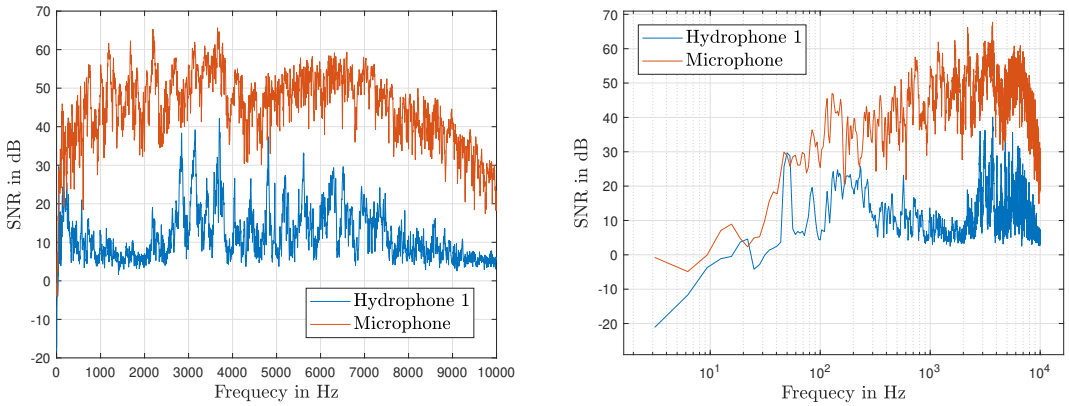

(a) Linear frequency axis **(b)** Log frequency axis

Figure 3.17: AutoSpectra of the subtraction-based SNR between the background noise and the noise from the OmniSource Loudspeaker

The measured sound pressure levels that resulted in the SNRs displayed in Figure 3.17 above was measured at position $L_x/2$, $L_y/2$, $L_z + 0.1$ m for the microphone air measurement and at position $L_x/2$, $L_y/2$, $L_z/2$ m for the hydrophone water measurement. As can be seen in Figure 3.17, the SNR in air is roughly between 30 and 60 dB, while for the water case, the SNR is centered somewhere around 10 dB. The microphone in air and the hydrophone in water had a distance from each other of 0.275 m.

4

Results and Discussion

4.1 Shaker performance

In order to evaluate the shaker performance in terms of producing a desired sound field in the tank, measurements were firstly undertaken using the underwater loudspeaker (item no 15. Table 3.2). This was for comparison purposes. The complete setup, instrument settings, signal processing parameters and more that was used for the following measurements are presented in Chapter 3. The theory behind the data processing is presented in Chapter 2. The comparison is made between the two sound-producing devices when they are driven to their respective highest points. These highest points are defined in Chapter 3.

4.1.1 Underwater Loudspeaker

The sound pressure level measurements using the underwater loudspeaker as sound source resulted in the autospectra presented in Figure 4.1 below.

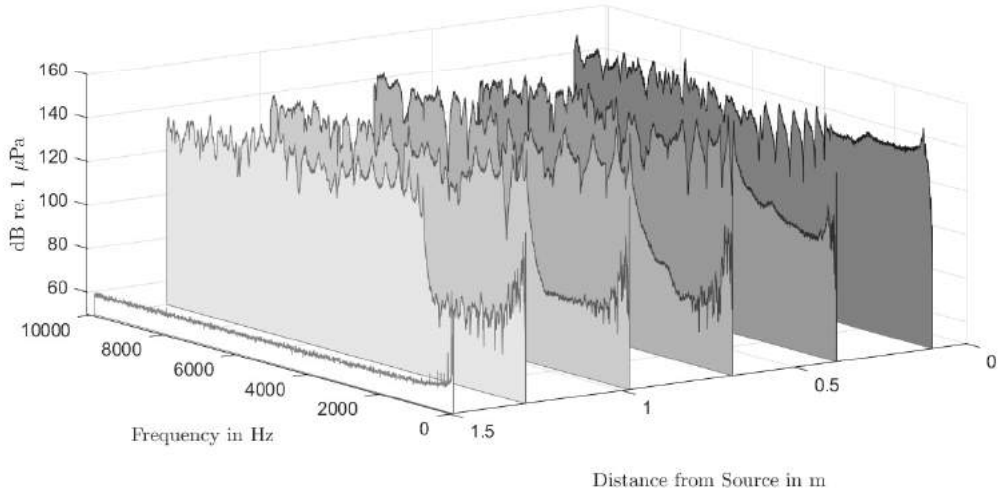

Figure 4.1: Autospectra from the sound pressure measurements using the underwater loudspeaker as a source. The signal is measured by the hydrophone at five different positions within the tank.

The five curves that are seen furthest away in the figure represents the SPL in dB re 1 μPa in the tank at positions $L_y/2$, $L_z/2$ and 0.1, 0.4, 0.7, 1,0, 1.3 m from

loudspeaker membrane, see Section 3.5.5.3. The last curve at 1.5 m is the measured background SPL in the tank. It is included as a reference and was measured at position $L_x = 1$, $L_y/2$ and $L_z/2$ m. As expected, the level below the cutoff frequency at around 2750 Hz is attenuated very quickly with distance from the source, and becomes much lower than the regions above the cutoff frequency already at 0.4 m from the source, see Section 2.2.7.

The corresponding coherence between the signal sent to the underwater loudspeaker and the signal that is picked up by the hydrophone from the same measurement is displayed in Figure 4.2 below. The closest curve at 1.5 m in Figure 4.2 is the coherence when no signal is sent to the loudspeaker.

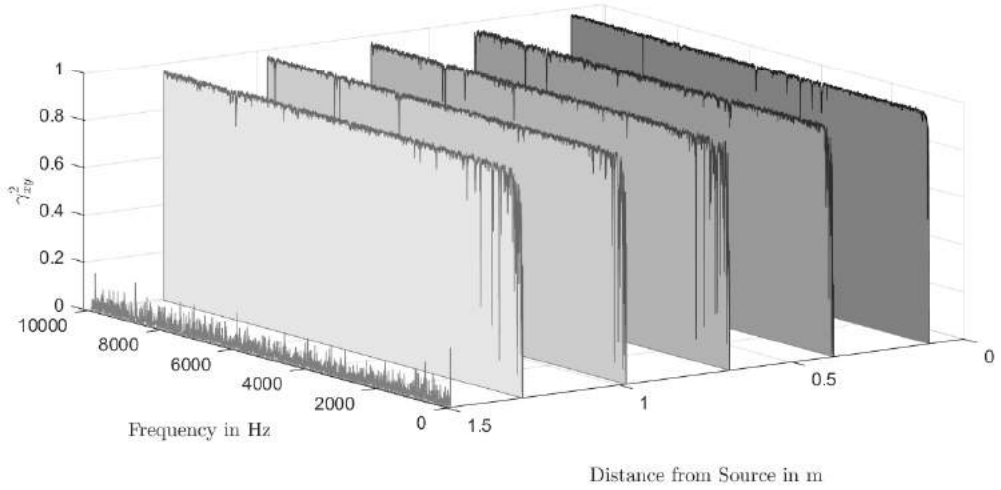

Figure 4.2: Coherence between the signal sent to the loudspeakr and the signal picked up by the hydrophones at five different positions in the tank.

The coherence is high for the regions above the cutoff frequency where the SNR[1] is high. The SNR in the tank is still high enough for the coherence to be close to 1 even for most frequencies below the cutoff frequency down to at least 1000 Hz. Below approximately 200 Hz, the coherence is closer to 0 than it is to 1. This is expected since the lower frequency range for the loudspeaker is 200 Hz, see Section 3.5.5.2 and because the background noise levels in the tank are high in these regions, see Section 3.9.2.

The FRF between the signal sent to the loudspeaker, and the signal that is picked up by the hydrophone is displayed in Figure 4.3 below. The low coherence below 200 Hz from Figure 4.2 indicates that the FRF probably is not a good representation of the system in this region.

[1]The SNR is not calculated here, but it should be visually clear enough by comparing the five SPL curves from the white noise measurements with the background noise level curve in Figure 4.1.

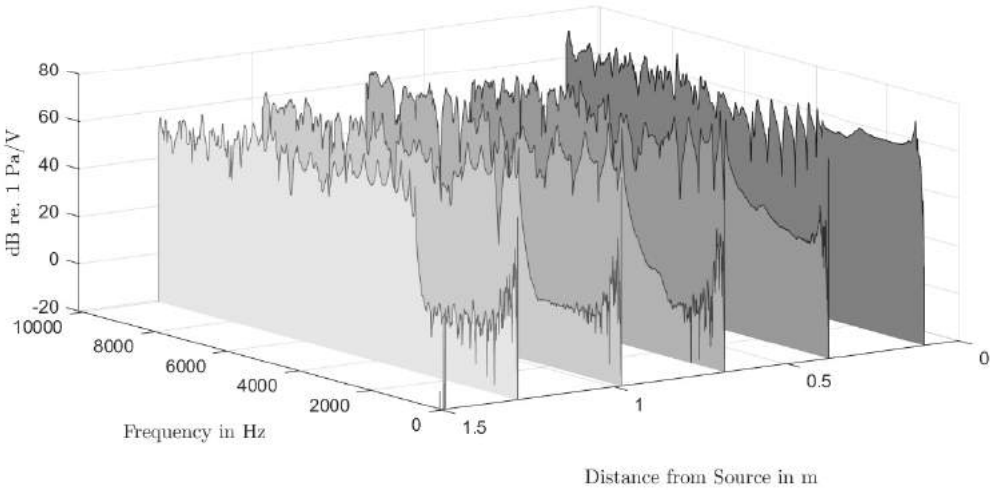

Figure 4.3: FRF between the signal sent to the loudspeaker and the signal that is picked up by the hydrophone at five different positions in the tank.

4.1.2 Shaker

The sound pressure level measurements using the shaker as a sound source resulted in the autospectra presented in Figure 4.4 below.

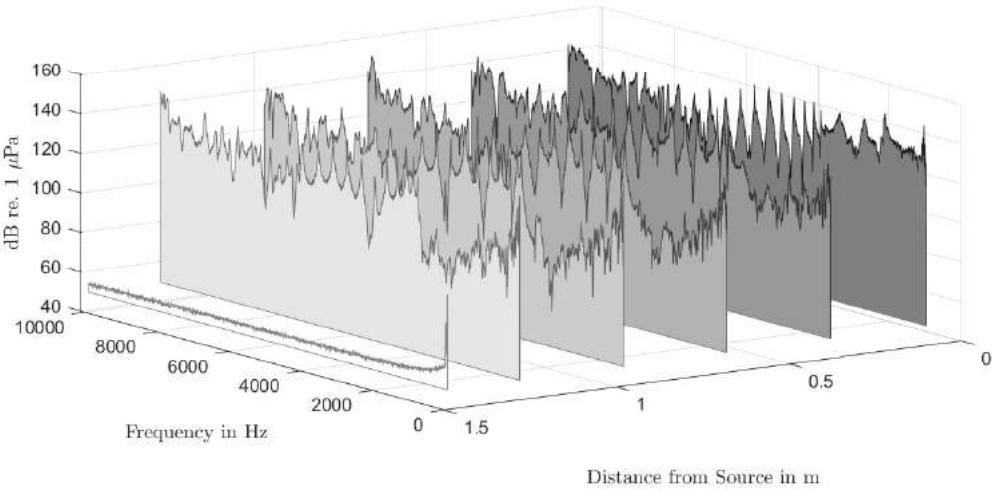

Figure 4.4: Autospectra from the sound pressure measurements using the shaker as a source. The signal is measured by the hydrophone at five different positions within the tank.

The measurement distances from the source, which in this case is the glass wall at the point closest to the shaker stinger, are the same as for the underwater loudspeaker measurements. By comparing Figure 4.4 above with Figure 4.1 in the previous section, it can be noted that the level below the cutoff frequency generally is higher with the shaker as a source, than it is when the underwater loudspeaker is the source. For example, the curve at 1.3 m from the source, is about 20 dB re. 1 μPa higher

for the shaker case. The difference in the level above the cutoff frequency is not as noticeable when comparing the shaker case with the loudspeaker case. The level generally is between 120 and 140 dB re. 1 μPa for both cases, but the level varies more for the shaker case.

The reason for the shaker case having levels below the cutoff frequency and above the cutoff frequency that are closer to each other than for the loudspeaker case was never understood. It was discussed whether the shaker is inducing vibrations in the glass walls and floor of the tank that is emitted as sound from all inner surfaces of the tank, including surfaces closer to the hydrophone than the surface at the shaker stinger. By studying Figure 2.12 and the theory leading up to it, it is understood that the level of the sound in low-frequency regions is attenuated very quickly with distance from the source below the cutoff frequency[2]. A sound source close to the receiving hydrophone, such as a vibrating side wall would thus be an explanation for the higher low-frequency levels in the shaker case.

The coherence that corresponds to the previous results in this section is displayed in Figure 4.5 below.

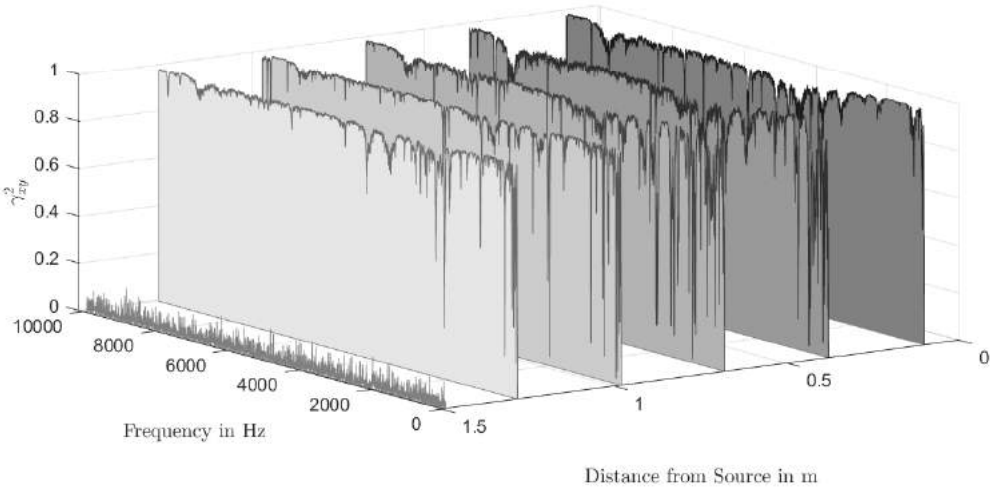

Figure 4.5: Coherence between the signal sent to the loudspeaker and the signal picked up by the hydrophones at five different positions in the tank. The curve closest to the distance 1.5 m on the m-axis is the coherence when no signal is sent to the system.

It is clear from comparing Figure 4.5 above with Figure 4.2 that the coherence is lower for the shaker case than it is for the loudspeaker case. This is expected, in short, since the shaker is not designed to produce a sound field in water, and the underwater loudspeaker is, see Sections 2.7 and 2.8. Additionally, although it was not audible by ear during these measurements, the shaker stinger might have tapped against the tank glass at some instances. This would surely be a cause for some of the lower coherence viewed in Figure 4.5, see Section 2.4.8. In Section 3.9.1, the

[2]This is also verified in the measurements and clear if looking at Figure 4.1.

occurrence of tapping against the glass is examined for a case when a low-frequency sine tone is sent to the shaker at a gain that is high enough for the tapping phenomenon to become very clear. Since this phenomenon is so clear during these specific tests, it is assumed that it might also occur while playing a white noise at a lower gain, but then being masked by noise.

The coherence, that is lower for the shaker case than it is for the loudspeaker case, indicates that the measured FRF in the shaker case will not have an as high quality[3] as for the loudspeaker case. The FRF displayed in Figure 4.6 below is used for the development of the equalizing algorithms described in Section 2.5. The quality of the FRF is good enough to use in the equalizing process to produce satisfactory results, which will be presented later in this chapter.

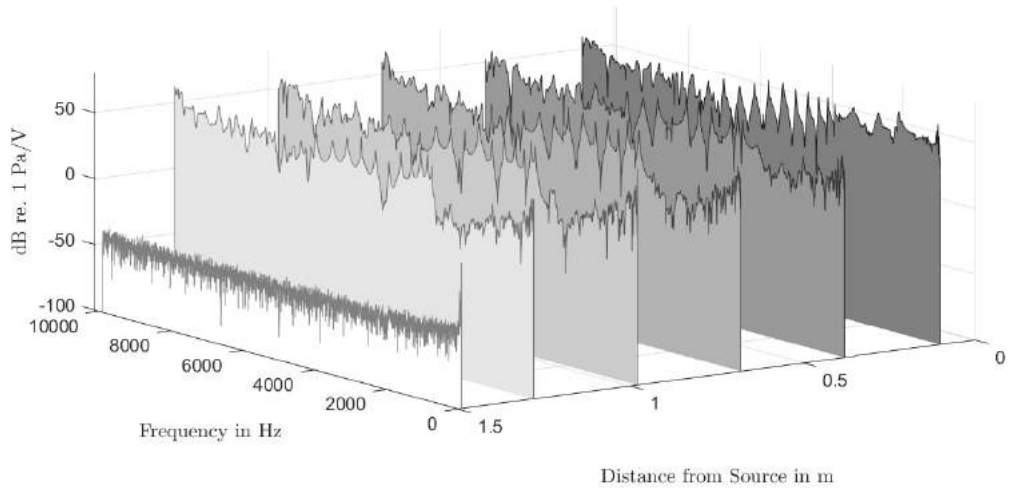

Figure 4.6: FRF between the signal sent to the shaker and the signal that is picked up by the hydrophone at five different positions in the tank.

One inconvenience with the use of a shaker as a mean for sound production is the loud background sound pressure levels that become present in the laboratory environment surrounding the tank, see Figure 4.7 below.

[3]I.e. the FRF for the shaker case might not show the actual response of the system as good as it does for the loudspeaker case.

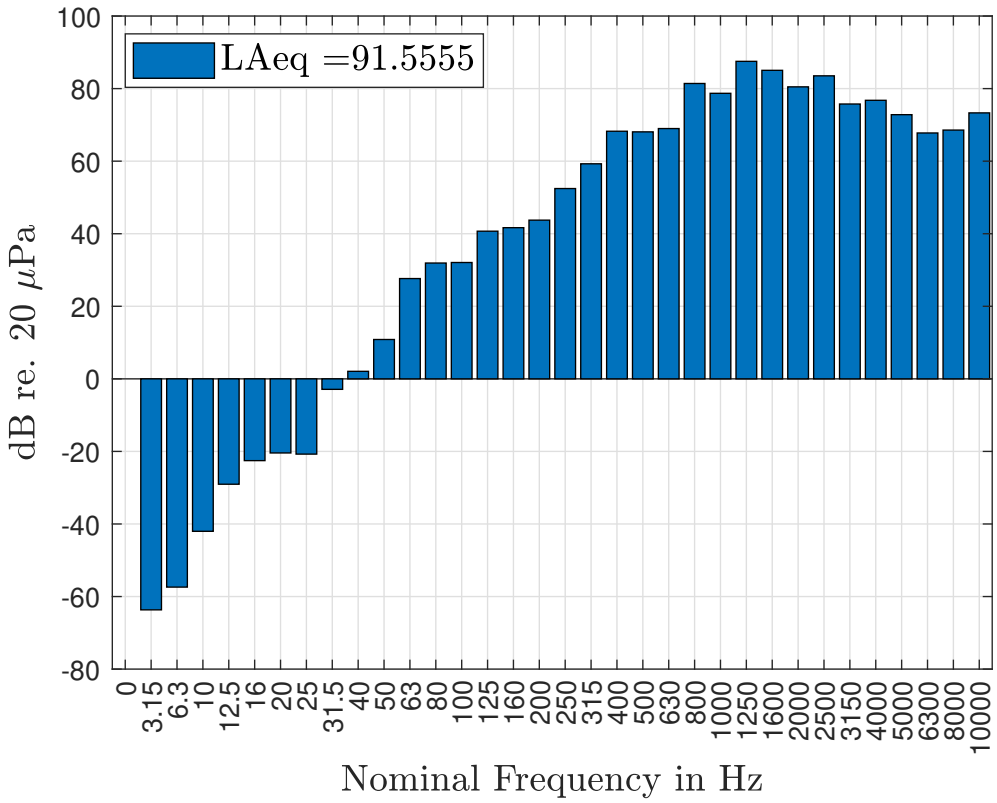

Figure 4.7: A-weighted SPL in dBA re. 20 μPa in the lab air.

The cause of the high background noise levels[4] that the shaker, in combination with the glass tank, produces in the lab air outside of the tank was never closely examined since it is beyond the scope of this thesis. It was however discussed whether the glass tank acted like a resonator[5] that transmitted the vibrations induced into it to the air outside of it. Eventual taps from the shaker stinger on the tank glass would further introduce impact noises, adding to the tanks emission of sound to the lab air.

4.1.3 The Potential of Low-Frequency Shaker Excitation

When focusing on narrowband shaker excitation, the shaker proved to have the potential to produce SPLs that were only limited by the authors' discomfort in knowing that the glass of the aquarium might break at any instance.

[4]The placement of the microphone measuring the sound pressure that resulted in the graph in Figure 4.7 above was the same as in Section 3.9.4.

[5]To clarify, this is to some degree indisputably true, since the shaker by itself only is able to produce a noise level of 82 dBA, measured at a distance of 1 m and at the height of 1.6 m above floor level in an enclosed cell, see the B&K Webpage for more information.

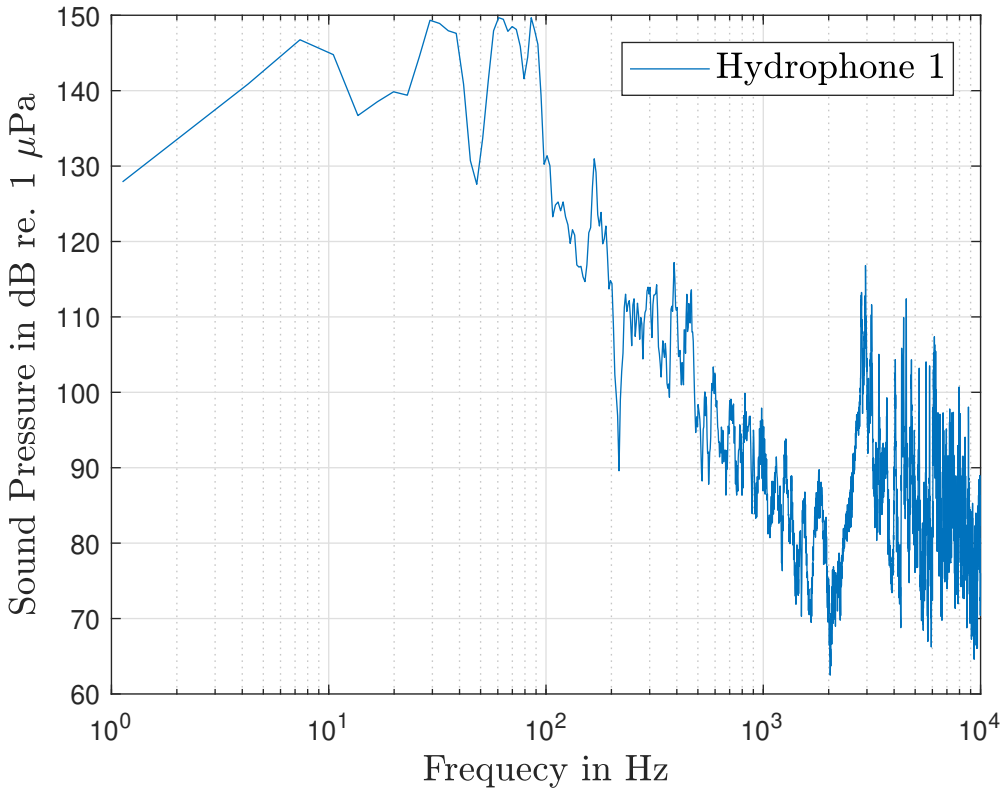

Figure 4.8: Auto Spectrum. Sweep between 5 and 100 Hz. Gain 2.5/10.

The amplitudes in Figure 4.8 above cannot be produced by the underwater loudspeaker, see Section 3.5.5.2. As can be seen in Figure 4.8, other frequency ranges of the sound field were excited than the intended frequency range between 5 and 100 Hz. This is partly due to some instances when the shaker stinger tapped against the glass of the tank. An observation that was made[6] was that the whole tank was moving[7] along with the shaker stinger at low frequencies[8]. It is not possible to exclude the possibility that this phenomena additionally lead to other frequency regions than the intended got excited by the signal[9].

4.2 A Comparison Between Measured and Modelled Results

In below Figure, the measured and the modelled FRFs for the tank under study is shown.

[6]Through looking at the glass tank during the measurements

[7]The ability of the whole tank to be able to move simultaneously was because the tank was standing on soft supports, see Section 3.5.5.

[8]"Low frequencies" is here referring to the region between 5 Hz and 100 Hz, which was covered by the sweep signal. The tank was moving less at some frequencies and more at other frequencies, probably due to eigenfrequencies of the system.

[9]Subjects for furhter research is covered in Chapter 6.

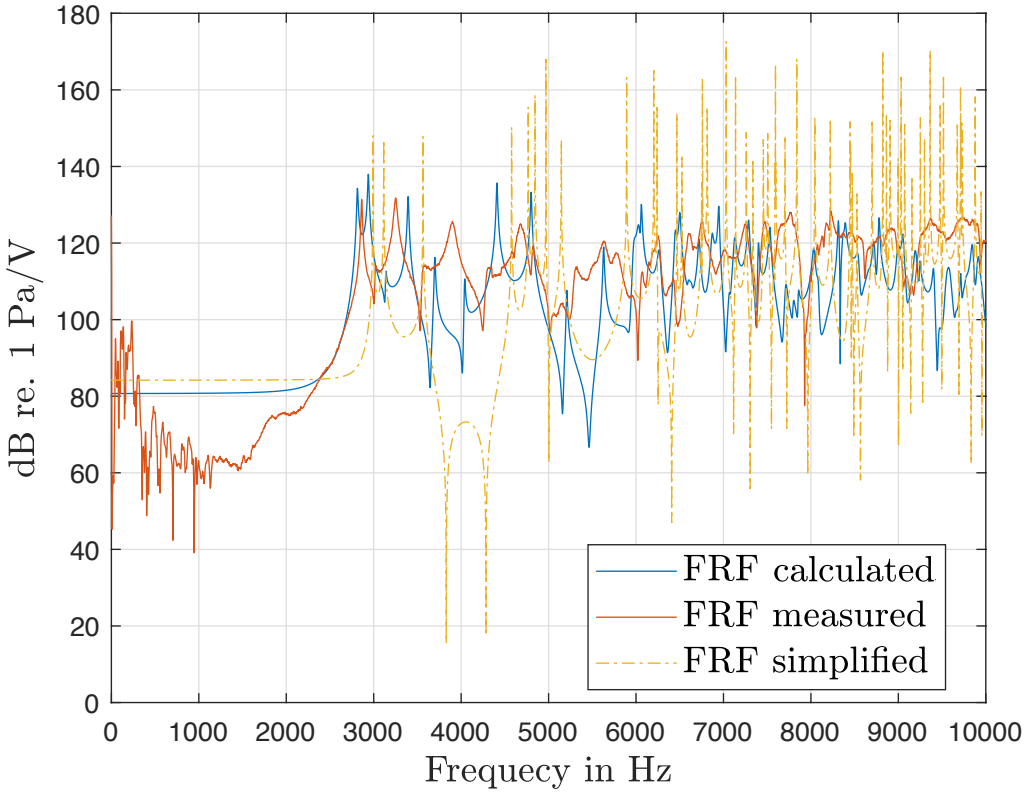

Figure 4.9: Measured and modelled FRF for a source at point [0.3, 0.37, 0.35] and receiver at point [1.0, 0.37, 0.35]

The FRF is calculated according to Section 2.2 with the material parameters and tank geometries given in Tables 2.1 and 2.2. Added in the plot is the resulting FRF when using Eq.2.5 to Eq. 2.7 together with Eq. 2.17 and thus bypassing the inclusion of damping, leakage and reflections within the tank.

As expected, the modelled response only correspond to the measured response on a qualitative level as clarified in Section 2.2.8. The model, however, corresponds better with the measured response than the FRF from the simplified model, as seen in Figure 4.9. This is in terms of the location of the first resonance frequency, level of the response below the first resonance frequency and the magnitude of resonances at and above the first resonance.

4.3 Equalization Algorithms

This section contains two subsections, where the results from the two equalization algorithms will be presented. Each subsection starts with modelled results, which referrers to the results from when the equalizing algorithm has been used to calculate the signal that is going to be sent to the system. After that, the result from when the calculated signal has been sent to the system and measured by the hydrophone will be presented. The FRFs used by the equalizing algorithms has been measured

using the shaker as a sound source, and the compensated signal that is calculated is again sent to the system by the shaker. The results are presented for a case when the hydrophone is placed at position [0.4 0.1850 0.1750] from the wall closest to the shaker stinger.

4.3.1 LMS - Inverse system Identification

The theoretical results from the LMS inverse system identification algorithm is seen in Figure 4.10 below.

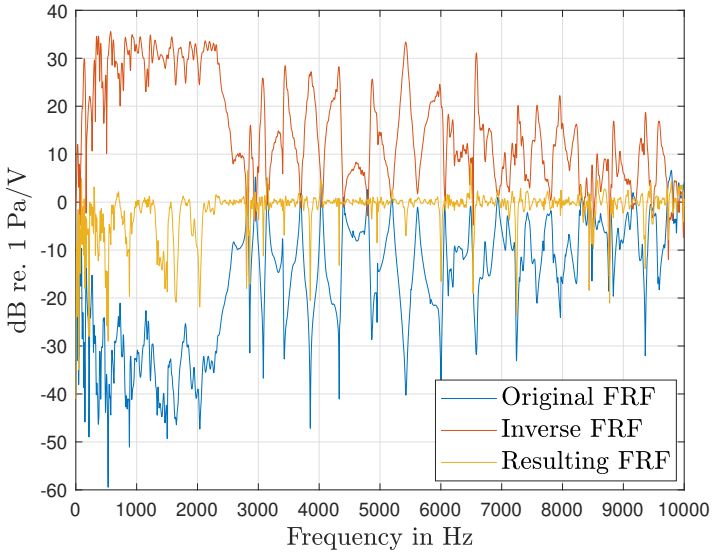

Figure 4.10: Theoretical results from the LMS algorithm. Blue curve: FRF between the signal sent to the tank through shaker excitation, and the signal measured by the hydrophone at position [0.4 0.1850 0.1750] ± 1 cm. Red curve: Inverse of the previous FRF using the LMS algorithm. Yellow curve: The resulting FRF after convolution.

The FRFs in Figure 4.10 are calculated as in Section 2.5.1 with the impulse response measured in the tank. As can be seen, the LMS algorithm, as it is used in this thesis, is not strong enough to completely equalize the FRF at low frequencies (yellow curve, approximately below the cutoff frequency). As exemplified in Section 2.5.1 in comparing Figure 2.15 with Figure 2.17, this is likely due to the comparatively extreme variations in amplitude in the tank IR. The coherence in the region below the cutoff frequency is also lower than for above the cutoff frequency (see Figure 4.5), which leads to a poorer measurement of the FRF, and thus a worse performance of the algorithm, see Section 4.5 and Section 4.1.2. Regarding this last statement, the influence of the low coherence on the performance of the algorithm is probably comparatively small. This is since it does not seem to affect the IFR algorithm much, as will be shown in the next subsection.

Below is the measured result before and after equalizing the input signal with the coefficients obtained from the LMS algorithm:

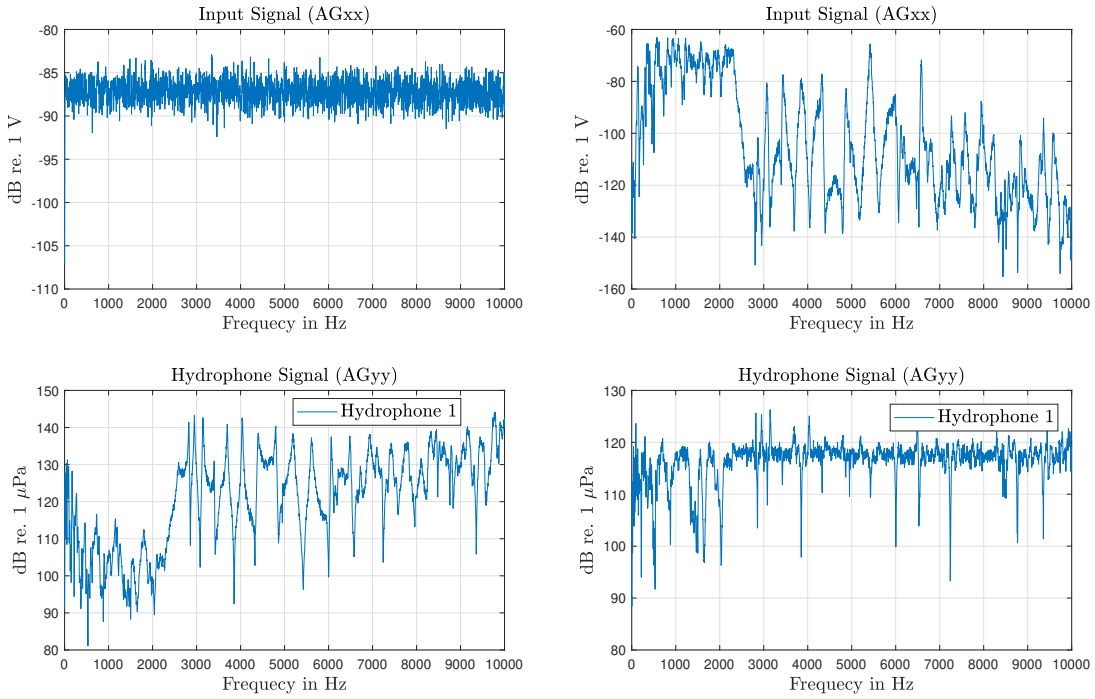

(a) Before equalization **(b)** After equalization

Figure 4.11: Autospectra of input signal (top) and output signal (bottom) before (left) and after (right) LMS equalization.

In Figure 4.18 above, the top left figure is the signal that is sent to the shaker during the measurement of the systems transfer function. In the bottom left, the signal that is picked up before equalization is seen. At the top right is the compensated signal that is calculated with the LMS algorithm. In the bottom right, the equalized signal that is measured by the hydrophone after the compensated signal is sent to the shaker is seen. The bottom left, and the bottom right curves are placed on top of each other in Figure 4.12 below, to illustrate the difference further before, and after equalization.

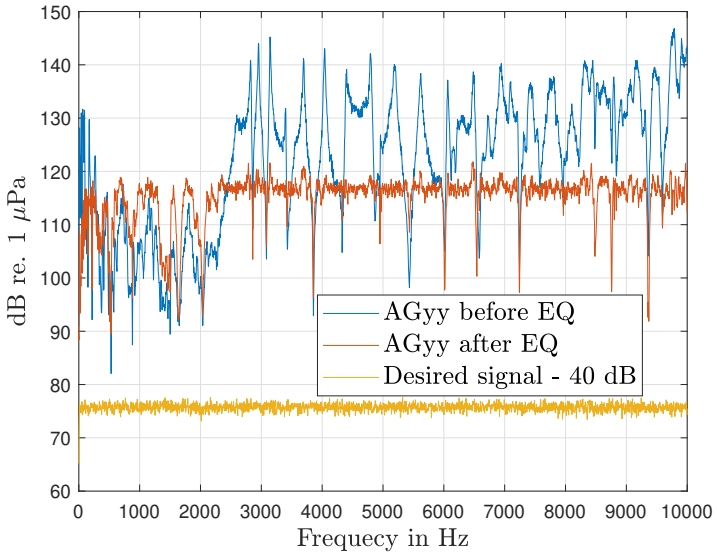

Figure 4.12: Autospectra. Blue curve: AGyy from down left in Figure 4.18. Orange curve: AGyy from down right in Figure 4.18. Yellow curve: The initial signal sent to the system, i.e. a white noise, plotted approximately 40 dB below the two other curves as reference.

The effect of the algorithms lack of performance in the lower frequency regions below the cutoff frequency is seen clearly below approximately 2500 Hz. This is in the form of dips in the orange curve reaching down to approximately 90 dB re. 1 μPa.

As stated in Section 2.5, the sound that is equalized for hydrophone position [0.4 0.1850 0.1750], as in Figure 4.12, will only give these results for that particular position. Figure 4.13 below is showing the autospectrum from a scenario when the same compensated signal as previously is sent to the shaker, but when the hydrophone is moved 0.1 m in a horizontal direction.

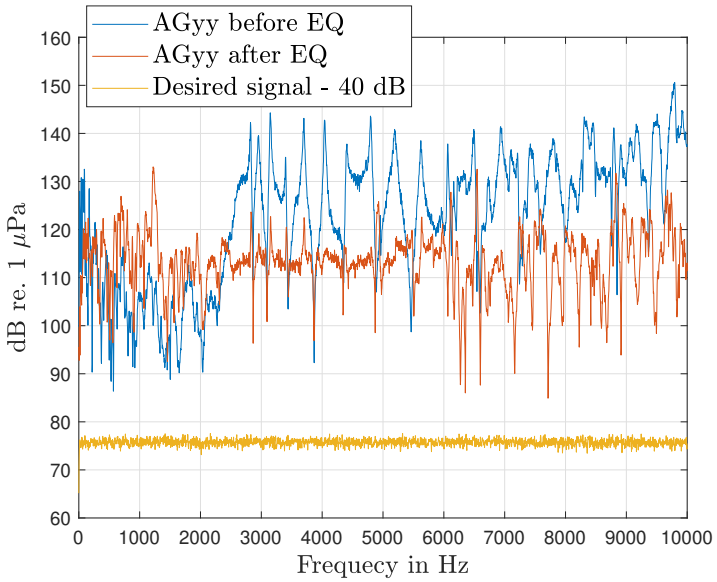

Figure 4.13: Autospectra. Hydrophone position moved from [0.4 0.1850 0.1750] m to [0.5 0.085 0.1750] m ± 1 cm.

In a comparison between the previous Figure 4.12 with Figure 4.13 above, it is seen that the orange curve (i.e. AGyy after EQ) is not as flat for the latter case. The reason for this is understood if looking at the mode shapes that were previously modelled in the top left Figure 2.10. Especially at higher frequencies, the response varies rapidly with changes in space.

4.3.2 Inverse Filtering with Regularization

The results corresponding to the ones displayed in Figure 4.10 in Section 4.3.2, but instead using the IFR algorithm, is displayed in Figure 4.14 below.

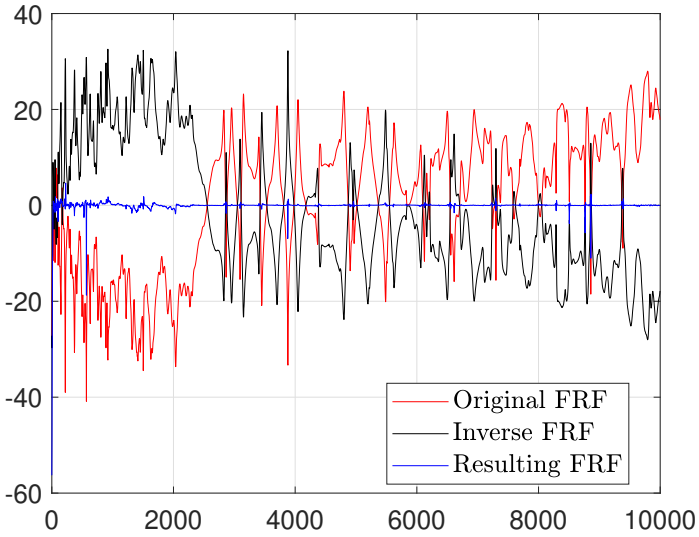

Figure 4.14: Theoretical results from the IFR algorithm. Red curve: FRF between the signal sent to the tank through shaker excitation, and the signal measured by the hydrophone at position [0.4 0.1850 0.1750] ± 1 cm. Black curve: Inverse of the previous FRF using the IFR algorithm. Blue curve: The resulting FRF after convolution.

As implemented in this project, the issues associated with poor algorithm performance in the low-frequency regions is smaller for the IFR case than it is for the LMS case. This is seen if comparing Figure 4.10 with Figure 4.14 above. This indicates that the coherence in the FRF measurements is probably high enough to produce an equalizing algorithm giving satisfactory results[10].

The results corresponding to the LMS results in Figure 4.12 and Figure 4.13, but with the IFR algorithm used instead are displayed in Figure 4.15 and in Figure 4.16 below.

[10]This probably reduces the problem with poor algorithm performance in the LMS case to the issue of bad implementation.

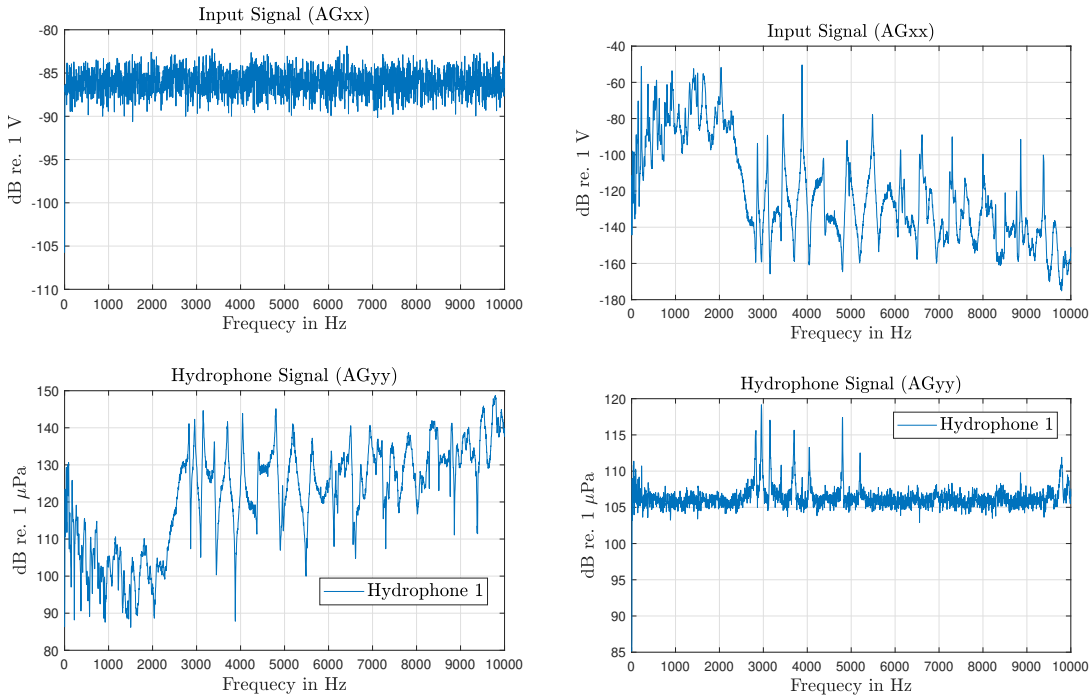

(a) Before equalization **(b)** After equalization

Figure 4.15: Autospectra of input signal (top) and output signal (bottom) before (left) and after (right) IFR.

In Figure 4.15 above and in Figure 4.16 below it can be seen that the level is more flat in the low-frequency regions below the cutoff frequency than it is for the LMS case. In fact, the issues with noise in both low and high-frequency regions[11] being modified by the systems impulse response, is in big settled. There are however seven major peaks in the spectrum starting from around 3000 Hz up to about 5000 Hz. The reason for these unwanted peaks was never understood[12] but could have to do with flaws in the algorithm.

[11] I.e. below, and above the cutoff frequency.
[12] Subjects for further research will be covered in Section 6.

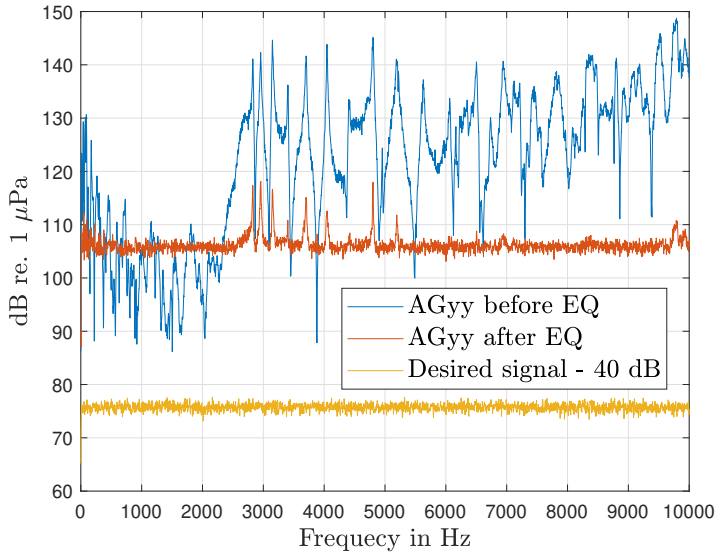

Figure 4.16: Autospectra. Blue curve: AGyy from down left in Figure 4.15. Orange curve: AGyy from down right in Figure 4.15. Yellow curve: The initial signal sent to the system, i.e. a white noise, plotted approximately 40 dB below the two other curves as reference.

As stated in Section 1.3 no claims are made in this thesis as to fundamental novelty regarding the implemented equalization algorithms used. Neither are any claims made as to optimize these algorithms. Part of the objectives of his thesis was, however, to show the potential of relatively easily implemented equalizing algorithms in marine biological research. Since the spectrum after equalization is closer to the desired spectrum than before equalization, this objective has been met.

4.4 Reproduction of Field Measurements

In this section, in Figure 4.17 below, an example of the shaker performance with the implemented IFR algorithm is shown.

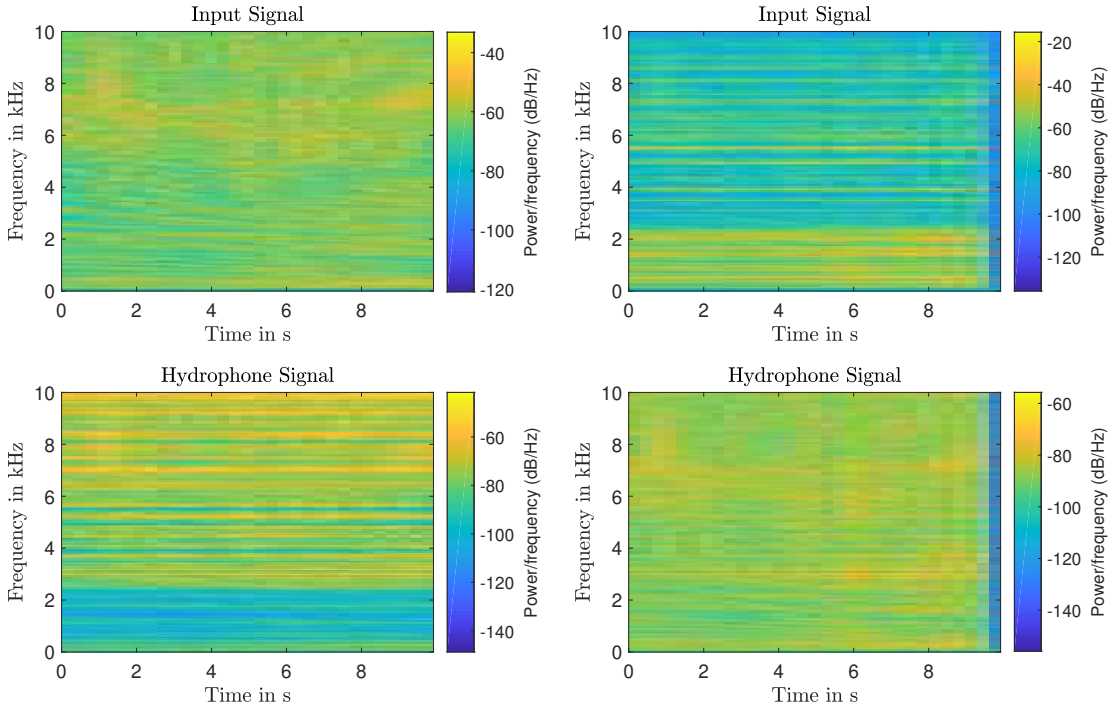

(a) Before equalization **(b)** After equalization

Figure 4.17: Spectrogram of the signal recorded from "Miami Vice" (top) and the corresponding singal measured in the tank (bottom) before (left) and after (right) inverse Filtering with Regularization equalization. The sound corresponding to the spectrograms can be listened to on https://youtu.be/$_TCCRkuS6sw$.

The transfer function of the system was measured using the shaker playing a white noise. After that, the IFR algorithm was used together with the transfer function to equalize the audio file "Miami Vice". A spectrogram of the audio file signal sent to the system before equalization is seen in the top left plot in Figure 4.17 above. The signal measured by the hydrophone before equalization is seen in the bottom left plot. The equalized audio file signal sent to the shaker is seen in the top right plot, and the resulting signal that was measured by the hydrophone is seen in the bottom right plot. The corresponding autospectra is seen in Figure 4.18 below.

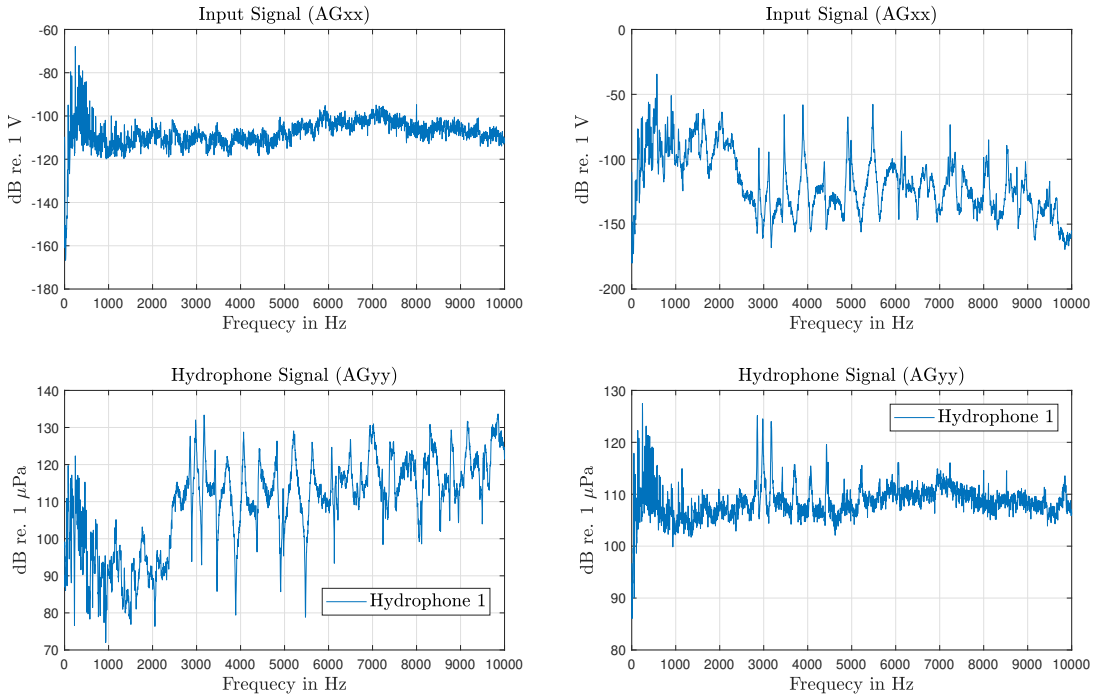

(a) Before equalization **(b)** After equalization

Figure 4.18: Autospectra of input signal (top) and output signal (bottom) before (left) and after (right) LMS equalization.

Visually and audibly (click the https://youtu.be/$_TCCRkuS6sw$ link) the shaker is now producing a sound field in the tank that is much closer to the desired sound field than before equalization.

4.5 Particle Velocity

As mentioned in the introductory Chapter 1 and the theory Chapter 2 of this thesis, fish and probably most invertebrates have hearing systems based on sensitivity for a relative contribution of pressure and particle velocity. Since the instruments for the measurement of particle velocity were not available, only the sound pressure in the tank could be studied. Unfortunately, reaching desired results in terms of sound pressure as was accomplished in this thesis so far, is merely one part of reproducing a valid sound field in the tank.

In the theory chapter of this thesis, a sound field in a glass tank was modelled both in terms pressure and particle velocity. Since the model was verified with measurements in terms of pressure, and the model is supported both in terms of pressure and particle velocity by findings in other academic works, it is assumed that the properties of the modelled particle velocity field is a reliable approximation. This

approximation suggests that a reproduction of a desired sound field[13] in terms of both pressure and particle velocity simultaneously probably is very hard[14]. This is because the relation between pressure and particle velocity in the tank is not linear as it is in the free far field. How the sound equalising algorithms are affecting the velocity field is unknown. If research would be conducted on the matter, the issue with limited distances to the sound source that causes a relative rise of the particle velocity in relation to sound pressure would reasonably be an early conclusion.

[13]It is assumed that the researcher wants to reproduce a sound field that, for example, a motor would produce in deep sea environments.

[14]with the boundary conditions associated with a glass tank as a water container.

5
Conclusion

To reach the aims in this thesis, a shaker was tested as a sound source and its performance was compared to the performance of an underwater loudspeaker. Additionally, sound equalising algorithms, whose utilization are well documented in other fields of science, were tested in this particular application.

5.1 Shaker Excitation

The following observations about the usage of the shaker as a sound source were made.

- The shaker had the ability to produce higher sounds levels than the underwater loudspeaker[1].
  - This is with emphasis on low frequency regions where the underwater loudspeaker generally had a lower ability to produce high level sound. The limiting factor as for how high levels that could be produced by the shaker were primarily the finite solidity of the glass. The upper limit was never tested because this possibly could have been the point were the glass tank cracked from the forces induced by the shaker. Additionally, increase[2] in gain gradually led to the shaker stinger loosing contact with, and tapping against the tank glass. The effect of this will be discussed below.
- The coherence in the shaker measurements was lower than for the underwater loudspeaker.
  - As the stinger started to tap against the glass, the coherence in the measurements dropped.
  - A generally lower coherence was expected since a shaker is not specifically designed for this sort of application, while an underwater loudspeaker is. If non audible tapping or masked tapping sounds were present in the measurements below the gain 5.5 remains unknown.
- The shaker produced high sound levels outside of the water filled tank.
  - These levels were high enough to be harmful without hearing protection.

[1] Without any instruments indicating overload, see Section 3.5.5.
[2] Particularly above gains around 5.5/10, as discussed in Section 3.5.5.

5.2 Sound Equalising Algorithms

As for the sound equalising algorithms, the following observations[3] were made.

- Through implementing sound equalising algorithms that are conventional in other fields of science, the spectrum and level produced by the transducers became closer to the desired spectrum and level.
  - The algorithms were however generally not able to equalize the extremes in the frequency response functions[4]. This is acceptable since the primary goal of implementing the algorithms was to show the potential of sound equalising algorithms in this particular application. Desirable ways in how to optimising will be covered in Chapter 6.
- The sound equalising algorithms showed distinguishable positive results[5] despite the lower coherence for the shaker case than for the loudspeaker case.
  - Increased coherence would however likely increase the precision of the algorithms.

[3] It this list, the observations are regarding the use of the shaker as a transducer.

[4] The extremes are referring to prominent peaks and dips in the spectra, see for example Figure 4.15 for the IFR case and Figure 4.18 for the LMS case.

[5] "Positive results" is here referring to results that are desirable in terms of reaching the aims of this thesis.

6
Discussion about Further Research

This chapter contains suggestions about what kind of research that would be suitable to conduct as a continuation of the work presented in this thesis. These suggestions are based on discussions between the author of this thesis, the supervisor of the thesis and the research institute client of the thesis. Additional suggestions come from discussions held at the thesis opposition that took place in November 2020.

The feasibility of the proposals has not been scientifically evaluated and is left to the reader to assess.

6.1 The Particle Velocity

All findings in this thesis in terms of pressure would also need to be examined for particle velocity[1][2]. The assumptions made about the particle velocity field need to be verified with physical measurements.

6.2 Analyses of the Walls

6.2.1 Forces and brittleness

The exact forces that the walls of the tank were exposed to from the shaker excitation are unknown. In the shaker datasheet[3], there is information about the forces that the shaker could theoretically produce. Still, these figures were never checked in combination with the specific signals that were sent to the shaker in this project.

It could easily be argued that knowledge about what forces that the walls are exposed to is essential in preventing breakage of the glass. The knowledge about the forces that the glass walls are exposed to would of course needed to be used together with knowledge about the brittleness of the glass material that the walls are made up of in order to prevent breaking.

[1]The instruments needed for measurements of particle velocity were not available during this project.

[2]Particle Velocity is an important aspect of research about the effect of noise on marine animals, see Section 1.1.

[3]See the B&K Webpage and Section 3.5.5 for more information.

The idea of using accelerometers or force transducers to examine the forces from the shaker stinger on the tank glass was discussed. How the forces were distributed in the tank walls, and perhaps also at what point the walls would break could be subject to a Finite Element Method (F.E.M) model.

6.2.2 Sound Emitting Properties

It was never explicitly examined how the glass walls of the tank emitted sound. Questions that would probably be interesting[4] to answer is how much vibrations are transferred via walls that are adjacent to the primary wall[5] and emitted as sound elsewhere than from the direction of the shaker.

The tank was standing on soft foam or Sylomer®, which seems to have lead to the whole tank moving along with the shaker stinger at low frequencies. Is this observation correct, and in that case, what effect does this have on the sound field in the tank?

As for the previous Section 6.2.1, it was discussed that a F.E.M analysis could be used to answer these questions.

6.3 Mounting of the Shaker Stinger

The shaker stinger was primarily pre-stressed against the tank glass for the tests in this project[6]. This lead to the shaker stinger tapping against the tank glass at high amplifier gain, and maybe also inaudibly at lower gains[7]. The tapping led to unwanted noise in the measurements. Thus, a method of preventing these taps is subject for further research.

6.4 Sound Equalising Algorithms

The desirable properties in a system developed for sound equalising that was not accomplished in this thesis, are listed below.

- The sound equalising algorithms implemented in this thesis are only effective in restricted areas in the tank[8]. Further research is needed in finding out ways of making the equalising algorithms effective in varying locations within the tank.
  - During this project, the possibility of using several sound sources instead of one as a means to accomplishing the above was discussed but never examined.

[4]Interesting because it could help answering questions about near-field contributions to the sound field, algorithm performance, etc.

[5]The wall in contact with the shaker stinger.

[6]See Section 3.5.5.

[7]See Section 4.1.2.

[8]See Figure 4.13.

  - To track the test subject[9] and making the algorithm adaptive with respect to the test subjects location was also suggested. This last approach would probably require continuous measurements of the systems transfer function and continuous filtering of the input signal.
  - Alternatively, the transfer function could be measured in a grid of many measurement points, and multiple inverse filters could be created out from these. If the movement of the test subject in the tank then was traced, the filter corresponding to the location at which the test subject is located could be activated, and the sound field at that point equalised.
- The sound equalising algorithms were not able to flatten all extremes in the autospectra. Since the algorithms were not perfect, there is room for improvements in this area.
- The sound field was equalised through first sending a white noise to the system, measuring its transfer function, creating an inverse filter from that, and then filtering the actual test signal with it before sending it to the tank (see Section 2). If any of the properties of the system[10] had changed between the measurement of the transfer function and the filtering of the test signal, the equalisation would not work as intended. Therefore, it is desirable to find out a way to continuously measure the properties of the system and adapt the filter from these measurements. The possibilities of using the actual test signal to continuously measuring the transfer function and simultaneously filtering the signal were discussed, but not further examined.

6.5 The Tank

The method for reproducing the desired sound field in the water-filled tank in this project is based on the principles of "accepting" the tanks boundary conditions and changing the sound field (see Section 2). An alternative approach that was discussed would be to change the boundary conditions themselves.

- This could, for example, be through creating an underwater anechoic chamber in some way. With absorbing boundary conditions, a free field would be simulated, which means that resonances and echoes would not be a problem anymore[11]. Obstacles to overcome in creating an underwater anechoic chamber are the probability of very large dimensions required, and the issue of finding a suitable and water-resistant material making up the sound absorbers.
- An approach that is similar to the anechoic approach is that of creating inclined beach boundaries, possibly out of some finely divided rock and mineral particles.
- Another approach that was discussed was that of using multiple sound sources and cancelling the sound close to the walls with anti-noise. This could possibly be realised by using several shakers as transducers.

[9] In practice, a marine animal.

[10] I.e. water temperature and amount, location of source and receiver, etc.

[11] However, the issue that areas of the measurement tank would be in the near field of the sound emitting device would still remain.

Bibliography

[1] A. Novak, M. Bruneau, and P. Lotton, "Small-sized rectangular liquid-filled acoustical tank excitation: A modal approach including leakage through the walls." *ACTA ACUSTICA UNITED WITH ACUSTICA*, vol. 104, no. 4, pp. 586 – 596, 2018.

[2] The MathWorks, Inc., "Matlab function reference," https://se.mathworks.com/help/pdf_doc/matlab/matlab_ref.pdf, 2020, [Online; accessed 11-May-2020].

[3] A. V. Oppenheim and R. W. Schafer, *Discrete-time signal processing.* Pearson Education, 2010.

[4] W. L. Whitlow and M. Hastings, *Principles of Marine Bioacoustics*, ser. Modern Acoustics and Signal Processing. Springer New York, 2008.

[5] A. N. Popper and A. Hawkins, *The Effects of Noise on Aquatic Life II.*, ser. Advances in Experimental Medicine and Biology: 875. Springer New York, 2016.

[6] N. Merchant, R. Faulkner, K. Brookes, A. Bicknell, B. Godley, and M. Witt, "Underwater noise levels in uk waters." *Scientific Reports*, vol. 6, 2016.

[7] E. McCarthy, *International Regulation of Underwater Sound. Establishing Rules and Standards to Address Ocean Noise Pollution.* Springer US, 2004.

[8] R. J. Dooling, M. R. Leek, and A. N. Popper, "Effects of noise on fishes: what we can learn from humans and birds." *Integrative zoology*, vol. 10, no. 1, pp. 29 – 37, 2015.

[9] S. D. Simpson, J. Purser, and A. N. Radford, "Anthropogenic noise compromises antipredator behaviour in european eels." *Global Change Biology*, no. 2, p. 586, 2015.

[10] E.-L. Blom, C. Kvarnemo, I. Dekhla, S. Schöld, M. Andersson, O. Svensson, and M. C. Amorim, "Continuous but not intermittent noise has a negative impact on mating success in a marine fish with paternal care," *Scientific Reports*, vol. 9, 04 2019.

[11] M. Gray, P. H. Rogers, and D. G. Zeddies, "Acoustic particle motion measurement for bioacousticians: principles and pitfalls," *Proceedings of Meetings on Acoustics*, vol. 27, no. 1, 2016.

[12] L. Thabane, J. Ma, R. Chu, J. Cheng, A. Ismaila, L. P. Rios, R. Robson, M. Thabane, L. Giangregorio, and C. H. Goldsmith, "A tutorial on pilot studies: the what, why and how." *BMC Medical Research Methodology*, 2010.

[13] T. Smith, "Empirical research." *Salem Press Encyclopedia*, 2019.

[14] L. Bjørnø, T. Neighbors, and D. Bradley, *Applied Underwater Acoustics.* Elsevier, 2017.

[15] L. Cremer, M. Heckl, and B. A. Petersson, *Structure-Borne Sound. Structural Vibrations and Sound Radiation at Audio Frequencies.* Springer Berlin Heidelberg, 2005.
[16] T. D. Rossing, *Springer Handbook of Acoustics.* Springer, 2014, vol. 2nd edition.
[17] G. Müller and M. Möser, *Handbook of Engineering Acoustics.* Springer Berlin Heidelberg.
[18] M. Kleiner and J. Tichy, *Acoustics of small rooms.* CRC Press, 2014.
[19] T. Akamatsua, N. Novarini, H. Yan, and T. Okumura, "Empirical refinements applicable to the recording of fish sounds in small tanks." *Journal of the Acoustical Society of America*, vol. 112, no. 6, pp. 3073–3082, 2002.
[20] L. Rade and B. Westergren, *Mathematics Handbook: for Science and Engineering.* Springer Berlin Heidelberg, 1999.
[21] A. Duncan, K. Lucke, C. Erbe, and R. McCauley, "Issues associated with sound exposure experiments in tanks." in *Proceedings of Meetings on Acoustics*, vol. 27, no. 1, Centre for Marine Science and Technology, Curtin University, 2016.
[22] T. Okumura, T. Akamatsu, and H. Yan, "Analyses of small tank acoustics: Empirical and theoretical approaches." *Bioacoustics*, vol. 12, no. 2-3, pp. 330–332, 2002.
[23] J. Mills, "Low frequency storage and loss moduli of soda-silica glasses in the transformation range." *Journal of Non-Crystalline Solids*, vol. 14, no. 1, pp. 255 – 268, 1974.
[24] J. Eargle, *Loudspeaker Handbook.* Springer US, 2003.
[25] J. Campbell, S. Shafiei Sabet, and H. Slabbekoorn, "Particle motion and sound pressure in fish tanks: A behavioural exploration of acoustic sensitivity in the zebrafish." *Behavioural Processes*, vol. 164, pp. 38 – 47, 2019.
[26] M. Gray, P. Rogers, and D. Zeddies, "Acoustic particle motion measurement for bioacousticians: Principles and pitfalls." in *Proceedings of Meetings on Acoustics*, vol. 27, no. 1, (1)Institute of Biomedical Engineering, University of Oxford, 2016.
[27] Committee on Potential Impacts of Ambient Noise on Marine Mammals, "Ocean noise and marine mammals. washington, dc: The national academies press." 2003.
[28] P. Enger, H. Karlsen, F. Knudsen, and O. Sand, "Detection and reaction of fish to infrasound," *ICES Mar. Sci. Symp.*, vol. 196, pp. 108–112, 01 1993.
[29] K. Shin and J. K. Hammond, *Fundamentals of signal processing for sound and vibration engineers.* John Wiley Sons, 2008.
[30] A. M. F. Miranda de Sá, "A note on the coherence-based signal-to-noise ratio estimation in systems with periodic inputs." *Journal of the Franklin Institute*, vol. 343, no. 7, pp. 688 – 698, 2006.
[31] O. Kirkeby, F. Orduna, P. A. Nelson, and H. Hameda, "Inverse filtering in sound reproduction," *Measurement and Control*, vol. 26, no. 9, pp. 261–266, 1993.
[32] L. Kong-Aik, G. Woon-Seng, and K. Sen M., *Subband Adaptive Filtering : Theory and Implementation.* Wiley, 2009.

[33] O. Kirkeby, F. Orduna, P. A. Nelson, and H. Hameda, "Inverse filtering in sound reproduction." *Measurement + Control*, vol. 26, 1993.
[34] O. Kirkeby and P. A. Nelson, "Digital filter design for inversion problems in sound reproduction," *J. Audio Eng. Soc*, vol. 47, no. 7/8, pp. 583–595, 1999.
[35] H. Tokuno, O. Kirkeby, P. A. Nelson, and H. Hamada, "Inverse filter of sound reproduction systems using regularization," 1997.
[36] S. W. Smith, *The scientist and engineer's guide to digital signal processing.* California Technical Publ., 1997.
[37] M. Kleiner, *Acoustics and Audio Technology*, 2012.
[38] *Low-frequency sound and marine mammals current knowledge and research needs.* Washington, D.C.: National Academy Press, 1994.
[39] S. Zuo, Z. Feng, J. Pan, and X. Wu, "Electromechanical coupling dynamic modeling and analysis of vertical electrodynamic shaker considering low frequency lateral vibration." *ADVANCES IN MECHANICAL ENGINEERING*, vol. 12, no. 10, n.d.
[40] Institute of Electrical and Electronics Engineers, "Ieee 100 : the authoritative dictionary of ieee standards terms." 2003.
[41] s. Butterworth, "On the Theory of Filter Amplifiers," 1930.
[42] The Acoustical Society of America, "Ansi s1.11: Specification for octave, half-octave, and third octave band filter sets," 2009.
[43] International Electrotechnical Commission and others, "Standard iec 61672-1: Electroacoustics-sound level meters-part 1: Specifications," 2013.
[44] M. G. Christensen, *Digital Audio Signals.* Cham: Springer International Publishing, 2019, pp. 31–43.

A

Appendix - Data Sheets

A.1 Hydrophone 1

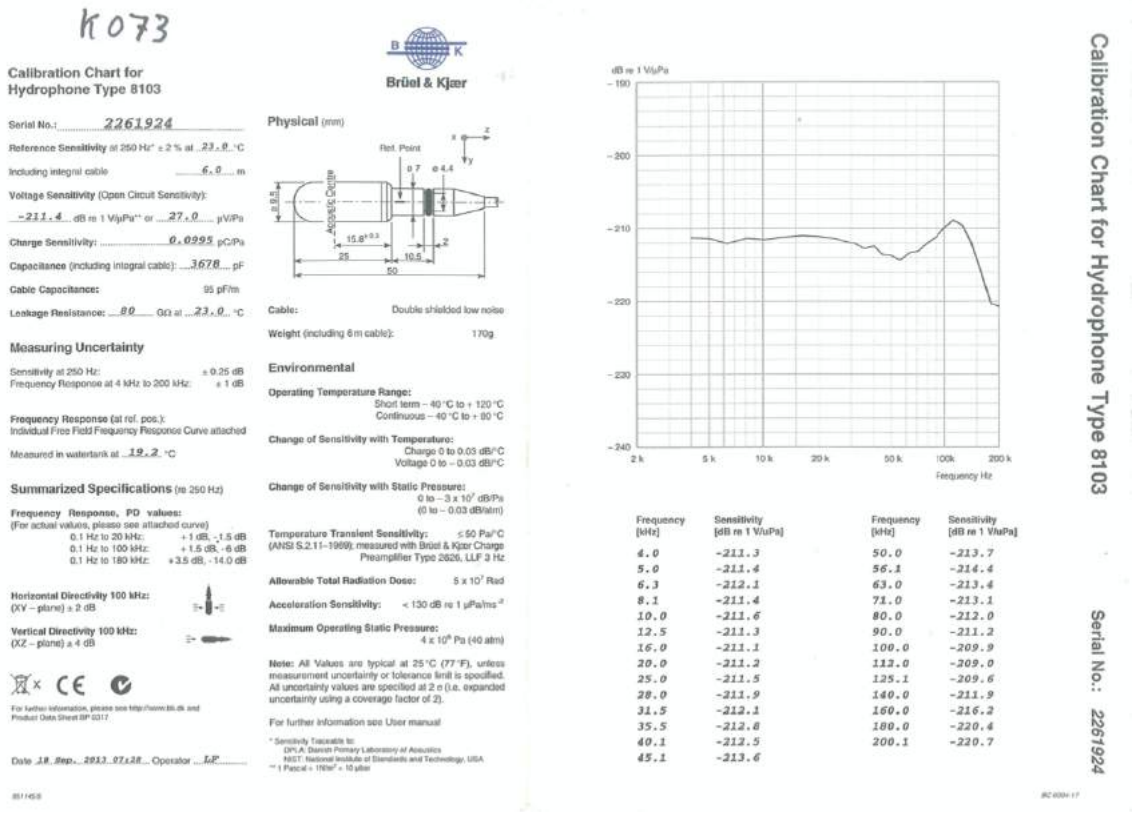

Figure A.1: Calibration chart for Hydrophone 1.

A.2 Hydrophone 2

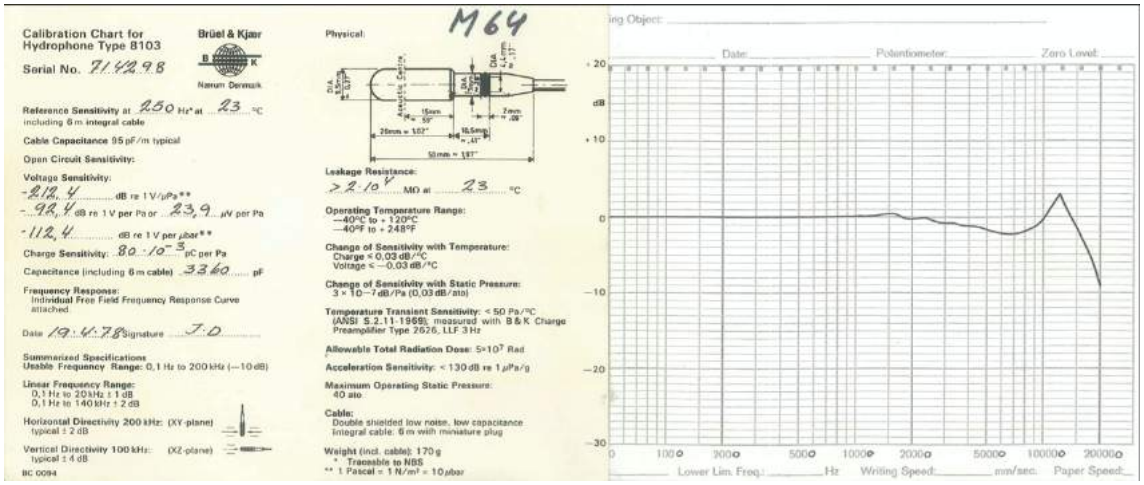

Figure A.2: Calibration chart for hydrophone 2.

A.3 Hydrophone Calibrator

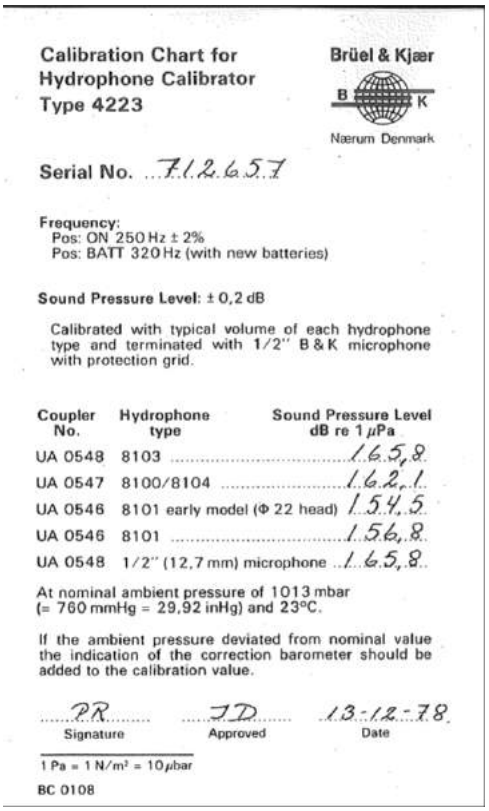

Figure A.3: Calibration chart for hydrophone calibrator.

A.4 Microphone

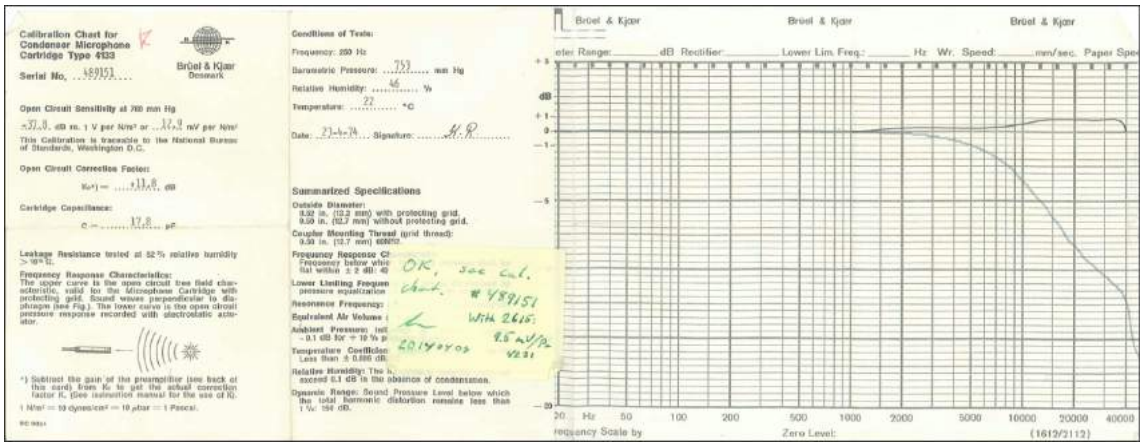

Figure A.4: Calibration chart for the microphone.

A.5 Microphone Calibrator

Figure A.5: Calibration chart for the microphone calibrator.

A.6 Underwater Loudspeaker

AQUAVOX

UNDERWATER LOUDSPEAKER TYPE UW60

This transducer is suitable for very large pools or in open water where clear speech is required or for acoustical research.

Typical acoustical range in reasonably quiet conditions, operating at 30 watts.

Clear speech - 30 metres.

Background music - 80 metres.

For temporary or test use it can be suspended by the side cleat, or alternatively, a cleat can be fitted to the base for suspending diaphragm downwards. For permanent installations the unit can be fitted with a stainless steel grille to suit a standard underwater lighting niche.

SPECIFICATION

POWER RATING (INPUT)	30 watts RMS. Peak 50 watts.
FREQUENCY RANGE	200Hz-7KHz
IMPEDANCE	Nominal 16 ohms
MAGNETIC SYSTEM	Permanent magnet.
MAXIMUM OPERATING DEPTH	20 metres.
DIMENSIONS	Overall diameter 125mm. Overall length 160mm. Weight in air 4Kg.
FINISH	White plastic. Cable white or grey twin PVC covered, standard length 5 metres, or to customer's requirements.

These specifications are subject to alteration without notice.

NOTE The loudspeaker must not be contaminated by strong chemicals if they are used for cleaning the pool, tank or associated equipment.

Figure A.6: Specifications for the underwater loudspeaker.

A.7 Sylomer®

CHRISTIAN BERNER

by getzner sylomer®

May 06, 2020

Project	**Isolering akvarium**		
Remark	Axel, Chalmers		
by	Rebecca Orvestad		
Material	**Sylomer® SR55**		
Quantity	6	Holes	
Length / Width	100 mm / 100 mm	Quantity	0
Surface	60000 mm²	Diameter	0 mm
Thickness	25 mm		
Shape factor	1		
Mass	250 kg	Dyn. Stiffness	1.84 kN/mm
Capacity	95 %	Dyn. Modulus of elasticity	0.77 N/mm²
Deflection	1.7 mm		
Natural frequency	12.5 Hz		

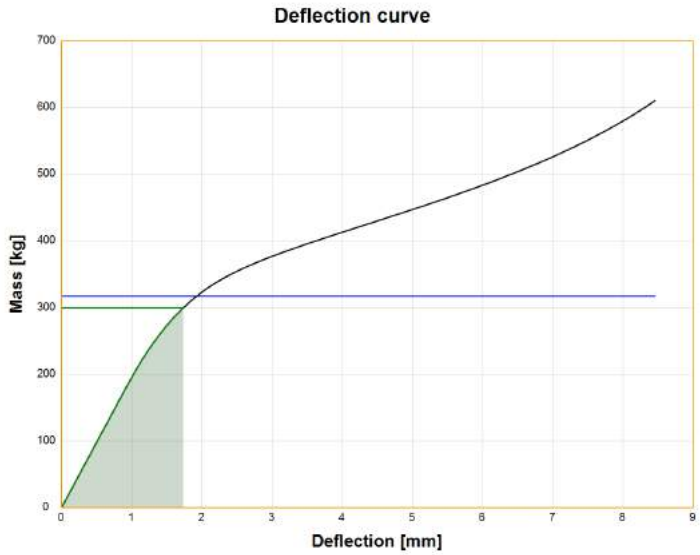

AUSTRIA – Bürs GERMANY – Berlin – Munich – Stuttgart FRANCE – Lyon JORDAN – Amman
JAPAN – Tokyo INDIA – Pune CHINA – Beijing USA – Charlotte www.getzner.com

getzner engineering a quiet future

Figure A.7: Part 1. Product data sheet for the Sylomer® used in the project.

CHRISTIAN BERNER

by getzner sylomer®

Project **Isolering akvarium**

Remark Axel, Chalmers

by Rebecca Orvestad

Graph of isolation

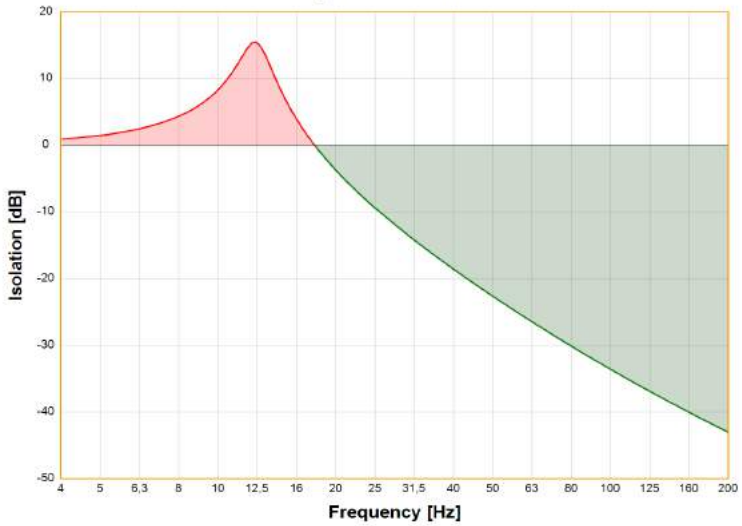

Frequency	Isolation
4 Hz	0.9 dB / -11%
5 Hz	1.5 dB / -19%
6.3 Hz	2.5 dB / -34%
8 Hz	4.5 dB / -68%
10 Hz	8.4 dB / -163%
12.5 Hz	15.5 dB / -497%
12.5 Hz	15.5 dB / -495%
16 Hz	3.5 dB / -50%
20 Hz	-3.8 dB / 35%
25 Hz	-9.3 dB / 66%
31.5 Hz	-14.1 dB / 80%
40 Hz	-18.7 dB / 88%
50 Hz	-22.6 dB / 93%
63 Hz	-26.4 dB / 95%
80 Hz	-30.2 dB / 97%
100 Hz	-33.6 dB / 98%
125 Hz	-36.8 dB / 99%
160 Hz	-40.2 dB / 99%
200 Hz	-43.1 dB / 99%

Figure A.8: Part 2. Product data sheet for the Sylomer® used in the project.

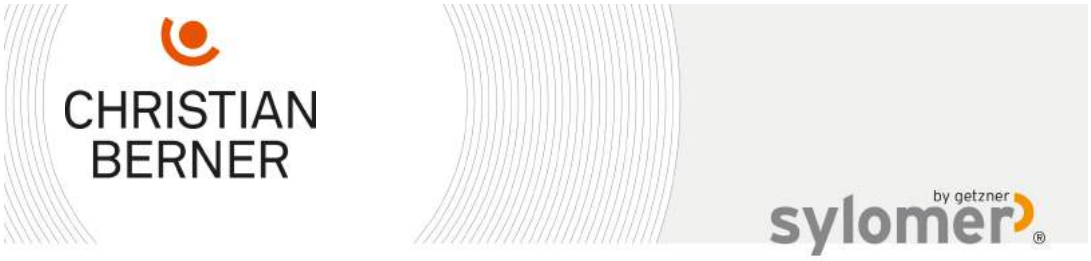

Basis of calculation:
The calculations base on the physical model of a harmonic oscillator with a massless spring on a rigid and plane subsoil. The calculation program FreqCalc makes calculations based on the assumption of a rigid mass in the centre of gravity. The calculated values are relevant for the degree of freedom in the vertical direction (single degree of freedom), taking into consideration the non-linear behaviour of the material.
The material data takes into account shape-factor-dependency and was last updated on 16-May-2019 | SW-Version 150610

All information and data correspond to the values on the Getzner data sheets, taking production- and material-tolerances into account. Furthermore, this information and data are based on the current knowledge of Getzner. These do not represent warranted properties, however.
The calculations and the associated results apply to and exist exclusively for the purpose of selecting materials from the Getzner range of products. Ensuring suitability for an intended use ultimately remains the responsibility of the customer or their authorised agent (e. g.: planner/structural engineer). All other rights are reserved. Sharing calculations with unauthorised third-parties in particular is expressly prohibited.
As far as is legally permitted, Getzner accepts no liability and gives no warranty regarding the use of the calculation results. This applies in particular to specific customer requirements. The customer shall not be entitled to pursue any claims whatsoever in relation to the use of calculation results.

Figure A.9: Part 3. Product data sheet for the Sylomer® used in the project.

B

Appendix - Code

B.1 White Noise Generation

```
function signal = Hn_signal(fs, T)
% Created by Axel Kindbom Jonsson, 2020

% Creates random signal having equal intensity at different frequencies
% The signal has a constant power spectral density.

% Example call:
% fs = 51.2e3;
% T = 30;
% signal = Hn_signal(fs, T)

Nf=round(fs*T);                          % Number of frequency components
signal = randn(Nf,1);                    % Create random numbers
signal = signal/max(abs(signal));        % Normalize to 1

end
```

Figure B.1: Function used for creating the white noise signal

B.2 Sweep Sine Generation

```
function signal = sweep_signal(fs, T, f_start, f_stop)
% Created by Axel Kindbom Jonsson, 2020

% Creates a logarithmically increasing frequency sweep with
% constant amplitude = 1.

% Example call

% T = 30;        % Length of sweep in s
% fs = 51.2;     % Samples per second defined by the sampling frequency
% f_start = 1;   % Starting frequency
% f_stop = 10e3; % Ending frequency

% signal = sweep_signal(fs, T, f_start, f_stop)

t = 0:1/fs:T;    % Time step
signal = (chirp(t,f_start,T,f_stop,'logarithmic',-90))'; % -90 makes a sine

end
```

Figure B.2: Function used for creating the sweep sine signal

B.3 Sine Wave Generation

```
function signal = sine(fs, T, f)
% Created by Axel Kindbom Jonsson, 2020

% Creates a sine wave signal

% Example call

% T = 30;         % Length of sweep in s
% fs = 51.2;      % Samples per second defined by the sampling frequency
% f = 500

% signal = sine(fs, T, f)

t = 0:1/fs:T;    % Time step
signal = sin(2*pi*f*t);
end
```

Figure B.3: Function used for creating the sine wave signal

B.4 Hn Estimator

```
function [H1, H2, coherence, AGxx, AGyy, fHn] = Hn_estimator(input, output, fs, ↙
window, overlap)
% Created by Axel Kindbom Jonsson, 2020
% Filter input variables:
% Input = Vector of input data
% Output = Vector of output data
% fs = Sampling frequency
% window = Scalar or vector for windowing the blocks
% Overlap = Amount of overlap btw the blocks.

% Filter Output variables:
% H1 = H1-estimator btw input and output
% H2 = H2-estimator btw input and output
% coherrence = Coherrence btw input and output
% AGxx = Autospectrum of input signal
% AGyy = Autospectrum of output signal
% fHn = Frequency vector to use for plotting

if isrow(input)                         % If row input, make column
    input = input';
end

if isscalar(window)                     % If scalar create hanning
    hw = hanning(window);
else
    hw = window;                        % If vector, use as window
    window = length(window);
end

hw_scale=sqrt(sum(hw.^2)/length(hw));   % Scaling factor

xb = buffer(input,window,overlap);      % Put input signal into blocks
yb = buffer(output,window,overlap);

Nb = size(xb,2);                        % No. blocks
Nf =  size(xb,1);                       % No. f-components / block
df = fs/Nf;
fHn = (0:Nf/2.56-1)*df;                 % Frequency Vector

xbhw = zeros(window, Nb);               % Allocate memory
ybhw = xbhw;
Xbhw = xbhw;
Ybhw = xbhw;
Sxx = xbhw;
Syy = xbhw;
Syx = xbhw;
Sxy = xbhw;

for nb=1:Nb

    xbhw(:,nb)=xb(:,nb).*hw/hw_scale;   % Window blocks
    ybhw(:,nb)=yb(:,nb).*hw/hw_scale;

    Xbhw(:,nb) = fft(xbhw(:,nb))./Nf;   % Convert to frequency domain
```

```
    Ybhw(:,nb) = fft(ybhw(:,nb))./Nf;

    Sxx(:,nb) = Xbhw(:,nb).*conj(Xbhw(:,nb)); %
    Syy(:,nb) = Ybhw(:,nb).*conj(Ybhw(:,nb));
    Syx(:,nb) = Ybhw(:,nb).*conj(Xbhw(:,nb));
    Sxy(:,nb) = Xbhw(:,nb).*conj(Ybhw(:,nb));

    if nb==1                            % Averageing
        ASxx = Sxx(:,nb);
        ASyy = Syy(:,nb);
        ASyx = Syx(:,nb);
        ASxy = Sxy(:,nb);
    else
        ASxx = ASxx - (ASxx - Sxx(:,nb))/nb;
        ASyy = ASyy - (ASyy - Syy(:,nb))/nb;
        ASyx = ASyx - (ASyx - Syx(:,nb))/nb;
        ASxy = ASxy - (ASxy - Sxy(:,nb))/nb;
    end
end

if mod(window,2) == 1                               % For odd window length
    AGxx(1) = ASxx(1);
    AGxx(2:(Nf+1)/2.56) = 2*ASxx(2:(Nf+1)/2.56);

    AGyy(1) = ASyy(1);
    AGyy(2:(Nf+1)/2.56) = 2*ASyy(2:(Nf+1)/2.56);

    AGxy(1) = ASxy(1);
    AGxy(2:(Nf+1)/2.56) = 2*ASxy(2:(Nf+1)/2.56);

    AGyx(1) = ASxy(1);
    AGyx(2:(Nf+1)/2.56) = 2*ASxy(2:(Nf+1)/2.56);

else                                               % For even length windows
    AGxx(1) = ASxx(1);
    AGxx(2:Nf/2.56) = 2*ASxx(2:Nf/2.56);

    AGyy(1) = ASyy(1);
    AGyy(2:Nf/2.56) = 2*ASyy(2:Nf/2.56);

    AGxy(1) = ASxy(1);
    AGxy(2:Nf/2.56) = 2*ASxy(2:Nf/2.56);

    AGyx(1) = ASyx(1);
    AGyx(2:Nf/2.56) = 2*ASyx(2:Nf/2.56);

end

H1 = (AGyx./AGxx);                          % Calculate transfer function

H2 = (AGyy./AGxy);

coherence = (abs(AGyx).^2)./(AGxx.*AGyy);  % Calculate coherrence
```

Figure B.4: Function for calculation of the auto spectra, transfer functions and the coherence

B.5 Code for Calibration

```
case 'hydro'
    % Created by Axe Kindbom Jonsson and Michael Sikora
    % In order to calibrate the hydrophone, this piece of code is added
    % to an in-house software for calibration of measurement instruments.

    % dataOfInterest = data from channel of interest
    % f_center = Measured frequency of peak from calibrator
    % info.fs = sampling frequency
    fprintf('Assuming a center frequency of 247 Hz. \n')
    f_center = 247;
    f_norm = f_center*[0.95, 1.05]/(info.fs/2);
    [num, den] = butter(2,f_norm);
    dataFiltered = filter(num, den, dataOfInterest);
    c = rms(dataFiltered)/186; % 186 = Pascals expected from the calibrator
    %       calibrator
    info.unit{channel+1} = 'Pa';
```

Figure B.5: Code for calibration with the Hydrophone Calibrator Type B&K Type 4229

B.6 LMS Algorithm

```
function [e_n,w] = LMSadapt(u_n,d_n,w_0,mu)
% Created by Axel Kindbom Jonsson, 2020
% Reference: L. Kong-Aik, G. Woon-Seng, and K. Sen M.,Subband Adaptive
% Filtering :Theory and Implementation.Wiley, 2009.

% y_n = Compensated signal
% e_n = Calculated error
% w = Coefficient of FIR filter. These coefficients are later used to
% modify the signal sent to the system.
% u_n = Product of convolution between signal x sent to the system,
% and the systems impulse response
% d_n = delayed version of input signal x. (Delayed with L)
% w_0 = Weight vector
% mu = Step size

% Example call %%%%%%%%%%%%%%%%%%%%%%%%%%%%%%%%%%%%%%%%%%%%%%%%%%%%%%%%%%%%%%%

% fs = 25.6e3;     % sampling rate for the Impuls Response
% dF = 1;          % frequency resolution
% f = 0:dF:fs-dF;  % frequency axis
% T = 15;           % Signal time
% [signal] = Hn_signal(fs,T); % Create white noise. (Check Appendix)
%
% IR = [0.1 -0.4 0.1 -20 8 1 -40 -2 0 1 1 1 -1 ]; % Arbitrary IR
%
% u = conv(signal, IR, 'full'); % SIgnal modified with the IR
% u = u(1:length(signal));
%
% u = (u./max(abs(u)))'; % Normalize to 1
%
% signal = (signal)'; % signal sent to the tank
%
% M = 2^8;         % Length of LMS filter
% L = fix(M/2); % Delay of LMS filter
% d = [zeros(1,L) signal(1,1:length(u)-L)]; % Delayed input signal
%
% w0 = zeros(M,1); % Weight vector (initially just zeros)
% mu = 2./(M.*var(u)); % Step size bound
% mu_crit = 0.1.*mu;
%
% [error, w] = LMSadapt(u,d, w0, mu_crit);

% %%%%%%%%%%%%%%%%%%%%%%%%%%%%%%%%%%%%%%%%%%%%%%%%%%%%%%%%%%%%%%%%%%%%%%%%%%%%

M = length(w_0);                % Length of LMS filter
w = w_0;                        % Zero padded weight vector of FIR filter
u = zeros(M,1);                 % Modified in
%
ITER = length(u_n);             % Length of input seque_nce
y_n = zeros(1,ITER);            % Initialize output vector to zero
e_n = zeros(1,ITER);            % Initialize error vector to zero

for n = 1:ITER
    u = [u_n(n); u(1:end-1)];   % conv(x, IR_tank, 'valid')

    y_n(n) = w'*u;              % Output signal
    e_n(n) = d_n(n) - y_n(n);   % Calculated error

    if n >= M
        w = w + (mu*e_n(n))*u;  % Filter coefficients
    end
end
```

Figure B.6: LMS algorithm code

B.7 Inverse Filter with Regularization

```
function [invIR]=RegInvFIR(IR, f_start, f_stop, RLST, L_out, n, fs)
% Created by Axel Kindbom Jonsson, 2020
% References:
% [O. Kirkeby and P. A. Nelson, “Digital filter design for inversion
% problems insound reproduction,”J. Audio Eng. Soc, vol. 47, no. 7/8,
% pp. 583-595, 1999]
% [H. Tokuno, O. Kirkeby, P. A. Nelson, and H. Hamada, “Inverse
% filter of soundreproduction systems using regularization,” 1997]
% and more papers signed Kirkeby

% Example Input %%%%%%%%%%%%%%%%%%%%%%%%%%%%%%%%%%%%%%%%%%%%%%%%%%%%%%%%%%%%

% fs = 25.6e3; % Sampling Frequency
% f_start = 500;
% f_stop = 6000;
% RLST = [50 -50]; % Regularization in the passband region and in the
% stopband region
% n = 2.^nextpow2(length(IR)); % Length of FFT.
% L_out = length(IR);
%
% [invIR] = RegInvFIR(IR, f_low, f_high, RLST, L_out, n, fs);

%%%%%%%%%%%%%%%%%%%%%%%%%%%%%%%%%%%%%%%%%%%%%%%%%%%%%%%%%%%%%%%%%%%%%%%%%%%%
if isrow(IR) == 1
    IR = IR';
end

RLST_pass = RLST(1); % Regularization in the passband region
RLST_stop = RLST(2); % Regularization in the stopband region

hwL = hanning(L_out); % Apply hanning window
hwn = hanning(n);
f = (0:fs/(n-1):fs/2)';

f_se = f_start-f_start/3; % Start of bandpass
f_ee = f_stop+3000; % End of bandpass

R = interp1([0 f_se f_start f_stop f_ee f(end)], ...
    [RLST_stop RLST_stop RLST_pass RLST_pass RLST_stop ...
    RLST_stop],f,'PCHIP'); % Amount of regularization in the passband
% and stopband

R = 10.^(-R./20);           % from dB to linear
R = vertcat(R,R(end:-1:1)); % Make double sided
r = ifft(R,'symmetric');    % Go to time domain.
r = circshift(r,n/2);       % Shifts the IR symmetrically to the middle
r = hwn.*r;                 % Applies HW to the regularization
[hello,r] = rceps(r);
R=fft(r,n);                 % Back to frequency domain

% Calculation of inverse filter

H=(abs(fft(IR(:,1),n)));
f_vec = linspace(1,fs/2,length(H)/2);
```

Figure B.7: Part 1. Inverse filter with regularization - code.

```
iH=conj(H)./((conj(H).*H)+(conj(R).*R));

ih=(circshift(ifft(iH','symmetric'),n/2))'; % Shifts IR to center
ih=hwL.*ih(end/2-L_out/2+1:end/2+L_out/2); % sqeezed to length L

[dummy,ym] = rceps(ih); % Reconstructed minimum phase signal
invIR = ym;

end
```

Figure B.8: Part 2. Inverse filter with regularization - code.